THE AUTONOMOUS LANDING OF ROTARY-WING UAVS ON UNDERWAY SHIPS IN A SEA STATE

by

Jordan Ross

Submitted in partial fulfillment of the requirements
for the degree of Doctor of Philosophy

at

Dalhousie University
Halifax, Nova Scotia
February 2020

Table of Contents

List of Tables

List of Figures

Abstract

There is a desire among researchers, governments, corporations and the public to learn more about our environment. To learn how it is changing, how it can be more efficiently used, interacted with, protected and understood. Some of these environments are also some of the harshest, meaning any tool that can help mitigate risks, decrease costs and maximize opportunities should be considered, such as unmanned aerial vehicles (UAV). In order to fully unlock the potential of these tools some infrastructure is lacking, mainly their recovery at sea. Current technologies focus on vision-based systems and very few end-to-end autonomous ship based algorithms have been demonstrated. Most current technologies also require very calm sea states. Here, a novel autonomous landing technique is presented.

The algorithm uses acoustic positioning to allow for landings in a wider breadth of conditions and reduces the reliance on specially designed landing targets. It also features a potential fields path planner to adapt for ship motion and provide some obstacle avoidance and natural biasing away from the heaving deck. The autonomy uses a sea state predictor to compensate for harsher sea conditions and ship motion, allowing the UAV to look for appropriate landing windows in higher sea states.

Autonomous landings are demonstrated in simulation and in a lab setting for sea conditions up to, and including, sea state 5. The ship motions in these sea states are defined using real sea trials data from the decommissioned Annapolis-class destroyer HMCS Nipigon.

List of Abbreviations and Symbols Used

Acronyms

ANN Artificial Neural Network

DOF Degrees-of-Freedom

EKF Extended Kalman Filter

FCU Flight Control Unit

GPS Global Positioning System

IMU Inertial Measurement Unit

IR Infrared

ISL Intelligent Systems Lab

MoCap Motion Capture System

MSE Mean-Squared Error

NOAA National Oceanic and Atmospheric Administration

PID Proportional-Integral-Derivative

RAO Response Amplitude Operator

UAV Unmanned Aerial Vehicle

Control

$e(t)$ System Control Error

K_d Differential Gain

K_i Integral Gain

K_p Proportional Gain

$u(t)$ Control Input

v_{MS} Measured Velocity

v_{SP} Set-Point Velocity

Kalman Filters

B_k Control-Input Model at Time k

$f(x_{k-1}, u_k)$ Non-Linear State-Transition Model at Time k

F_k Linear State-Transition Model at Time k

$h(x_k)$ Non-Linear Observation Model at Time k

H_k Linear Observation Model at Time k

I Identity Matrix

K_k Kalman Gain at Time k

P_k State Covariance Matrix at Time k

Q_k System Covariance Matrix at Time k

R_k Measurement Covariance Matrix at Time k

u_k System Inputs at Time k

v_k Measurement Uncertainty at Time k

w_k Unmodelled System Contributors at Time k

x_k System State at Time k

y_k State Measurement at Time k

Neural Networks

b Network Biases

C Neuron Scaler

$g(x)$ Neuron Output

nh Number of Hidden Neurons

nx Humber of Input Neurons

W Network Weights

x Activation Energy

y Neural Network Output

Potential Fields

ζ Potential Scaling Factor

d_o^* Critical Distance to Obstacle

d_{q,q_g} Distance Between Robot and Robot Goal

d_{q,q_o} Distance Between Robot and Obstacle

F Resultant Potential Force Acting on Robot

q Robot Current Location

q_g Robot Goal Location

U Artificial Potential

Acknowledgements

This thesis was completed with financial support from MEOPAR, the Irving Chair in Marine Engineering and Autonomous Systems and NSERC Chair in Design Engineering.

I would like to thank my supervisors Dr. Mae Seto and Dr. Clifton Johnston for their support and expertise through my time at Dalhousie. I would also like to thank my fellow researchers at the Intelligent Systems Lab for their willingness to help and make suggestions towards my thesis.

I would also like to extend a special thank you to Kevin McTaggart and DRDC for supplying all of the sea state data for the HMCS Nipigon.

Finally I would like to thank my friends and family, and especially my wife, for supporting and encouraging me as I have worked towards achieving one of my life's goals. No one achieves anything alone.

Chapter 1

Introduction

For all the time humans have spent on planet Earth, there is still so much to discover and understand. So much in fact that there are researchers who still refer to the Earth as an alien planet. Evidence corroborates the sentiment when one looks at the facts. For instance, the National Oceanic and Atmospheric Administration (NOAA) suggests that more than 80% of the world's oceans remains unmapped, unobserved, and unexplored, while less than 10% has been mapped with sonar [1]. The Russian Navy has mapped 5 small islands recently discovered hidden beneath the Nansen Glacier, in addition to the 30 or more islands, capes and bays found in the same region from 2015-2018 [2]. New species of plants, animals, bacteria and marine life are being found on land, in water and in the atmosphere. Hundreds of sub-glacial lakes that have been environmentally sealed in Antarctica have been found and some have even begun to be studied [3]. The planet's climate is changing and becoming a major priority politically and scientifically to monitor, understand and perhaps even rectify. There is without a doubt still much to learn, understand and discover. One of the reasons so little is known about so much of the planet is that the environments where there is information to be gained are also among the harshest. One example is the Arctic; which can present some of the world's most interesting and challenging conditions. Shifting and melting ice creates an ever-changing landscape that only worsens as the global temperatures increase. This, coupled with high winds, rough

seas, limited satellite exposure and six months of darkness every year means the Arctic presents unique challenges not present in other regions. On the other hand, the Arctic also presents a lot of potential. The Arctic is warming faster than any other region on Earth and is the location best suited to study the effect climate change has on the planet and how it may cause further changes if not mitigated. Environments and habitats that are now endangered need to be protected and others that were previously inaccessible can now be exploited, explored or monitored. The melting ice creates the possibility for the North-West passage to be used as a shipping lane, allows for the potential mining of resources like gold, natural gas, oil and other minerals like nickel, iron and copper, and creates incredible new research opportunities.

Exploration within this type of ecosystem requires the use of tools that can mitigate the inherent risks to people, property and environment. One group of tools that has seen increased use in virtually every scientific field are robots. Robots create opportunities to search, explore, map, test and analyse a variety of environments and complete tasks that may be mundane, dangerous, expensive or difficult for humans to accomplish alone. They can be designed and equipped to meet specific needs in a variety of ways. For example, returning to the Arctic environment described previously, unmanned aerial vehicles (UAVs) in particular can be used to make observations at high altitudes (for example, at a modest altitude of 50 m, the UAV horizon is ≈ 25 km compared to 5-8 km at sea level) and can monitor marine protected areas with a much lower environmental impact than direct human observation. UAVs can increase a ship's situational awareness by looking for leads in the ice that are wide enough for a ship to travel and maneuver through without being trapped while also used as scouts to look for visible navigation hazards that the ship should avoid. They can be used along with merchant vessels to take persistent measurements, that is a measurement taken in the same location at different times of the year (this is a project that is currently proposed). Militaries can use UAVs to map and image derelict ships or other floating bodies to decrease the risk to themselves before they move into range and many other applications.

To optimize the use of UAVs in these applications, there are a few pieces of infrastructure that need to be developed and implemented that are currently challenges to

the potential range of applications. For use in Arctic sea-based missions in general, one piece of infrastructure that still requires development is the recovery of the vehicle i.e. ship-based landing. How UAVs are recovered on a ship is highly dependent on what type of UAV is used. UAVs themselves fall into three broad categories: fixed-wing, rotary-wing and hybrid rotary and fixed-wings, known as vertical take-off and landing vehicles (VTOL). Each of these have different constraints when it comes to landings, however within the context of this thesis, in reference to UAV landing, only the latter two categories are considered. Currently UAVs can land in calm seas with good visibility. They can land autonomously and semi-autonomously with a pilot, however there are a lot of environmental conditions where the only method to recover the UAV is a controlled crash landing. This is due to the complexities in fusing the motion of a high frequency response UAV with low frequency slower ship motion. Pilots, by nature, can only sense what one of the two vehicles is feeling depending on where they are located while piloting and therefore can take advantage of all the available information. Wind and poor visibility conditions further complicate the human operator's responsibilities. As such, this is an area that could benefit from increased autonomy and robustness with regards to environmental conditions.

A robot that can function autonomously has many advantages; the largest being that it does not rely on human input. It can fuse information that may not be available to a human operator and make better decisions faster. Even though there are applications where a robot cannot, and should not, replace human intuition, having a robot that can make decisions and carry out actions for itself can drastically increase its potential applications. Robotic autonomy is a very broad and abstract distinction with no real agreed definition [4]. Some researchers define autonomy as the full/ partial replacement of a function that was originally carried out by a human operator [5]. The classic example here is the use of robotic arms and manipulators in manufactoring plants to assemble products, or having a planetary rover (like the Mars Exploration Rover) explore the Mars instead of an astronaut. Others go deeper and define robotic autonomoy as where the robot follows high level orders but exactly how the task is completed is left open to the robot [6]. For example, telling a planetary rover to go to a certain location and let it determine how to get there. Then, telling it to take a sample and let it determine how to actuate to have it take the sample.

The most common notion for robotic autonomy states it is the robots active use of its own capabilities to pursue its goals, without intervention by any other agent in the decision-making processes [7]. This definition emphasizes the decision-making aspect. Returning to the rover example it would look like a broader high level goal-based command. Telling the rover to take a sample of a rock and have it determine where and how to go to the best location, have it search for the rock, take the rock and return. It just has a goal, and is able to determine for itself all the steps necessary to complete the goal. This is the definition used within this thesis.

This thesis will present a novel solution to the autonomous recovery/landing of UAVs on an under-way ship traversing in the Arctic experiencing typical Arctic conditions. The goal of the autonomy is to have the UAV land safely on the ship in harsh seas and environmental conditions while minimizing damage to people and property. The autonomous landing of UAVs is a topic that has been at the forefront of many research projects and has been explored in great depth over the last decade. The autonomy involved can be viewed as a very high-level problem that is accomplished with a collaboration of highly coupled, but also independent, low-level subsystems all contributing to the overall behaviour. As such, there are numerous approaches and components for researchers to focus on. Therefore, in the bigger picture, there is a need to categorize the different contributions; this is usually based on the low-level components of the landing architecture. There is a precedent to divide these subsystems into four fundamental topics:

- how the UAV senses its environment (Pose Estimation);
- how the UAV moves within its environment (Guidance);
- how the UAV is captured or lands on the ship (Recovery);
- how the UAV handles uncertainties and external disturbances (Control).

Based on the existing literature, the vast majority of the work in the field has gone into the pose estimation and control problems and to the guidance and recovery problems. There are several good surveys published already detailing the state-of-the-art with regards to autonomous landing. The reviews by Guatam et al. [8] and Kong et

al. [9] provide an excellent overview of the current existing technologies. It is important to note that there are very few researchers that focus on the marine environment and researchers also tend to focus on one element of the landing problem instead of addressing the event in its entirety. This thesis will propose a solution featuring an acoustic-based position estimator, potential fields guidance system, prediction-based recovery and feedback PID controller, as shown in Figure 1.1.

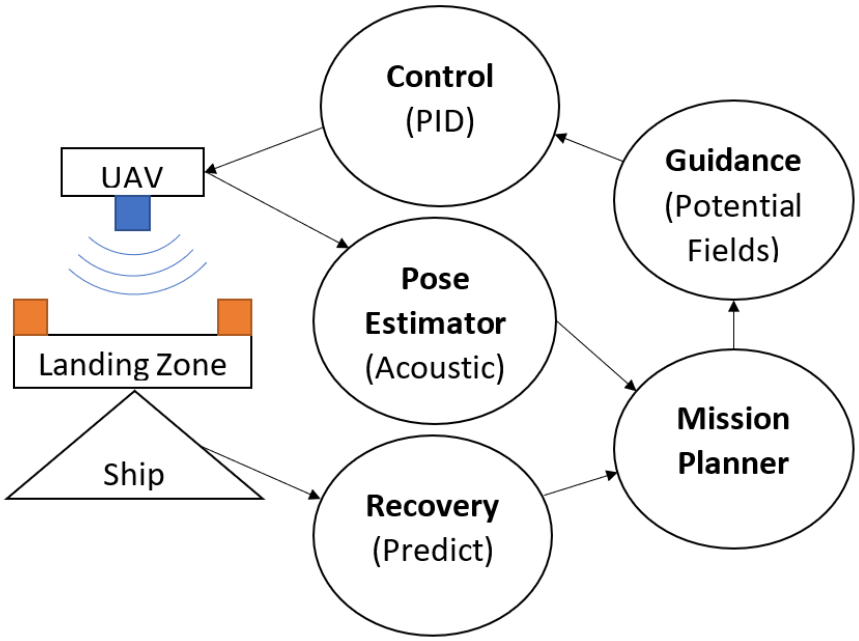

Figure 1.1: Schematic detailing the components of the proposed landing autonomy.

This thesis will first explore in detail the state-of-the-art for autonomous UAV landing, followed by background information to build the proposed solution. Next, it will introduce the proposed landing algorithm, detail the simulation and experimental environment used for testing and finally present the results, discussions, conclusions and contributions of the research project.

Chapter 2

Literature Review

This chapter will explain in detail the state-of-the-art for UAV autonomous landing with regards to the four areas used in the industry. Even though this thesis focuses on the landing of rotary-wing UAVs, some of the research specific to fixed wing UAVs will also be presented for situations where the technology and techniques are transferable. Before getting into the low-level building blocks, there are a few full-scale autonomous systems that have been demonstrated and are currently used in marine-based missions today. The most relevant is the techniques used by Northrop Grumman for their large Fire Scout UAV [10]. They have demonstrated autonomous landings full-scale in missions and are currently deployed by the US military. These landings are vision-based and use the helipad, or another known target, for localization. The UAV assumes the landing site is clear of obstacles, the seas are calm and the ship motion is negligible. It simply centers above the platform and descends.

2.1 Pose Estimation

The "pose estimation" is the environment sensing part of the landing. The UAV must perceive/sense its pose relative to where and what it is trying to land on. It is the primary source of feedback used in the guidance and control subsystems as needed

through-out the landing process. The term "pose" refers to both the position and orientation of the vehicle, however in this section not all pose elements are found using the described technique; the pose is fully defined using the proposed solution coupled with other techniques. The most common pose estimation techniques with UAVs and robots in general is the use of a Global Navigation Satellite system like the Global Positioning Systems (GPS). GPS works through trilateration; if the UAV knows how far it is from at least 3-4 satellites, it knows it is located at the intersection of all the spheres created by the known distances. GPS however is not ideal for many landing applications, especially in cases where the area available for landing is constrained since civilian GPS accuracy is on the order of 3-5 m (this could potentially be improved with the new L5 broadcast signals [11]). GPS also requires a minimum set of available satellites (3 or 4: if only 3 are available it will be assumed the user is at sea level) to be available at all times. The American GPS system consists of 31 satellites, and while it can be used in conjunction with some other satellite constellations (such as the 24 satellites that are part of Russia's GLONASS constellation and the 7 that are part of India's NAVIC constellation). The satellite coverage is adequate for most environments but at some more extreme zones, namely the Earth's poles, there will be many times of the day where the satellite coverage is insufficient due to the low orbital elevation. Therefore, the pose estimation problem, in reference to autonomous landing of UAVs, is an area where many researchers have focussed since it is one of the larger deficiencies.

Most research into pose estimation for autonomous UAV landing uses vision-based techniques. Theoretically, other light-based sensors could also fall into this category; light detection and ranging (LiDAR) systems being a prominent example. Not a lot of research and development has gone into autonomous landing using these systems, however NASA has been developing a Doppler LiDAR under their Autonomous Landing and Hazard Avoidance Technology project [12]. The goal of the project is to design a sensor to extract velocity and attitude measurements to assist in landing rovers for planetary missions. This technology is still in the testing phase and has yet to be used in actual application.

2.1.1 Single Camera Vision

Computer vision-based pose estimation for use in UAV systems was first proposed and demonstrated by Shakernia et al., who showed that the pose for a landing UAV can be determined through ego-motion estimation and visual odometry [13]. Their system functions essentially as a velocimeter, where the relative motion of specific salient areas in subsequent images are used to extract the relative velocity of the UAV. This type of system was also proposed by Saripalli et al. who also applied it to an autonomously landing helicopter [14]. They found that with their estimation they could land the helicopter within 30 cm and 7 degrees of a desired landing position and orientation [15, 16]. These results were expanded on by Merz at al. by using a wider envelope of starting positions and testing the robustness of the applied algorithm/controller against varying environmental perturbations like wind and lighting [17].

The feature detection and recognition algorithms that use moment invariants to detect the salient features can be computationally challenging. To reduce the computational requirements of the algorithm, Sharp et al. devised a set landing pad design that has high contrast from any background and other features designed into the target [18]. The landing pad consisted of a large black square on a white background. Smaller white squares of set sizes and orientations were placed within the large black square (this landing pad design is shown in Figure 2.1).

With a set landing platform image, the computation time to recognize the target between subsequent images and to extract the corners of the squares was found to dramatically reduce. Sharp then used a model-based camera pose estimation technique with both linear and nonlinear optimization algorithms to estimate the pose. It essentially worked by matching the 2D camera image to the 3D known landing zone and estimating the UAV pose based on the distortions. This team of researchers later added to this work by incorporating multiple camera views to incorporate all algebraically independent constraints and improve the robustness of the solution [19]. While the proposed algorithm was meant to be applied in landing operations, autonomous landings were not actually demonstrated.

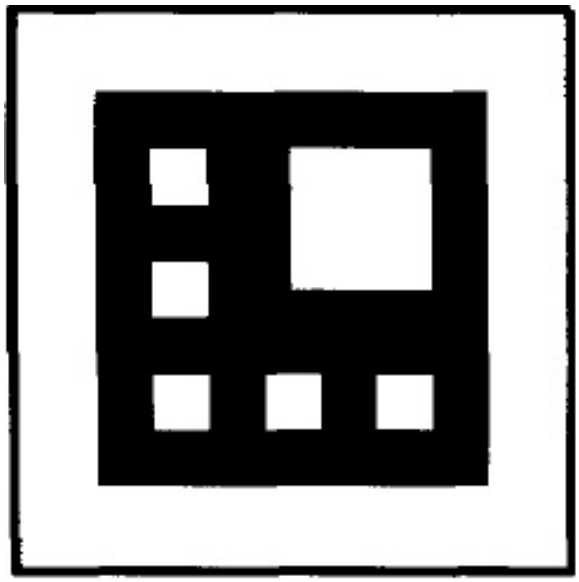

Figure 2.1: Landing target proposed by Sharp et al. based on high contrast and known dimensions. The UAV must be able to see the entire target throughout the landing. Reprinted with permission from IEEE © 2001 [18]

After the techniques shown by Sharp et al., the majority of the research into monocular vision-based pose estimation has gone primarily to improving the landing pad design and to a lesser degree into devising better target detection algorithms. Fan et al. focused on a solution to the detection problem. They proposed using a simple "H" shaped target similar to what is used for helipad sites and showed with this design Zernike moments could preform better than the Hu moment invariants used by Sharp [20]. Pose was extracted using the image region similar to what was previously done. Martinez et al. on the other hand showed good pose estimation capabilities using the pyramid approach of the Lucas-Kanade algorithm then estimating the pose through the pinhole camera model, which was similar to what was done by Fan [21]. A similar algorithm was applied by Arora et al. to track the landing zone on a ship for full scale helicopters with good results [22].

Up to this point, the landing targets designed had a few limitations:

- the targets only allowed for position to be extracted, not attitude;
- the target extraction was time intensive; and
- the target needed to be completely visible and fully extracted to work.

Designs To Extract Full Pose

Yang et al. devised a landing pad that focused on extracting more elements of the pose. They adapted the classic "H" also used by Fan by adding a circle around it. The advantage of this design is that it could extract the orientation (attitude) of the robot as opposed to just the position like the other landing target designs at the time. The pose was extracted using the elliptical deformation of the circle relative to the letter [23], similar to the perspective-n-point problem for locating calibrated cameras. A similar system was applied by Lopez et al. with the intention of being used for shipboard landings. They placed the circled "H" landing pad on a Stewart platform and were able to estimate the relative pose of the landing platform and robot while the landing pad was moving as if on a ship in a sea state [24] (shown in Figure 2.2).

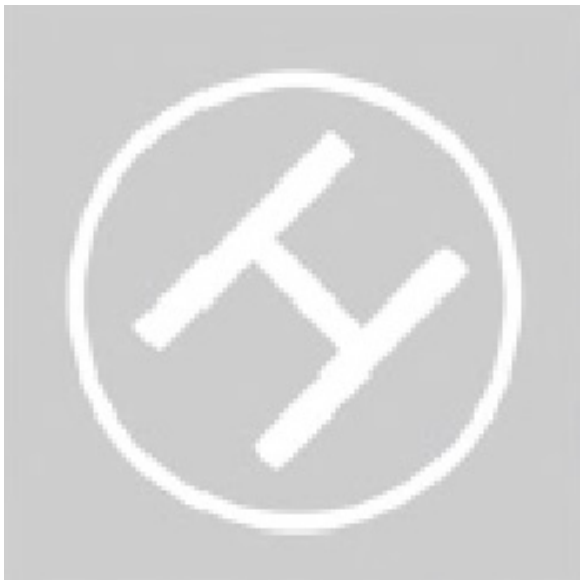

Figure 2.2: Landing target proposed by Lopez et al. in order to extract UAV attitude. The UAV still requires good visibility for line-of-sight and must have the target in its field-of-view at all times. Reprinted with permission from Springer Nature © 2014 [24]

Solutions To Speed Up Estimation Time

In contrast to a solution that can extract more pose elements, other researchers focused on designing targets that could speed up the feature extraction phase. These

designs however have not been used as much as those already mentioned. Mebarki et al. for instance designed a landing pad with 4 black circles [25] and showed through hardware experiments successful landings. Shuo et al designed a landing pad consisting of "L" shaped holes and used SRUKF to estimate the $x - y$ position to within 5 cm [26]. Edwards et al. proposed a system specifically designed for fixed-wing applications, with the goal to work in real-time [27]. They used a distinctly colored target, which after filtering and saturation were used to estimate the $x - y$ position of the UAV relative to the target. The theory is that it is easier to extract locations of high color densities than specific features. Masselli et al. applied a similar approach to rotary wing UAVs. They used 4 orange balls placed in a single plane; the camera would detect the markers and estimate the 6DOF pose of the robot using the Perspective-n-Point algorithm ($n = 4$ in this case) [28]. Bi et al. also went this route and developed a colored landing pad consisting of a green "H" with blue and red fill [29] (shown in Figure 2.3). This assumes that there is daylight to make the distinction between colours.

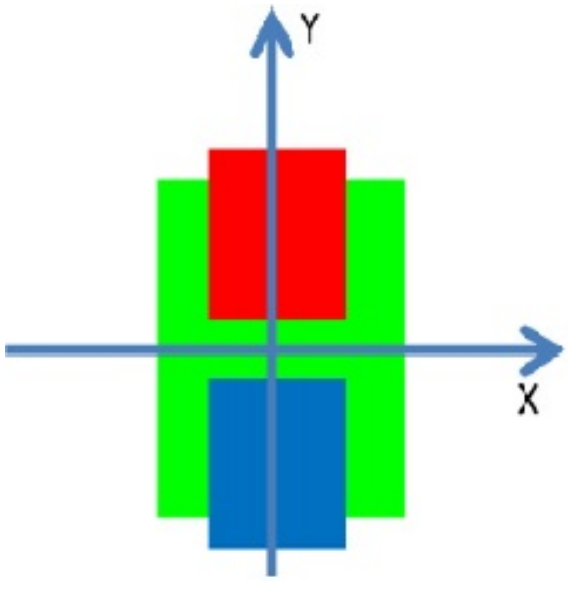

Figure 2.3: Landing target proposed by Bi et al. to reduce target extraction time. The Pose estimates are still based on line-of-sight and require the UAV to land directly on the target. Reprinted with permission from Elsevier © 2013 [29]

Borshchova and O'Young demonstrated autonomous UAV landing on a moving target using color-based object detection; the advantage being it does not require

finding depth within the image and is computationally less intensive [30, 31]. They demonstrated their solution in simulation with validation in real-time hardware trials.

Beyeler et al. proposed to simplify the problem and focus primarily on the elevation estimate. Instead of calculating the optic flow, they proposed reducing the problem to 2 dimensions and estimating the height by minimizing the difference between an interpolated image and a raw sensor image [32]. Barber et al. applied a similar system with the addition of a barometric sensor for increased precision [33].

Designs That Work With Partial Detection

Lange et al. proposed a completely different type of landing pad, concerning themselves more with extracting a pose estimation even if the entire landing pad cannot be detected. Their design consisted of white and black concentric circles; only 2 of which needed to be visible to be used for position and elevation estimations [34, 35] (shown in Figure 2.4). This allowed the UAV to fly much higher and lower since the size of the circles allowed for at least 2 to be visible at a much larger range of elevations. It also allowed for more motion and deviation by the UAV as it tried to hold its position above the platform as the entire target did not have to be detected; it could be slightly cut off and still have 2 visible circles. Araar et al. proposed a different but very similar solution to this same problem using AprilTags that decreased in size towards the center of the pad. They showed good position estimation and tracking of a moving target with their design [36].

Donenco et al. proposed a solution that eliminated the assumption that the downward facing camera can already detect the landing pad. They first detect the target with a forward-facing camera, use PTAM SLAM to track it then switch to a downward camera once over the target [37]. This could also be used to relocate the landing target should the UAV lose it from its field-of-view. Kim et al. proposed a different system to handle the field-of-view issues with a downward facing camera. They introduced an omnidirectional camera with a "fish lens" and a solid colored target. This allowed for a larger field-of-view making it more robust to wind and

Figure 2.4: Landing target proposed by Lange et al. to reduce the dependence on full target detection. While the UAV no longer needs to have the entire target in its line of sight, it still is requires good visibility and must land on the target. Reprinted with permission from IEEE © 2009 [35]

moving targets while still extracting pose estimates [38].

Relevance to Thesis

Monocular camera-based pose estimation is convenient since most UAVs are equipped with cameras. They have been shown to be able to work effectively for autonomous UAV landings on targets that are stationary and translating in one or two degrees-of-freedom. They can be used to extract very accurate pose estimates very quickly using a variety of techniques. However, they require clear line-of-sight. In all the cases above, if the UAV could not see some or all the targets/known features on deck, then it could not estimate its position. This cannot be guaranteed in environments that experience lots of precipitation, fog and six months of darkness. The line-of-sight requirement could limit the usefulness of UAV in these environments. Many of these techniques also required a uniquely designed landing pad to be used. The UAV needed to be able to see the landing pad (often in its entirety) through the entire decent, meaning the air column in which the UAV can fly is limited by the camera field-of-view and focus. The UAV is also constraint to land directly on the

landing pad and this can not be changed should something happen on deck. For these reasons, monocular camera pose estimation is not suitable for the problem studied in this thesis.

2.1.2 Stereo Vision

Single camera systems have been shown to adequately estimate the position and orientation of a UAV and have been used to autonomously land UAVs. There are however still limitations associated with using a single camera. Specifically, the depth is difficult to extract from imagines, meaning the elevation estimation can be difficult to accurately achieve. In an attempt to correct this issue with monocular camera solutions, Gui et al. proposed to instead use a stereo vision camera. Similar to the single vision solution, the target is filtered, its features extracted, and the pose is estimated through Hough transforms based on the relative locations between the features in the image and known existing features [39]. Their system required no specially designed target and compensated for the previously discovered feature detection and extraction time delays by only using 3 points for the estimation. They applied their system to a full-scale unmanned helicopter used in a marine application. Xu et al. took this idea and applied it back to the distinct and specifically designed landing pads. Their design consisted of 4 squares that highly contrast with the environment. They showed that this design, which gave 16 easily extractable features, and a least-squares pose estimation that could extract position while still operating in real-time [40].

Hsia and Yang worked separately, but similarly tried to simplify the computational requirements without using a predefined target for stereo vison systems. They both focussed solely on getting the elevation of the UAV with the stereo cameras; the theory being it is the most important variable and the x-y position can be extracted from the single camera techniques previously demonstrated. Hsia et al. used epipolar geometry to estimate the elevation to within 10 cm for up to 8 m [41] while Yu et al. used a plane-fitting method to estimate the height [42]. They used the same concept to land fixed-wing UAVs as well.

Pan et al. used this combined monocular/stereo system to land fixed-wing UAVs

on runways. They were able to use the monocular camera with the vanishing line geometry (from using Hough transforms and RANSAC [43]) and then determined the elevation using Harris corner extraction [44]. Still for use with fixed-wings UAVs, Sereewattana took the combined stereo/mono camera system and applied it back to use with landing pads. His design consisted of 4 colored circles. The pose could be estimated using homography with a monocular camera and the elevation estimated with homography using the stereo cameras [45]. More recently, Patruno et al. show potential with the use of "Point-to-Line" distance methods. Their overall methodology is a coarse-to-fine search similar to that described by Lange where coarse estimations are taken when the UAV is further away and as the UAV descends, it looks at finer (small and better defined) elements in the landing pad to make more accurate estimations [46]

Relevance to Thesis

Stereo camera-based pose estimation is shown to be able to work well for autonomous UAV landings while making improvements on some previously known deficiencies with single-camera pose estimation. However, the improvements made do not address the previously stated problems involving single-camera pose estimates as it still requires line-of-sight and special landing pad designs to land on. For these reasons, stereo camera pose estimation is also not suitable for the problem studied in this thesis.

2.1.3 Ground-Based Vision

UAV mounted cameras are convenient because many UAVs are fitted with cameras so no additional sensor needs to be integrated for the landing. These cameras also have their drawbacks, as occasional inaccuracies redundant in the embedded systems due to vibrations, unknown landing geometry and weather conditions can reduce their effectiveness. The effort to reduce these errors and restrictions gave way to the idea of using ground-based cameras; the cost being additional hardware and infrastructure required at the landing site. Pebrianti et al. proposed such a system where a single ground-based stereo camera system could track a specific part of the UAV using the

Figure 2.5: Ground-based stereo vision position estimation as shown by Martinez et al. The UAV vibrations are remove from the pose estimate at the cost of accuracy. Landing targets are no longer required, however line-of-sight is. Reprinted with permission from Springer Nature © 2011 [21]

CAMSHIFT algorithm; the position of the UAV would be estimated using triangulation [47]. The part of the UAV being tracked would be colored for easier detection, extraction and to accelerate the overall estimation effort. His method showed only marginal improvements compared to GPS, with errors still on the scale of 2 m for the elevation estimation. Martinez et al., at the same time they were experimenting with monocular on-board systems, also demonstrated a ground-based system with a similar setup to Pebrianti. They instead used an array of three ground-based monocular cameras. This provided some redundancy and allowed for the baseline between cameras to be increased. They used more points on the UAV and a backpropagation algorithm for the pose estimation itself. They did not show a lot of improvement however, and found that errors for the elevation estimate were still on the order of 2 m [21] (shown in Figure 2.5).

Kong et al. proposed a similar technique to Martinez et al. except for the application to fixed-wing UAVs. They used 2 single camera systems, as opposed to 1 stereo or 3 monocular cameras, mounted on either side of a runway. This increased the baseline for the stereo vision algorithm much more than the trinocular system. They found that this change allowed for the elevation of the UAV to be estimated to within 40 cm [48] (shown in Figure 2.6).

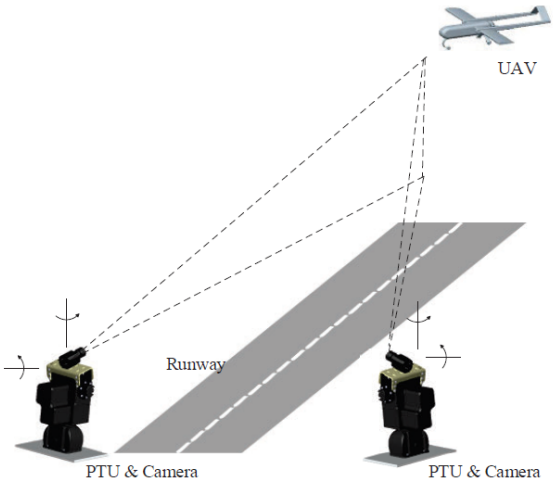

Figure 2.6: Ground-based stereo vision position estimation as shown by Kong et al. They improved the accuracy of these systems however they now require more space and still rely on line-of-sight. Reprinted with permission from IEEE © 2014 [48]

Relevance to Thesis

Ground-based cameras attempted to reduce the effects vibrations and some weather conditions had on the pose estimation. While these techniques did increase the robustness of the pose estimate to weather conditions and eliminated the requirement for special landing pads and set landing locations, they still require clear line-of-sight to function. They also sacrifice some accuracy especially in the elevation estimate. For these reasons ground-based cameras do not fit the requirements of this thesis.

2.1.4 Infrared Vision

One of the issues associated with vision-based pose estimation that was previously touched upon was the issue of line-of-sight. Many of the proposed targets require the entirety of the landing pad to be visible and even the best needed at least a portion of the target to be fully extracted. In many environments, targets can be partially or fully obscured by other objects, distance or weather (rain and snow). One proposed solution to make pose estimation more robust to these situations is to reduce the dependence on the availibility of the visible spectrum and to instead consider the infrared (IR) part of the spectrum. This method is also one of the

techniques that has been applied specifically in marine environments. Yakimenko et al. were the first to use IR in this capacity. They showed that the position of an UAV relative to a ship can be estimated with an IR camera and the position of 3 known IR targets (which can be lamps, engines, exhaust stacks, etc...) using the well established P3P triangulation algorithm [49] (shown in Figure 2.7). Wenzel added to this by later showing that the yaw of an UAV can also be determined with the addition of a 4th known IR source. Assuming the roll and pitch can be extracted from an inertial measurement unit (IMU) or gyroscope with a bounded error, this allows the UAV pose to be completely estimated [50, 51]. Other researchers have also expanded on this theory, either by applying the algorithm to larger scale systems [52] or increasing the number of points and spreads to attempt to extract more/better pose information [53].

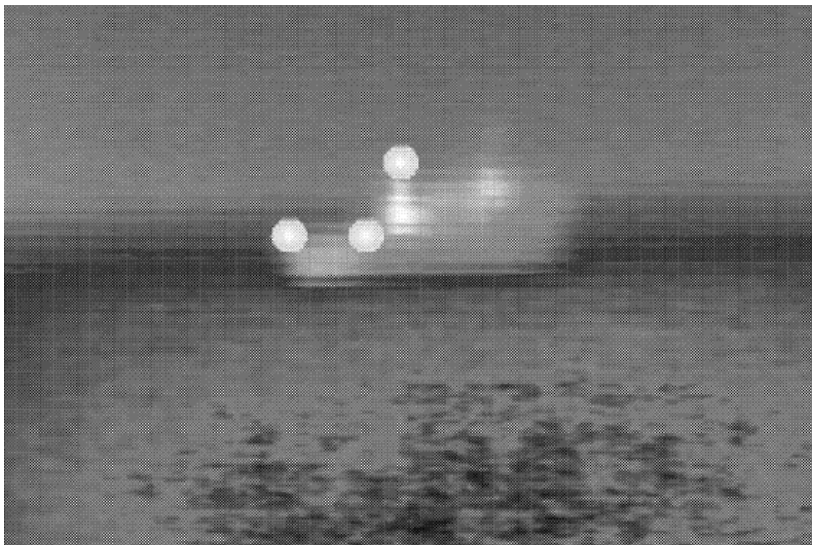

Figure 2.7: Infrared returns from a ship with 3 known IR tagrets shown by Yakimenko et al. They do not require set landing pads and can work in poor visibility, however are not as accurate as some other systems and still require line-of-sight. Reprinted with permission from IEEE © 2002 [49]

From here, researchers followed the same progression as with monocular camera techniques, where specific landing pads were designed and used instead of pre-existing features. Xu et al. for instance designed a specific IR target in the shape of the letter "T" at the landing site [54, 55] (shown in Figure 2.8). The known shape allows for the extraction of the orientation in addition to the 3D position. Xu has also shown

his system can be used to find the ship itself through a spiral search for the IR target. He also found that the greater contrast between target and background inherent to the IR detection algorithm meant the IR technique was more effective than simple vision searches alone [56]. Xiaa-Hong et al. later applyed a Tsai calibration to this system which reduced the errors caused by camera lens distortions [57].

Figure 2.8: Infrared landing target as shown by Xu et al. They improved the pose estimate accuracy for IR however returned to requiring special landing pads. Reprinted with permission from Elsevier © 2009 [54]

Since the IR cameras were mounted on the UAV, they had similar issues with vibrations and weather patterns as the UAV-mounted vision cameras. Similar to the progression with vision to ground-based vision cameras, Kong et al. demonstrated a system using ground-based stereo IR cameras at the landing zone to track the UAV position through its natural IR signature [58]. This proved to be successful for position estimations but once again reduced the portability of the landing system and once again saw an error increase to the elevation estimate relative to UAV mounted systems.

Relevance to Thesis

IR camera pose estimation techniques can address and increase the conditions for which the UAV can estimate its pose, since IR cameras can be used in the dark.

They do not however address the problems involved with flying in precipitation and once again require special landing pads (that need to be quite large compared to the other vision landing targets). While IR gets closer to meeting the requirements of this thesis, it still does not do so.

2.1.5 Acoustics

The existing research shows a clear gap in the existing technologies for pose estimation- the reliance on computer-vision. The design environment under consideration (the Arctic) however is not always conducive for computer-vision and will limit the conditions and times the UAV can be landed autonomously. There is a clear need for different pose estimation techniques that rely on a different sensing modality. The technique demonstrated in this thesis is based on acoustics. At the time of writing, there has not been an attempt to use acoustics for position estimation to land UAVs. Acoustics have however been used for position estimation in GPS denied environments, specifically for indoor flight (and other indoor position estimation applications). The Massachusetts Institute of Technology (MIT) was the first to develop this technology. Traditionally with UAVs, acoustic sensors are used for elevation estimates. The sensor emits and then records the rebounded sound waves, meaning it only measures distances to surfaces. The distance is estimated using the time-of-flight and the known speed of sound. MIT on the other hand developed an acoustic device that could be used as part of an array to make point-to-point acoustic estimations (shown in Figure 2.9). They demonstrated their system by placing beacon (emits sound) sensors around a building and tracking a listener (records sound) sensor. They were able to estimate the position of a moving train set to within 3 cm using the point-to-point measured ranges from 3 beacons and trilateration [59]. Marvelmind Robotics later commercialized these sensors and demonstrated their integration with UAVs for indoor flight. They also use trilateration for their system and advertise a 2 cm position error, however this claim has not been published in a peer-reviewed publication.

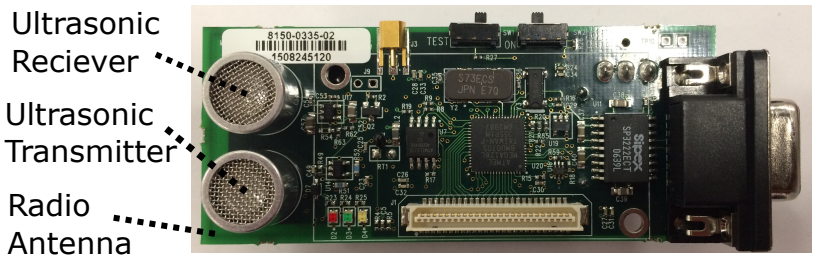

Figure 2.9: Cricket mote as developed by MIT. These sensors can make peer-to-peer acoustic range estimates which can be used to triangulate the location of a UAV without relying on computer vision.

2.2 Guidance

The "guidance" subsystem for landing determines not only the best path from the vehicles current pose to the landing site but also how it moves to the desired site by determining the required actuation forces, velocities or accelerations. It is the path planner subsystem in the autonomous landing paradigm.

2.2.1 Traditional Approaches

The most traditional techniques include proportional guidance where the goal of the guidance algorithm is to maintain a constant angle to the landing site. This is similar to pursuit guidance, another common paradigm where the aim is to maintain a velocity vector continuously pointing to the target [60]. While most researchers use these two basic techniques, a few have proposed new algorithms. Min et al. proposed a guidance strategy based on a time-to-go polynomial [61]. In this instance, control inputs are determined based on an estimate of the time remaining before touchdown and the current pose of the UAV. The polynomial has a pair of constraints: the acceleration at the final time instance must be 0 and the velocity at the final time instance must be 0.

On the other hand, Saripalli expanded on his previous pose estimation formulations with the addition of a trajectory controller based on Hamiltonian and Euler-Lagrange equations and showed the ability to track arbitrary trajectories on moving targets [62, 63].

Wu et al. proposed a method for landing autonomous helicopters using a path planner based on linear programming (LP). The landing procedure is broken into 4 stages; the linear constraints in each stage are established respectively which include the UAVs flight envelope and target kinematic constraints. Based on the established LP formulations, the optimal velocity expectation is derived [64].

Relevance to Thesis

The guidance techniques currently used work well as demonstrated in the research. They all however make some large assumptions about the landing conditions, like that the ship deck being clear of obstacles or that the UAV will always be able to approach from a certain angle-of-attack. They also do not allow for changes to be made to the approach, the goals to quickly change or for a lot of motion, especially in the heave direction, in the landing site. This thesis looks to design a landing algorithm that can be used in a variety of environments with a variety of vehicles involved, and therefore, these techniques are not ideal for this thesis in their current state.

2.2.2 Biomimedic Approaches

Chahl et al. applied a biomimetic approach strategy to the landing of UAVs using observations of how honey bees land [65] (shown in Figure 2.10). They found that when honey bees land on a flower, they attempt to maintain a constant magnitude of optic flow in their visual field. The landing site is centered within their field-of-view, and as the honey bee gets closer, it needs to slow down to maintain the constant optic flow. The descent velocity is selected to be proportional to the forward velocity, meaning both become 0 as the bee hits its target.

The advantage of this technique is that the elevation and position are not specifically solved for. As such, this algorithm is not meant for velocity control or hovering. Ruffier et al. applied this algorithm to an UAV using their OCTAVE autopilot. Their findings showed reliable terrain-following and robustness to environmental disturbances and the potential for use in landing [66]. McCarthy et al. expanded this

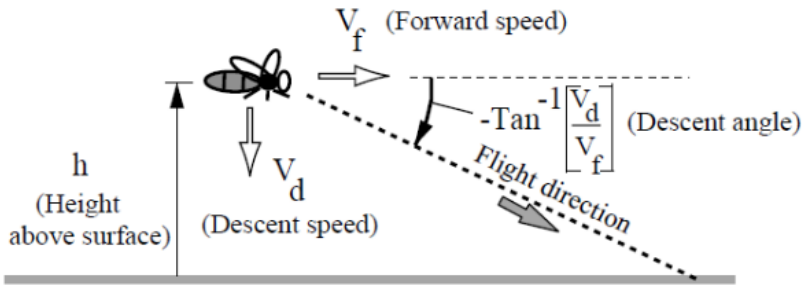

Figure 2.10: Bee-like optic flow as shown by Chahl et al. This technique simplified the overall landing problem and can be used for obstacle avoidance. This technique however, relies on vision. Reprinted with permission from SAGE © 2004 [65]

model by looking at the Time-to-Contact and optic flow fields. They calculate the flow divergence with respect to specific flow expansion points, which considers the shifting focus of expansion. This set up also allows for more control in approach speeds, decent speeds and how the robot approaches the target. This system was applied to a mobile robot approaching a wall and was shown to be effective [67]. Herisse et al took the algorithm proposed by McCarthy and applied it to the autonomous landings of a quad-copter. They showed that autonomous landing could be achieved using the optic flow divergence theory for both stationary targets [68] and moving targets [69, 70]. On the other hand, Thurrowgood found that for fixed-wing systems at least, optic flow was inefficient at low altitudes. He proposed instead a combination of optic flow with stereo vision for the landing phase [71] (shown in Figure **??**).

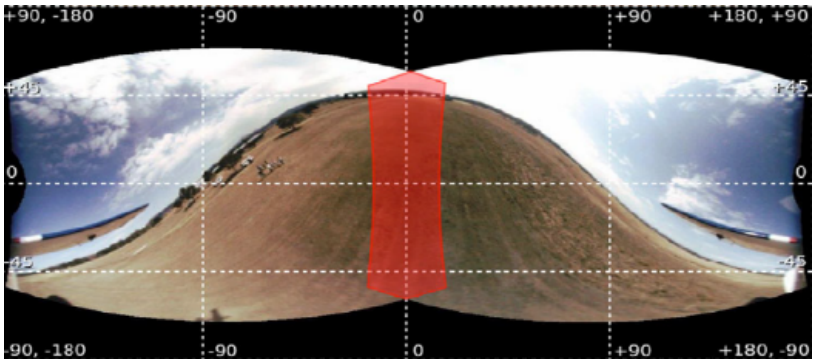

Figure 2.11: Optic flow landing approach proposed by Thurrowgood. This technique simplified the overall landing problem and can be used for obstacle avoidance. This technique however, relies on vision. Reprinted with permission from Wiley © 2014 [71]

Kendoul proposed a different biologically inspired system based on Tau theory, which states that animals and humans use the Time-to-Contact variable and simple guidance strategies to control movements. This is related to the optic flow divergence stated above with a few different challenges. The strategy works by creating a guidance strategy and control-loop based solely on the Time-to-Contact variable [72, 73]. It was shown to work for autonomous landing of rotary wing UAVs.

Relevance to Thesis

The biomimetic approaches have been shown to work for autonomous UAV landing. They can simplify the overall problem and reduce the dependence estimating the pose and can be used for some obstacle avoidance. They however, like before, require clear landing sites and cannot the react quickly to changes should they be needed. Furthermore, they require cameras which has been discussed at length at this point. These approaches while effective, are not adequate for the problem studied in this thesis.

2.2.3 Potential Fields

Existing guidance solutions mostly rely on clear landing sites and, in some cases, computer-vision. There is still a need for a robust guidance solution to be applied to autonomous landing that can adapt for obstacles on the ship deck while also limiting the risk during approach and touchdown. An artificial potential fields approach is proposed in this thesis. While it has not been applied specifically to landing, potential fields has been widely used in robotic path planners. In general, potential fields discretize the space and assign each node a potential that is calculated based on the location of the goal (low potential) and any obstacles (high potential). The robot then traverses through the space following the decreasing potential gradient. For UAVs specifically, potential fields are used for obstacle avoidance [74–76] and swarm robotics [77].

2.3 Recovery

The "recovery" part of landing is concerned with the final touchdown. It is how the UAV finally comes to rest on the landing site along with any considerations for mitigating damage to it. In most cases, and in all the work presented previously, there were no complex recovery methods. The UAV simply lands gently on the target and the friction between the UAV and landing site holds it in place. The UAV velocity is also reduced during touchdown to reduce the potential for damage. Such systems, as previous explained, require good pose estimates, detailed guidance laws and accurate controllers to prevent failures during the touchdown. They also require landing site that are either stationary or moving predictably as no consideration is given for what the landing site might be doing at the time. This is not often sufficient for ship-based landings as ship motions create unpredictable and sometimes extreme landing site motions. As far as ships are concerned, there are two areas that researchers have focussed for vehicle recovery: crash landing-based recovery devices and landing site predictors.

2.3.1 Mechanical Recovery

The majority of recovery devices are designed with the intention of the UAV essentially crash landing on the ship. The goal of the recovery device is only to mitigate or limit the damage to the UAV and the ship during the crash landing. Possibly the most well-known recovery device is the bear-trap style device, since it is also the one used for manned helicopters today. Oh et al. proposed using this system for autonomous helicopters as well. This recovery device tethers the vehicle to the landing site. When it was time to land, the tether provides tension while the helicopter thrusts upward while being reeled in [78] (shown in Figure 2.12). This effectively removed the need for exact UAV pose estimation but added the constraint that the UAV must either be tethered or attached to a tether while hovering and ready to land.

One crash-landing style recovery device is a net, which is primarily used in military applications for fixed-wing UAVs. Mulligan et al. demonstrated the use of such nets

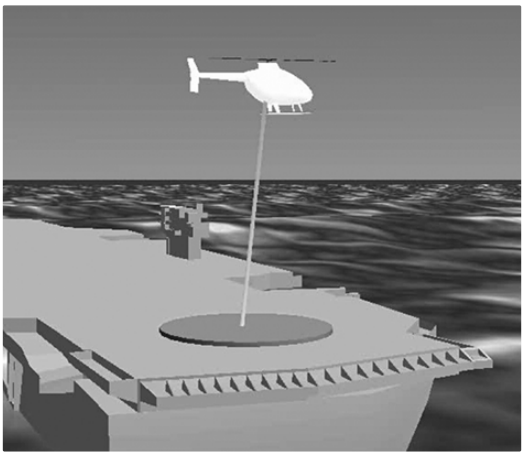

Figure 2.12: Beartrap for the landing of autonomous helicopters proposed by Oh et al. The beartrap requires a tether to be attached to the UAV and for the it to thrust upward, increasing the risk for damage during landing. Reprinted with permission from IEEE © 2006 [78]

in a variety of situations: ground-based where the net is on the ground held up by posts, moving ground-based where the net is traveling on the back of a truck, air-based where the net is suspended between two parasails and marine-based where the net is attached to a ship [79]. They also proposed an algorithm for guidance in the landing phase to fly the UAV into the net system. They used vision, and the UAV would estimate its position relative to the net using visual cues or GPS; the UAV would then use GPS estimates for navigation. The net was large enough to accomodate errors in the GPS estimation during the recovery. Yoon et al. also worked with net recovery devices, focussing more on the guidance of the UAV over the net design [80–82]. They propose a spiral approach before a smooth recovery. This method reduced the number of "misses"/failures and limited the amount of airspace needed for landings. Kim et al. took this system a little further by introducing net designs that are easier to see with vision algorithms (shown in Figure 2.13), which allows for more accurate positioning and thus smaller nets [83,84]. Kai et al. proposed using nets again in the application of ships however they showed that using an angle-of-sight (similar to the proportional guidance law discussed previously) guidance law provided better results with the ship motion [85].

The other common crash-landing recovery device is the airbag. Once again, this

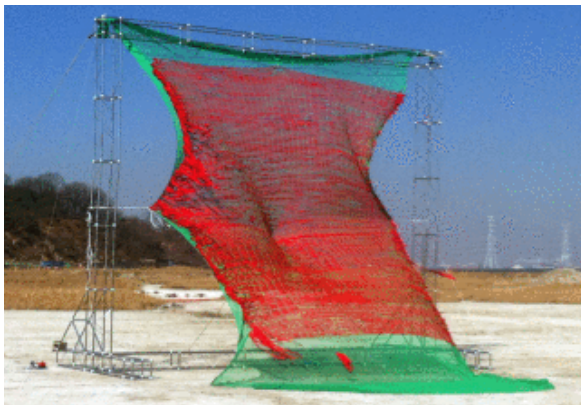

Figure 2.13: Recovery net proposed by Kim et al. This technique recovers the UAV with a crash landing, which is not desired for this thesis. Reprinted with permission from IEEE © 2013 [84]

recovery device is primarily designed for fixed-wing UAVs. Huh proposed placing a large airbag at the landing site [86, 87] (shown in Figure 2.14). The UAV would determine the location of the landing site and fly directly into the airbag - similar to what was done with the net. The advantage of this scheme is that the target airbag is easier to see and identify than the nets. Spinning parts are also less likely to get caught and the final resting place of the UAV is on the ground as opposed to still being in the air with most net configurations.

Figure 2.14: Recovery air bag proposed by Huh et al. This technique recovers the UAV with a crash landing, which is not desired for this thesis. Reprinted with permission from Elsevier © 2010 [86]

Relevance to Thesis

Mechanical recovery devices (except for the bear trap) work to simply limit, not prevent, crash landings. They all require extra hardware present at the landing site and increase the hazards involved in the whole process. It limits the turnaround time for UAVs as the UAVs need to be checked for damage and repaired, which also increases the technical personal needed on the ship as well. These landings are not idea, and the goal for this thesis is to instead have controlled landings.

2.3.2 Predictive Recovery

More recent studies into ship-based UAV landing and recovery have begun to move away from recovery devices and crash-landings and more towards attempting to land at opportune moments. This often involves predictions of when the ship might be in a suitable state (pose) for landing. Depending on how far into the future the prediction is made, it could give the UAV the opportunity to begin its landing phase early. Ferrier et al. first demonstrated this using energy indices to predict lull periods in the ship motion, which required measurements of the ship motion to be transmitted to the UAV [88]. Moriarty et al. demonstrated that an artificial neural network could predict the state of the ship up to 5 s into the future [89]. Their predictor was shown only in simulation and used only simulated ship motion, however with a simple two-layer network they managed to have a 5 second prediction accurate 98.8% of the time. Their system also used a backpropagation training law which was trained offline which means it could not adapt to changing sea conditions. Abujoub et al. used a different predictor, based on LiDAR and signal prediction algorithms. It worked on the assumption that both the roll and pitch ship motion are periodic and can be decomposed into sine waves [90]. They evaluated their system in simulation based on how many attempts were require before the drone could safely land and showed this number reduced by 2 with their prediction and did so without requiring UAV-to-ship communications.

Relevance to Thesis

Predictive recovery presents a unique solution to the autonomous landing of UAVs, especially for active landing zones. The research by Moriarty et al. [89] is especially relevant to the work being proposed in this thesis. However, there is still a lot of room for development. Their predictor was only demonstrated in simulation using simulated ship motions derived from sine waves; which are easier patterns for a neural network to learn. Their predictor was also batch trained meaning it was designed for use in specific sea conditions and would be obsolete if the sea conditions changed. They also did not demonstrate any landings with their predictor. This thesis will look to fill these deficiencies.

2.4 Control

The "control" part of landing is primarily interested in determining the control signals to have the UAV implement the desired behaviour and adapt to disturbances like wind and rain. For autonomous UAV landings, along with the pose estimation, the control subsystem is the one of the most heavily researched topics. The focus however for these researchers is largely fixed wing UAVs, since their control is more complex than hover-capable rotary wing UAVs; most of these techniques can still be applied to rotary wing UAVs. There are numerous control paradigms that can and have been used for landing UAVs autonomously, the most relevant control architectures being described here.

2.4.1 Linear Control

The Proportional-Integral-Derivative (PID) controller is the standard control architecture used in feedback linear control systems. PID controllers use a linear combination of the error (the difference between the measured and desired state variable, P), the rate of change of the error (D) and the accumulated error to form the control signal (I). Often times, different terms of the PID controller are used. For instance,

Erginer et al. proposed using separate PD controllers to control the elevation, pitch, yaw and motion of a rotary wing UAV [91]. Hervas et al. proposed a technique for ship-based landing using feedback control and showed in simulation the ability to land on a ship that was heaving [92]. The majority of researchers mentioned in the previous 3 sections of this chapter also used PID control to test their pose estimation, guidance and recovery techniques.

Even though PID control is popular for control systems, their performance depends heavily on the dynamic system. This means a well-defined dynamic system is required for optimal performance, which is challenging, especially in dynamic environments. Bodson et al. proposed to instead use a linear-quadradic controller for the tracking of a ship by a fixed-wing UAV towards landing. The controller was a combination of a linear-quadratic estimator and a linear-quadratic regulator which allowed the UAV to adequately track the longitudinal and vertical motions of a ship [93].

More recently, Feng et al. demonstrated in simulation a system using model predictive control. With this, they were able to land a UAV within 37 cm of the center of a mobile platform moving in 2D at a constant speed of 12 m/s [94].

Relevance to Thesis

Linear control is often used with rotary-wing UAVs since their dynamics are more linear than fixed-wing UAVs. They have been shown to work will for rotary wing UAV tracking at high speeds and winds, and with autonomous landing. These systems are simple and often UAVs come with some form of linear controller pre-existing in the software. Controllers are often case specific and while linear controllers have their flaws, they should be adequate for use in this thesis, however other options were still explored.

2.4.2 Non-linear Control

Linear control techniques are, by definition, designed for linear systems, or in cases where the non-linearities are negligible. However, if the non-linearities in the system

are large, they are not adequately addressed with linear control techniques and the controller is not optimized. As a result, researchers investigated non-linear control techniques. The aircraft dynamics and degrees-of-freedom (DOF) in non-linear control are coupled and therefore are all controlled with single controllers and control loops. There are several techniques that have been applied.

Prasad et al. demonstrated the use of feedback linearization in the context of landing a fighter aircraft [95]. Feedback linearization is a technique where nonlinear feedback is designed and used so the system can be treated as linear, about an equilibrium point, for the purpose of control and has worked effectively. Voos et al. applied feedback linearization to a quadcopter and were able to use non-linear feedback to decouple 3 out of the 6 DOF; allowing them to apply linear controllers to altitude and 2D-tracking [96].

Marconi et al. applied an internal-model-based error-feedback dynamic regulator to a fixed-wing VTOL attempting to land on the back of an oscillating platform meant to emulate the deck of a ship. The internal-model-based error-feedback dynamic regulator uses internal non-linear dynamic models to determine the response of the UAV to disturbances then closes the loop with feedback position estimates. They found this control technique to be robust against the uncertainties caused by the motion of the platform [97, 98].

Lee and Kim applied a backstepping controller, along with neural networks to the landing problem of full-scale planes [99]. The backstepping algorithm recursively stabilizes the origin of a system in strict-feedback form. In other words, backstepping uses subsystems that radiate out from an origin that can be stabilized using some other method. This structure allows the controller to start at a known-stable system and "back out" new controllers that progressively stabilize each outer subsystem. The process terminates when the final external control is reached. In Lee and Kim's model, the backstepping controller tracked the angle-of-attack, side-slip angle and roll while the neural network adaptive controller compensated for modeling errors. Bouaboudallah et al. applied a backstepping controller to the rotation and linear translation tracking [100]. Ahmed at al. applied the algorithm to a UAV landing with a tether by applying a correction to the flapping dynamics [101]. They later

expanded this work with the addition of a hovering controller and by decoupling the angular and linear motion, similar to the work by Bouabdallah [102]. Yoon et al. proposed an adaptive backstepping controller for a fixed-wing UAV landing with wind using hedging techniques. The backstepping controller tracked a desired glide slope towards the runway while adaptive control was used to estimate the modeling errors of aerodynamic coefficients in the nonlinear model while in flight (error in this case was a stuck actuator) [103].

Along with the backstepping controller, Bouaboudallah et al. also proposed a sliding mode controller for UAV landing [100]. Sliding mode control alters the dynamics of a nonlinear system by applying a control signal that forces the system to "slide" along a cross-section of the system's normal behavior in a finite amount of time and remain at that behavior. The trajectories in sliding mode control are defined as solutions to a set of discontinuous sliding functions that the control can switch between. Bouabdallah et al. found that the sliding mode approach provides average results partly due to the switching nature of the controller; introducing high frequency, low amplitude vibrations that cause the sensor to drift. Lee et al. applied a sliding mode controller to the landing of an UAV using visual servoing and showed the capability to land but experienced similar difficulties [104].

Shin et al. proposed a non-linear controller based on time-delay control. Time-delay control is an adaptive controller that uses the previous control output as feedback to be used as the control input for the next time-step to cancel out the model uncertainties. Their algorithm was applied to the autonomous helicopter landing on a ship in cross-winds and showed stable tracking in simulation only [105].

Relevance to Thesis

Non-linear controllers in this context are used more with fixed-wing UAVs since their motion in the six degrees-of-freedom is more coupled. These controllers were used for UAVs that needed precise control, special landing procedures (were not hover capable) and to perform complex maneuvers. As this thesis is focusing on rotary-wing vehicles, non-linear control should not be required. It could however be part of

future research.

2.4.3 Artificial Intelligence

Artificial intelligence-based controllers are systems that perceive their environment and take actions to maximize their likelihood of success for a goal. They are usually combined with linear controllers and can be designed to fit a wide variety of goal-based control problems. A few artificial intelligence-based controllers have been used in autonomous UAV landing projects.

One example in this category is fuzzy logic control. Fuzzy logic is a mathematical representation that is able to analyze analog input signals, which are continuous and range from 0 to 1, as opposed to classic digital control systems that use discrete inputs of either 0 or 1. This allows the controller to handle partial truths and accommodate for non-linearities due to aerodynamics, actuators, sensors, environmental disturbances, etc. It can also be combined with conventional feedback controllers to form a hybrid system, where the control system defines the operational semantics with both discrete and continuous dynamics. Livchitz et al. proposed a fuzzy logic controller for the landing of a fixed-wing UAV, where fuzzyfied inputs were evaluated using a linguistic rule and fuzzy logic operations to yield an appropriate control output. The output was defuzzyfied and combined with a PID controller for landing [106]. Nho et al. applied fuzzy logic and PD control to simulated linear and non-linear fixed wing models [107]. Mendex et al. combined the altitude pose estimation techniques presented above with a fuzzy logic altitude controller for a rotary wing UAV. They were able to demonstrate landing from as far as 5 m with as little as 30% of the target visible [108].

Koo et al. presented a different hybrid control design for UAV landing by modeling the multi-modal behaviors in the outer-inner loop of the vehicle as a hybrid system. A hybrid controller controls the discrete evolution of the hybrid system based on its continuous state. They carry out the landing by encoding switching sequences for the phases in the landing scenario [109].

Malaek et al. built four logic-based controllers to compensate for gusts and strong winds for the landing of fixed-wing UAVs. The base architecture for three of the four controllers were neural networks. They showed that in strong winds, adaptive fuzzy logic combined with a PID controller was able to derive the desired performance, where the conventional PID, neural and hybrid neural-PID controllers fell short [110]. They also noted that the hybrid neural-PID results were acceptable.

Khantsis et al. used generic algorithms in an attempt to evolve control laws for the landing of a small fixed wing UAV on the back of a ship. They show through a six degree-of-freedom non-linear UAV model simulator that an effective controller can be designed with little knowledge of the aircraft dynamics using appropriate evolutionary techniques [111].

Relevance to Thesis

Similar to non-linear controllers, artificial intelligence-based controllers are used primarily with fixed-wing UAVs and should not be required for this project. It could however be part of future research.

2.4.4 Robust Control

Robust control methods deal explicitly with uncertainties in control design. Robust methods are designed to function provided that uncertain assumptions or disturbances are found within a set. Robust methods aim to achieve robust performance and/or stability in the presence of bounded modeling errors. The most common form of robust control used in these applications is mixed H_2/H_∞ control. This structure meshes the strengths of H_2 control, which can achieve a good dynamic response with H_∞ control, which is robust to disturbances. Laio et al proposed using H_2 control for landing a fighter plane [112]. H_2 control minimizes the H_2 norm of a system against a cost function to obtain and track the optimal trajectory. Laio applied this control architecture to tracking in the cases of stuck actuators, noise, faults, wind, shear and turbulence in simulation, showing acceptable performance in the cases of wind and

stuck actuators.

Shue et al. proposed using robust control for the automatic landing of commercial airplanes. They applied a H_2/H_∞ controller to the longitudinal motion of the aircraft and show that the control is able to adequately handle the glide slope capture motion and flare maneuver of the aircraft [113]. Wang et al. applied the H_2/H_∞ controller to rotary wing UAVs and tested their ability to track, hover and land relative to a classical PID controller. They found that not only did the mixed controller provide stability to the design uncertainties, but also had a smaller tracking error than the PID controllers [114, 115]

Relevance to Thesis

Once again, robust control is applied primarily to fixed-wing UAVs and should not be required for this project. It could however be part of future research.

Chapter 3

Background

The solution presented in this thesis assumes prior knowledge of algorithms, techniques and concepts commonly used in engineering, robotics and oceanography. Since the work as demonstrated requires some background knowledge, this chapter will introduce the prerequisite information in its most general form. Specifically, the following topics will be covered:

- state estimation and Kalman filters;
- path planning and potential fields;
- neural networks;
- response-amplitude operators.

These items will all be applied and further developed in the following chapter when the theoretical development of the work is presented. The baseline for these topics will also be used to demonstrate the theoretical contributions made within the project.

3.1 State Estimation

One of the challenges in the thesis is to accurately determine the pose of the UAV and the landing pad (ship transom motion) with the intent to land or "dock" the UAV on the ship. Towards that end, state estimation techniques will be used to determine the pose. State estimation is the process of assigning value to unknown or uncertain system state variables. Within the field of robotics, in the context of pose estimation, the "state" of the vehicle usually includes elements like position, orientation, angular/translational velocity and angular/linear acceleration. More advanced algorithms will also include maps of the immediate area, distances to obstacles, positions relative to other robots, etc. The state is used primarily within the control and path planning parts of robot missions.

In general, state estimation techniques use measurements of the state and a filtering element that reduces the effect of erroneous measurements and noise. Other techniques use defined models of the system to predict how the state may change due to known inputs, however these systems usually still require some measurement to prevent the state estimate from diverging too much. One of the most commonly used solutions that uses both a model prediction and state measurement to estimate the state is the Kalman filter. Kalman filters are appropriate for this work given the uncertainty of the motion models, sensor measurements and environment.

3.1.1 Kalman Filters

The Kalman filter, also known as a linear-quadratic-estimator, is an optimal estimator. It combines a systems kinematic or dynamic model and known control inputs with measurements of the state that is subject to noise. This combination forms a state estimate that is better than relying on the model/inputs or measurements alone. The Kalman filter adapts to approximations in models and noise in measurements by taking a weighted average of the two information sources. The weighting for the Kalman filter is calculated from the covariance of the model and measurements. Therefore, the filter will bias itself towards the element that has the least uncertainty.

Another advantage of the Kalman filter is that each state estimate depends only on the previous estimate and current measurements, not its entire time history (i.e. the Markov condition). It also is able to track the covariance of the estimate itself which can be tuned to gain a desired response.

The Kalman filter has two distinct phases within the algorithm: the prediction phase and the update phase. In the prediction phase, a predicted state is determined based on the previous state estimate (or initial state estimate if this is the first time step) and known control inputs. The whole process begins with a linear, discrete time system. This system can be defined by the following general form:

$$x_k = F_k x_{k-1} + B_k u_k + w_k. \tag{3.1}$$

In this form, x_k is the state (ie: the minimum set of data that uniquely defines the behaviour of the system) at time t_k. The first term in this equation propagates the state from the previous time step x_{k-1} to the current time step using the process function or state-transition model F_k. The second term considers the effects of the control inputs u_k to the system through the control-input model B_k. The final term represents the unmodeled elements in the system, assumed to be normally distributed zero mean Gaussian white noise with covariance Q ie: $w_k \sim N(0, Q)$. All variables and corresponding symbols can also be found within the nomenclature at the beginning of the thesis.

The state prediction can be found from the linear discrete time system directly, and the covariance for the predicted state P_k can also be found within the prediction phase as well:

$$x_k = F_k x_{k-1} + B_k u_k, \tag{3.2}$$

$$P_k = F_k P_{k-1} F_k^T + Q. \tag{3.3}$$

The update phase then fuses the predicted state estimate and covariance with a state measurement. This phase does not have to run at the same frequency as the predict phase if the control inputs are being determined faster than the state measurements. In that case, many prediction estimates may be calculated before being updated with state measurements. Once again, the update phase uses a linear measurement model. The general form of this equation can be defined by the following equation:

$$y_k = H_k x_k + v_k. \tag{3.4}$$

The measurement y_k is defined simply as the current state x_k transformed by the observation model H_k. As with the state model, uncertainty in the sensors is modelled through the addition of zero mean Gaussian white noise with covariance R ie: $v_k \sim N(0, R)$.

In order to update the predicted state to obtain the filtered state estimate, it must first defined a scaling factor. The scaling factor K is known as the Kalman gain and is used to bias the end result towards either the model or measurements, depending on which source has the least uncertainty. The Kalman gain is defined by the following equation:

$$K_k = P_k H_k^T (H_k P_k H_k^T + R)^{-1}. \tag{3.5}$$

The Kalman gain is proportional to $Q/(Q + R)$. This relation is in essence how the Kalman gain is used to bias the filtered state towards either the prediction or the measurement, again depending on which has the least uncertainty. If the ratio is close to 1, it means that $Q > R$ and there is more uncertainty in the kinematic/dynamic motion model than in the measurements. The filtered state would thus put more

weight into that information source and the filtered state would track closer to the measured values. These cases often lead to noisier filtered state estimations that are very responsive to rapid changes. If the ratio is small, then the opposite is true and $Q < R$. More weight is put into the model rather than the measurements and the filtered state would more closely track the kinematic/dynamic motion model. This often leads to much smoother filtered estimation time series at the cost of reduced responsiveness to rapid system changes.

Once the Kalman gain is determined, the filtered state and covariance can be calculated as follows:

$$x_k = x_k + K_k(y_k - H_k x_k), \tag{3.6}$$

$$P_k = (I - K_k H_k) P_k. \tag{3.7}$$

This state becomes the previous estimate (prior) used for the next time step. The whole process is shown in Figure 3.1.

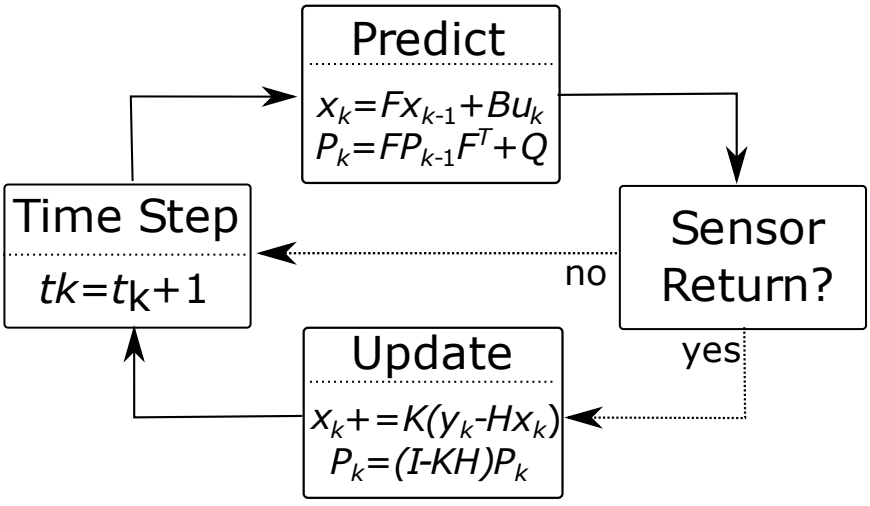

Figure 3.1: Process flow diagram for the Kalman filter.

3.1.2 Extended Kalman Filters

By definition, the Kalman filter is designed for linear discrete time systems. Many engineering problems however are non-linear and thus the Kalman filter as defined above is often unsuitable for these applications. To mitigate the issues involved in estimating the state of a non-linear system this way, the extended Kalman filter (EKF) was designed. The extended Kalman filter linearises the state and/or measurement model by using the first order Taylor series expansion (i.e. the first two terms) for the non-linear components. The drawback from this linearisation is that the extended Kalman filter is no longer an optimal estimator and has a greater tendency to diverge. This is because the first order Taylor series approximation is expanded around the current state estimate; if the initial estimate of the predicted state has large errors, then the extended Kalman filter models will have more noise than expected and the state can result in a local minima. The EKF follows the same process and has the same two-phase process as the linear Kalman filter: prediction and update. The general form of a non-linear system can be defined as follows:

$$x_k = f(x_{k-1}, u_k) + w_k. \tag{3.8}$$

The predicted state and covariance are found in a similar manner to what is shown in equations 3.2 and 3.3:

$$x_k = f(x_{k-1}, u_k), \tag{3.9}$$

$$P_k = F_k P_{k-1} F_k^T + Q_k. \tag{3.3}$$

The predicted state can still be found directly from the non-linear motion model, however the covariance requires linearisation. Naturally, if the model is already linear, this step can be skipped. The state is linearized by taking the partial derivative of

the motion model with respect to the state expanded around the current (prior) state estimate:

$$F_k = \frac{\partial f}{\partial X}\Big|_{X_{k-1}}. \tag{3.10}$$

Likewise, the measurement model can also be non-linear and generalized to the following form:

$$y_k = h(x_k) + v_k. \tag{3.11}$$

The expected measurement can be found directly with the non-linear model but the Kalman gain and updated covariance require the motion model to be linearised. Like the linearisation of the motion model, this occurs by taking the partial derivative of the measurement model with respect to the state expanded about the predicted state:

$$H_k = \frac{\partial h}{\partial X}\Big|_{X_k}. \tag{3.12}$$

Now that the measurement model has a linear approximation, the EKF can finish the update state in the same way that it did for the regular Kalman filter. First the Kalman gain is found:

$$K_k = P_k H_k^T (H_k P_k H_k^T + R)^{-1}, \tag{3.5}$$

then finally the state is updated:

$$x_k = x_k + K_k(y_k - h(x_k)), \tag{3.13}$$

$$P_k = (I - K_k H_k)P_k. \tag{3.7}$$

3.2 Robotic Path Planning

Path-planning will be performed in this thesis as a step in the UAV landing to account for obstacles and motion of the ship while also tracking the landing site. Robotic path planning is concerned with how a robot moves within its environment. It can be as simple as moving directly from the current position to a desired goal position to more complex global search algorithms, obstacle avoidance (local path planning) and goal-tracking, where the desired goal and required path are constantly changing and updating.

There are many different methods used for path planning, each with their respective advantages and disadvantages. Techniques such as A* and D* grid-based searches, interval-based searches, reward-based algorithms and geometric-based algorithms have all been applied successfully to robot missions in a variety of environments and operating conditions. One type of path planner that is seeing more use today is the artificial potential fields approach.

The potential fields algorithm assigns a "potential" to every point in the world using potential field functions (to be defined below). In essence, the goal location is defined to have the lowest potential while obstacles by definition have high potentials. With this approach, the robot is driven to travel from higher potential to lower potential; it is continuously pulled towards the goal location and pushed away from any obstacles. Another way to express this is that the robot follows the negative potential gradient. This is expressed mathematically by defining the total artificial potential U at the robots location q as the sum of the attractive potential (i.e. the goal) U_a and repulsive potential (i.e. the obstacles) U_r:

$$U = U_a + U_r. \tag{3.14}$$

The differences between different potential fields path planning applications are usually based in how the attractive and repulsive potentials are defined. Traditionally, the attractive potential created by the goal pulling the robot towards it is defined as either a conical function, a quadratic function or, more commonly, a combination of both.

A conical function increases the attractive potential at each point linearly with distance as it moves away from the goal location. This works well for larger distances as the potential gradient does not become too large at long distances, however as it gets closer to the goal the potential might be too low to create a distinct gradient to finish the traverse or the final stages of the traverse may happen very slowly. The final resting place will often have a larger error when compared to the quadratic function. The conical function is defined as the following equation:

$$U_a = \zeta d_{q,q_g}. \tag{3.15}$$

In this equation, ζ is a scaling factor and d_{q,q_g} is the distance between the robot and the goal.

A quadratic attractive function increases the attractive potential at each point exponentially with distance as it moves away from the goal location. This works well for short distances as the larger gradients make for better motion, however at large distances the potential can quickly become too large and create unstable motion. This attractive function is defined as the following equation:

$$U_a = \frac{1}{2}\zeta d_{q,q_g}^2. \tag{3.16}$$

The most common solution is to use a combination of the two methods. When a combination of the conical and quadratic function is used, there must also be a rule for the transition, which is usually a function of the distance between the robots current position and its goal position. This creates a piece-wise function for the attractive potential:

$$U_a = \begin{cases} \zeta_a d_{q,q_g} & \text{if } d_{q,q_g} > d^*, \\ \frac{1}{2}\zeta_b d_{q,q_g}^2 & \text{if } d_{q,q_g} <= d^*. \end{cases} \tag{3.17}$$

The critical distance at which the function changes is denoted by d^* and the raw distance between the robot and the goal d_{q,q_g}. This allows the conical function to be used at large distances and the quadratic function to be used at smaller distances taking advantage of the strengths in each method, while minimizing some of each method's biggest detractors. Due to the nature of piece-wise functions and to ensure a smooth transition between the conical and quadratic regions once the robot is at the distance d^* from the goal, the constants ζ_a and ζ_b can be selected to satisfy the relationship:

$$d^* = \frac{\zeta_a}{\zeta_b}. \tag{3.18}$$

Continuing with the combination attractive potential function, the gradient at the location due to the attractive potential can then be defined:

$$\nabla U_a = \begin{cases} -\frac{\zeta_a (q - q_g)}{d_{q,qg}} & \text{if } d_{q,q_g} > d^*, \\ -\zeta_b (q - q_g) & \text{if } d_{q,q_g} <= d^*. \end{cases} \tag{3.19}$$

The repulsive potential is generated by any obstacle within the space a robot may need to avoid. Traditionally for the repulsive function, it is generated only when the robot is within some critical distance d_o^* relative to the obstacle itself. To satisfy this,

the repulsive potential is also a piece-wise function:

$$U_r = \begin{cases} \frac{1}{2}\zeta_r\left(\frac{1}{d_{q,q_o}} - \frac{1}{d_o^*}\right)^2 & \text{if } d_{q,q_o} < d_o^*, \\ 0 & \text{if } d_{q,q_o} >= d_o^*. \end{cases} \tag{3.20}$$

The gradient is then determined in the same way as with the attractive function:

$$\nabla U_r = \begin{cases} -\zeta_r\left(\frac{1}{d_{q,q_o}} - \frac{1}{d_o^*}\right)\frac{1}{d_o^{*2}}\frac{q-q_o}{d_o^*} & \text{if } d_{q,q_o} < d_o^*, \\ 0 & \text{if } d_{q,q_o} >= d_o^*. \end{cases} \tag{3.21}$$

The attractive and repulsive forces are summed to determine the artificial potential at all points in an area:

$$F_{tot} = F_{att} + F_{rep} = -\nabla U_{att} - \nabla U_{rep}. \tag{3.22}$$

The potential forces can then be applied to the robot as generalized accelerations, velocities or forces depending on the situation. Figure 3.2 demonstrates what a simple map might look like once the forces are found and summed.

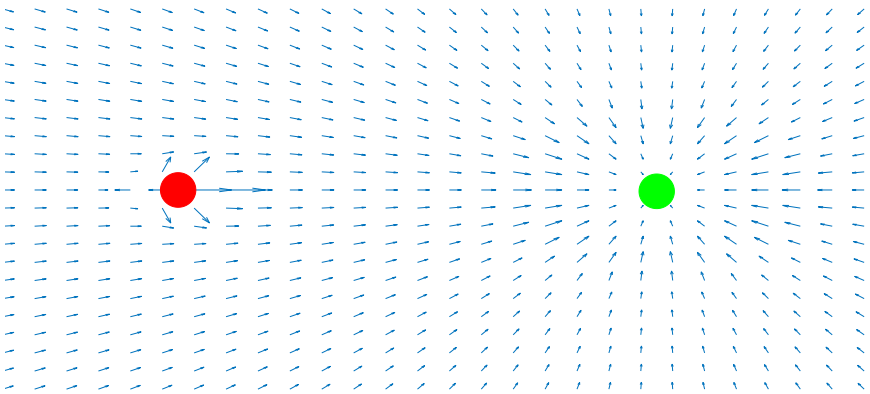

Figure 3.2: Potential fields gradients. Goal is shown in green and an obstacle is shown in red.

There are a few weaknesses associated with the potential fields approach. The most prominent issue is that the algorithm is susceptible to local minima, where the robot finds itself in a location where there is no gradient at its current location. In these cases the robot gets stuck and requires some assistance. The biggest advantages are that in simple environments the robot can quickly and effectively navigate through obstacles, the robot is very responsive to its environment and the robot can handle moving goals and obstacles.

3.3 Neural Networks

A neural network can be best described as a function mapper or emulator. They are essentially designed as a "black box" where inputs go in, go through a process, and outputs come out. Neural networks were originally designed to model human brain function and are used today to model complex systems where the dynamics are not fully known using a series of simple non-linear computations to replicate a more complex function. A neural network-based predictor will be designed to learn the ship motions prior to the UAV landing, which will in turn be used to attempt to predict when the ship is best suited to be landed on. This is done to optimize the landing and minimize the risk of failure.

A neural network can be broken down into smaller structures called neurons. These neurons are then grouped into different layers. The parameters of a neural network are usually how many neurons are used, how many layers in-between the input and output and how the neurons are connected to each other. Some of the more common network structures include deep networks, feedforward networks, recurrent networks, NARX networks etc [116]. They all have different applications and design motivations, however the most basic network structure is the feedforward multilayer perception (MLP) model. The MLP network typically has an input layer, an output layer and one or more hidden layers; however it has been shown that one hidden layer of sufficient neurons is able to replicate most functions [117]. The MLP network can be seen in Figure 3.3.

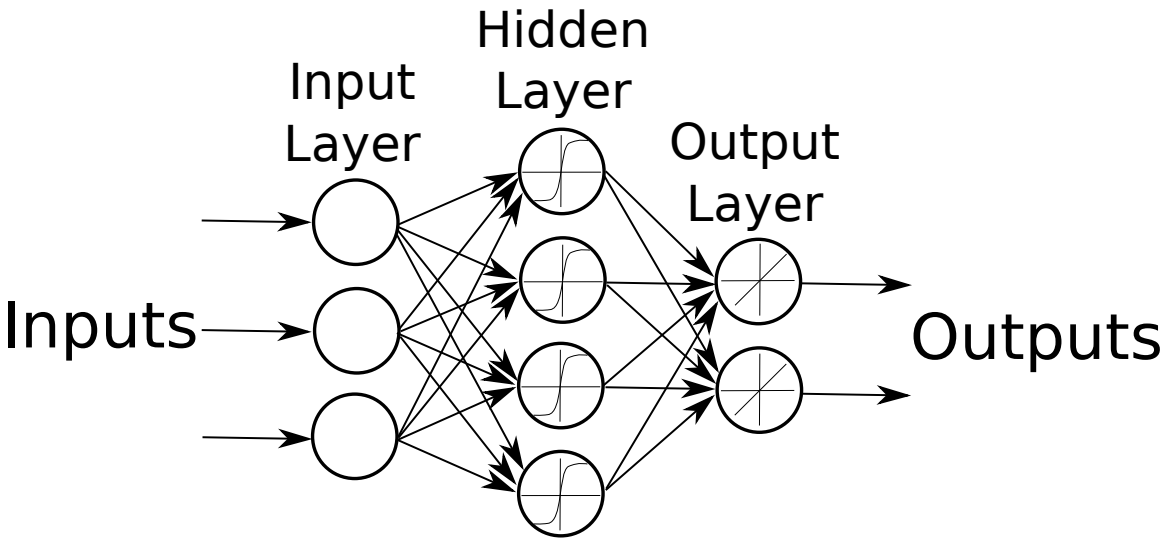

Figure 3.3: Feedforward multilayer perception neural network structure.

Each neuron has an activation energy. The activation energy is the sum of weighted outputs from each neuron in the previous layer in addition to a bias. The neuron output is then calculated using this energy and an activation function. The activation function will scale the activation energy to a corresponding value between [0,1] or more commonly between [-1,1] [118]:

$$g(x) = \frac{1}{1 + e^{-Cx}} \quad \text{if } [0, 1], \tag{3.23}$$

$$g(x) = \frac{1 - e^{-2Cx}}{1 + e^{-2Cx}} \quad \text{if } [-1, 1]. \tag{3.24}$$

In these equations, $g(x)$ is the neuron output, C is the neuron scaler and x is the activation energy. In order for the network to work, the inputs and outputs are scaled between [0,1] or [-1,1] depending on the activation function used.

The neurons in the input layer have their output energy set equal to the black box inputs. These values are then passed to the hidden layer where each input neuron is connected to each neuron in the hidden layer with its own specific connection weight. Each hidden layer neuron sums all incoming connection values with a bias

and calculates its activation energy before passing it off to the next layer, usually the output layer. The output layer once again sums all incoming energy, adds a bias to it, passes it though an activation function (usually this is just a linear function in this layer) and then passes it to the next layer. In the case of the output layer, this is just the black box output.

One of the difficulties in designing a neural network is selecting the number of hidden layer neurons, as the number of neurons in the input and output layers are constrained by the number of system inputs and outputs. Each hidden layer needs to consist of enough neurons to adequately emulate the desired model without too many redundancies that slow the overall system performance. In general, the pruning of neural networks involves beginning with more hidden neurons than necessary, then slowly removing neurons until there is too large of a change in the network performance (as measured by mean square error and variance). A MLP neural network consisting of an input, output and single hidden layer can be summarize into a single equation:

$$y = \sum_{i=1}^{nh} W_i^o tanh(\sum_{j=1}^{nx} W_{j,i}^h x + b_i^h) + b^o. \tag{3.25}$$

In this equation, nh is the number of hidden neurons, nx is the number of input neurons, $W_{j,i}^h$ are the connection weights from the input layer to the hidden layer, W_i^o are the connection weights from the hidden layer to the output layer, b_i^h are the biases for the hidden layer neurons and b^o are the biases for the output layer neurons.

For networks to be used in a meaningful way, they first need to be trained. The training process tunes the weights of every neuron connection and the biases of each individual neurons to produce the desired response. There are three common learning paradigms for neural networks: supervised, unsupervised and reinforcement learning.

Neural networks trained through supervised learning are provided both a set of inputs paired with their desired outputs. The weights are adjusted using the error between the current network output for a set of weights and the desired network output.

Traditionally these networks are batch-trained using a backpropagation training law, meaning they see all of the training data set at once and after training the weights are frozen. This makes the system less adaptable if the environment changes the network cannot change with it. In unsupervised learning the network does not have the desired outputs to go with the training inputs. In this case, the network itself decides what features to focus on and how to adjust and group the network connections. This is referred to as self-organization or adaptation. Finally, reinforcement learning does not provide a training data set but generates its own signals through interactions with its environment. The environment is modelled as a Markov decision process (MDP) [119] where at each point in time, the agent performs an action and the environment generates an observation and a cost. The goal of the learning paradigm is to perform its actions through minimizing the long term cost.

3.4 Quantifying Sea Conditions

Within oceanography and naval architecture, the sea conditions are often categorized into easily defined and relatable categories. Since sea conditions can have large extremes and are hardly repeatable, for the purposes of design and study, sea conditions are categorized using scales. There are many scales in existence used to define sea conditions, however for this thesis there are two that are most applicable: the Douglas Sea Scale and the Beaufort Scale. These two scales are used to quantify different but related properties, namely wave height and wind speed. In the research here, the response of a ship will be quantified, and emulated with a Stewart platform, to follow these scales. The ability of an UAV to land will be evaluated against the sea states the ship (landing pad) is in.

3.4.1 Douglas Sea Scale

The Douglas Scale was created in the early 1900s and relates a “degree” or “sea state” value to a distribution of wave heights (the distance between the wave crest and a neighbouring wave trough). The scale is broken into two parts for two different types

of waves: wind waves and swells. Each has their own definition and categorization, as well as physical description. Naturally, these scales can be arbitrary given the randomness that is inherent with ocean waves; however they are still used to help quantify the conditions.

The first classification in the Douglas scale is for wind waves. Traditionally, and for this thesis, when the term "sea state" is used, it is refering to the scale for wind waves. Wind waves are surface waves that occur on the free surface of any body of water. They are caused by the direct air-water interaction and are the result of energy transfering from the air to the water. In general, there are five factors that influence the formation of wind waves [120]: wind speed, fetch length (the distance over the water that the wind blows in a single direction), fetch width, wind duration and water depth. While all 5 of these factors affect wave height, their individual contributions are not considered in the Douglas scale: ie. there is no subcategory or modifier for wind speed, water depth, fetch, etc. The Douglas Sea Scale for wind waves, as well as their physical descriptions, are shown in Table 3.1.

Table 3.1: Douglas sea scale for wind waves [121]

Degree	**Wave Height (m)**	**Description**
0	0	Calm (Glassy)
1	0 - 0.1	Calm (Rippled)
2	0.1 - 0.5	Smooth
3	0.5 - 1.25	Slight
4	1.25 - 2.5	Moderate
5	2.5 - 4.0	Rough
6	4.0 - 6.0	Very Rough
7	6.0 - 9.0	High
8	9.0 - 14.0	Very High
9	> 14.0	Phenomenal

The second table in the Douglas Sea Scale is for "swells". Swells are, for all intents and purposes, a form of surface wave. Surface waves themselves once formed are a very effective mode of energy transfer. Once formed due to local weather and wind patterns, these waves can continue to travel on their own hundreds of kilometers; long after the wind that created them has ceased. Once the surface waves have decoupled from the wind that formed them they are swells. As swells are products of weather

patterns in other regions, they have no relation to the local wind speed or weather patterns. As such, they can seem a bit random and are harder to predict. The Douglas Sea Scale, as it pertains to swells, relates the degree of the sea state to the swell wave height and wave length. This scale can be viewed in Table 3.2.

Table 3.2: Douglas sea scale for swells [121]

Degree	**Description**
0	No Swell
1	Very Low (short and low wave)
2	Low (long and low wave)
3	Light (short and moderate wave)
4	Moderate (average and moderate wave)
5	Moderate rough (long and moderate wave)
6	Rough (short and heavy wave)
7	High (average and heavy wave)
8	Very high (long and heavy wave)
9	Confused (wavelength and height indefinable)

For use in table 3.2, wavelengths and wave heights are defined as the following:

Description	**Wave Height (m)**	**Description**	**Wavelength (m)**
Low Wave	< 2.0	Short Wave	< 100
Moderate Wave	2.0 - 4.0	Average Wave	100 - 200
Long Wave	> 4.0	High Wave	> 200

To report the sea state using the Douglas convention, the conditions for both scales are defined. For example, the sea state for 1m waves and 0.5m swells would be Sea:3, Swell:1. However, sometimes only the wind waves are considered i.e. the above example would be just sea state 3.

3.4.2 Beaufort Scale

The Beaufort Scale was created in the early 1800s and focuses primarily on relating a "degree" value to a distribution of wind speeds. This scale was not designed specifically for conditions at sea and is often used to describe wind conditions on land as well. As such, the traditional Beaufort scale makes no reference to the Douglas

scale. However, for simplification, the Beaufort table shown in Table 3.3 has had the approximate wave heights and Douglas wind sea scale correlations added to it.

Table 3.3: Beaufort scale for wind speeds [121]

Degree	**Wind Speed (m/s)**	**Wave Height (m)**	**Sea State**	**Description**
0	0 - 0.3	0	0	Calm
1	0.3 - 1.5	0 - 0.1	1	Light Air
2	1.5 - 3.3	0.1 - 0.5	2	Light Breeze
3	3.3 - 5.4	0.5 - 1.0	3	Gentle breeze
4	5.4 - 7.9	1.0 - 1.5	3 - 4	Moderate Breeze
5	7.9 - 10.7	1.5 - 2.5	4	Fresh Breeze
6	10.7 - 13.8	2.5 - 4.0	5	Strong Breeze
7	13.8 - 17.1	4.0 - 5.5	5 - 6	Near Gale
8	17.1 - 20.7	5.5 - 7.5	6 - 7	Gale
9	20.7 - 24.4	7.0 - 10.	7	Strong Gale
10	24.4 - 28.4	9.0 - 12.5	8	Storm
11	28.4 - 32.6	11.5 - 16.0	8 - 9	Violent Storm
12	> 32.6	> 14.0	9	Hurricane

This combined table allow the wave heights and wind speeds to be estimated and quantified for any given sea state and vice versa. The table will be used in the experimental set-up to define and tune the test platforms to ensure a proper correlation to what is seen in real-world applications.

3.4.3 Response Amplitude Operators

Even though the sea state may be categorized and roughly defined using the Douglas and Beaufort scales, it does not necessarily mean (and in fact, is quite unlikely) that all ships will respond in the same way. A 1 m wave does not necessarily mean that a ship will move up and down 1 m as well. Two different ships may also move to completely different heights, pitch and roll at different angles or otherwise move differently with the same 1 m forcing waves. As such, in ship dynamics and naval engineering, Response Amplitude Operators (RAOs) are used to define the ship response to different excitations.

Response Amplitude Operators are essentially transfer functions in the form of engineering statics that relate the expected ship motion to set sea state conditions and aspects. The transfer functions are usually found through computational fluid dynamics and numerical modelling, however they can be found experimentally as well. This is done by measuring the motion of the ship at its centroid (with a motion capture system like an IMU) in all 6 degrees-of-freedom (surge, sway, heave, roll, pitch and yaw) over a period of time while traversing through a variety of sea states. These RAOs are specific to the ship they characterize and can be used to model expected ship motions in a sea state. RAOs are also usually specific for the aspect into the sea state itself (as shown in Figure 3.4).

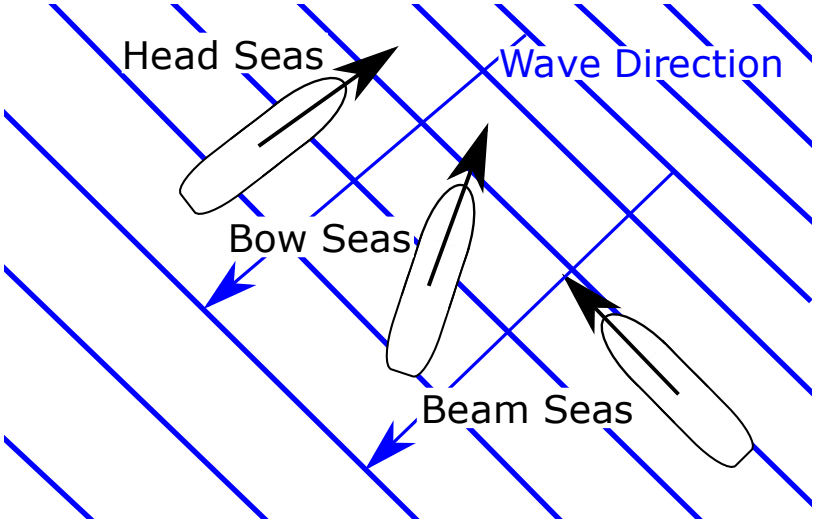

Figure 3.4: Visualization of head, bow and beam seas.

Assuming traditional ship designs, the longitudinal inertia is often much greater than the lateral one. This means that in head seas (wave motion is 180 degrees to the ship heading) the motion of the ship is often reduced relative to a ship in beam seas (wave motion is perpendicular to the ship heading) due to the width of the ship usually being much smaller than the length. For this reason, the worst ship conditions are often incurred when the ship is travelling at beam seas while the best are usually found at head seas. Bow seas are when the ship and wave crest angles are somewhere between parallel and perpendicular to the wave crests. Bow seas are in between head seas and beam seas thus couple more DOF in their resultant motions.

Chapter 4

Theoretical Development

As previously discussed, the autonomy involved in landing can be viewed as a high level abstract control problem consisting of highly coupled low level subsystems/ components. It has also been established that within the literature and existing research there is a precedent to categorize the low level elements into 4 categories: pose estimation, guidance, recovery and control.

This chapter will introduce the theoretical elements of the autonomous controller design. To be consistent with what currently exists, this technology will be presented and explained through two lenses: the high level landing autonomy and low level subsystems that realizes the autonomy as a whole. The subsystems in this thesis will once again be broken into the four common categories as to remain consistent with what currently exists, as well as the addition of a fifth, the mission-planner. The specific theoretical contributions made by this thesis will be highlighted and summarized later in the chapter.

4.1 High Level Autonomy

The high level autonomy is the general overall behaviour the UAV should demonstrate during the time the landing autonomy has the control authority. It is not concerned

with how the UAV achieves the landing, only with what the landing should look like. The details of how it achieves this will come in the next part of the chapter. For the purposes of this research it is assumed that prior to the UAV beginning the landing process, it was deployed, completed its mission, located the ship and returned to it. At the time the landing commences, it is assumed the UAV is hovering above the ship (5-20m) and located roughly above the selected landing site (in range of the ship-based sensors). Once the landing autonomy has the control authority, the UAV will enter a three-phase landing procedure:

- Phase 1: Hover (goal set $\sim 5 - 10$ m)
- Phase 2: Ready (goal set $\sim 1 - 2$ m)
- Phase 3: Land (goal set to 0 m)

The primary differences physically between the phases is the elevation that the UAV is hovering. It is always station-keeping over where it is attempting to land. While physically there is not much difference between the phases, the actual goals of each phase differ notably. This process is shown visually in Figure 4.1.

4.1.1 Landing Phase 1: Hover

Phase 1 is defined as the "Hover" phase. In this phase, the UAV has just returned to the ship. It has completed its mission, is hovering high above the ship and is now beginning the landing procedure as per the assumptions made previously. The overall goal of this phase is to characterize what kind of landing conditions it is expecting to encounter. It is trying to determine the max/min pitch and roll angles, pitch/roll bias, motion frequency etc. Anything that may contribute to a more difficult landing. The majority of this characterization can be done before the UAV has returned since the measurements that are being used in the characterization are ship-based. Therefore this phase may last anywhere from a few seconds to up to a few minutes depending on how the UAV plans to use the ship motion measurements it just captured. While

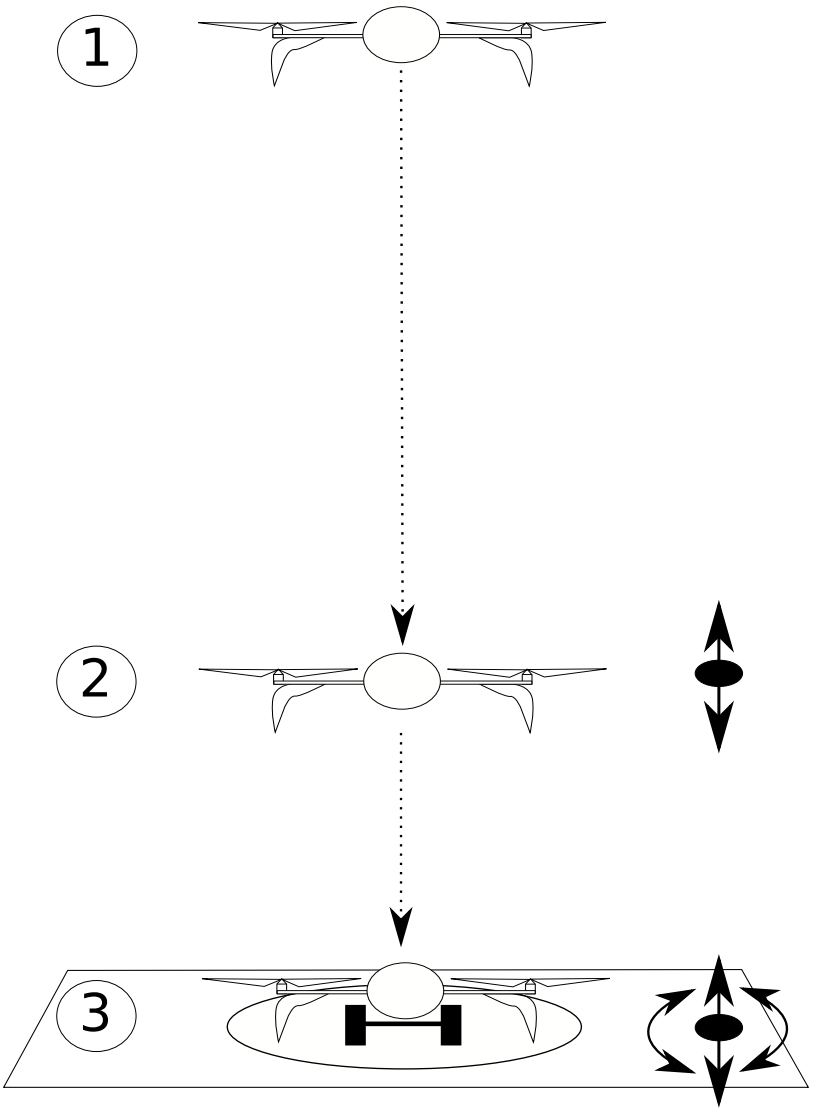

Figure 4.1: High level autonomous landing highlighting the individual landing phases: Phase 1 is Hover, Phase 2 is Ready (with motion matching) and Phase 3 is Land. Ship is moving in 4 DOF throughout.

in this phase, the UAV will naturally be performing some motion-matching (station-keeping) since the position estimates used to control the motion of the UAV will be relative to the ship motion. The UAV will also be performing some obstacle avoidance as needed while keeping itself centered over the landing site. The actual location of the UAV in this phase and how well it holds that position is of low importance so longs as it is not in danger of colliding with objects or parts of the ship. Once the UAV has characterized the current landing conditions it moves into the "Ready" phase.

4.1.2 Landing Phase 2: Ready

Phase 2 is defined as the "Ready" phase. In this phase, the UAV has finished the characterization of the ship motions and it is now ready to use this knowledge to land. The overall goal of this phase to get into a landing position and to make the decision as to when to attempt a landing. To do this, the UAV first drops to a low elevation where it can respond quickly once a landing window is identified ($\sim 1-2$ m). The position of the UAV has become more important as it is trying to remain above its landing site in case it has to come down quickly to avoid damaging itself in rough seas. The reaction time of the UAV needs to be considered here as well since it is low enough to collide with the ship if the heave amplitude and velocity are large (usually the UAV is more responsive than the ship). As such, the elevation defined in this phase can be set higher for less responsive vehicles. The UAV is continuing to match the translational motion of the ship while also using the characterization of the ship prepared in the "Hover" phase to look for potential landing windows. In some cases the ship state will be such that the UAV can simply land whenever it is ready, while in others the landing windows may be few and far between. In the most extreme cases the landing window may be too short for the UAV to safely land so the UAV will need to use the characterization to predict a future landing window. Anywhere from 1-5 seconds may be needed to give the UAV enough time to land before the landing window closes. It is also tracking the accuracy of the characterization itself, and should it find that errors are arising or the characterization is no longer valid due to changing sea states or changes in ship heading (the ship should hold a constant heading while landing, however the algorithm cannot be constrained by that

assumption), it can drop back to the previous phase. Once the UAV has identified a landing window and is prepared above the landing site, it enters the final "Land" phase.

4.1.3 Landing Phase 3: Land

Phase 3 is defined as the "Land" phase. In this phase, the UAV has identified a landing window (either a future landing window it thinks is coming or one it currently sees depending on the situation) and is in the best position above the landing site. The overall goal of the phase is to get the UAV to touchdown safely, as it has already made the decision to land and now just needs to execute it. It does so by descending towards the landing site, slowing as it approaches the surface of the ship and touches down. Once the UAV touches down, it is able to go through its shut down procedure and power down. There are a few safe guards built into this phase as it is during this phase that the UAV and ship are at the highest risk for damage. Should the UAV realize that it is drifting too far from the landing site, in danger of colliding with a known object or the landing window it predicted does not materialize, the UAV has the ability to drop into any previous phase at any time.

4.2 Low Level Design

The high level abstract autonomy is achieved through the collaboration of specific and highly coupled subsystems that are designed to produce the desired actions. These subsystems realize landing algorithm. Once again, the subsystems are broken into the previously defined categories of pose estimation, guidance, recovery and control. A mission planner is also included to handle the communication and decision making as the UAV demonstrates the high level behaviour. The subsystems are designed to be modular to facilitate using different techniques and algorithms.

4.2.1 Pose Estimation

For the UAV to be able to maneuver around and land in appropriate locations on the ship, it must have some idea of its own location with respect to the ship. This estimated relative pose is the primary feedback the UAV uses in the control and guidance elements of the landing autonomy.

Before the pose estimations can be used, the coordinate frame for the pose needs to be defined. In this application, the pose of the UAV is estimated relative to the ship, not the world frame. As such, the origin of the coordinate frame can be defined at any reference location on the ship, however in this work a point on the transom of the ship, like the landing site, is used as it is the most convenient location. It is also convenient to orient the reference frame so that it is aligned with the axis of the ship, meaning the x-axis is pointing forward along the longitudinal axis of the ship, the y-axis pointing to port (left) and the z-axis pointing up (this could also use the NED convention. It is chosen as such here to match with what is native to the flight controllers used in testing in future chapters). The reference frame is attached to the ship and moves with it. The coordinate frame is shown in Figure 4.2. In the figure, the x-axis is green, y-axis is red and z-axis is blue.

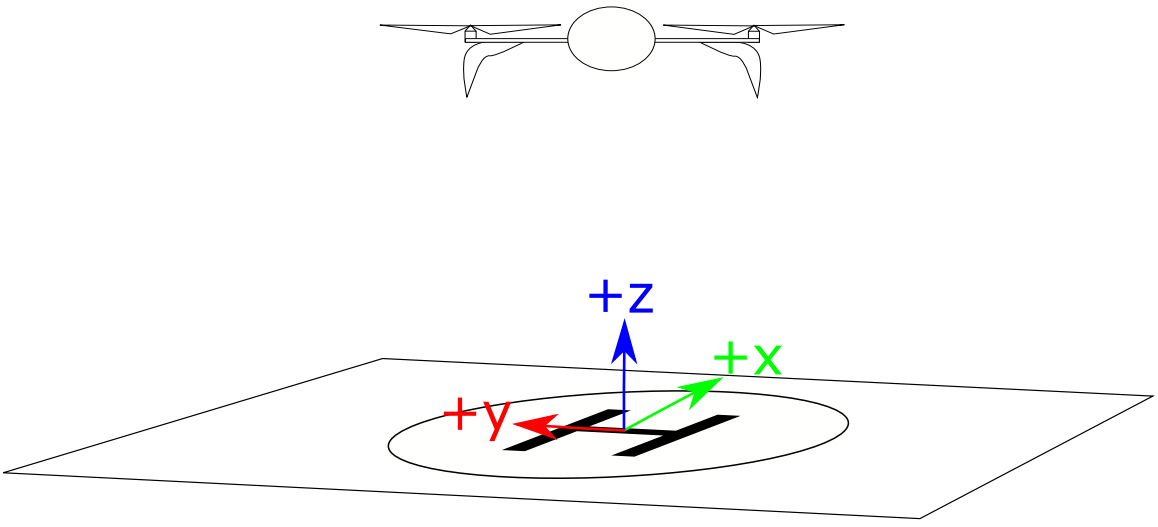

Figure 4.2: Reference frame while the ship is even keel.

While having the reference frame translate with the ship works well for control

purposes, it would be more convenient if the z axis of the relative coordinate frame was always pointing up (ie: parallel to the world z axis) as that is the axis gravity affects. Therefore, the coordinate frame is fixed in the pitch and roll directions and does not rotate as the ship rotates. The yaw of the reference frame can still yaw as the ships heading changes. This can be seen visually in Figure 4.3.

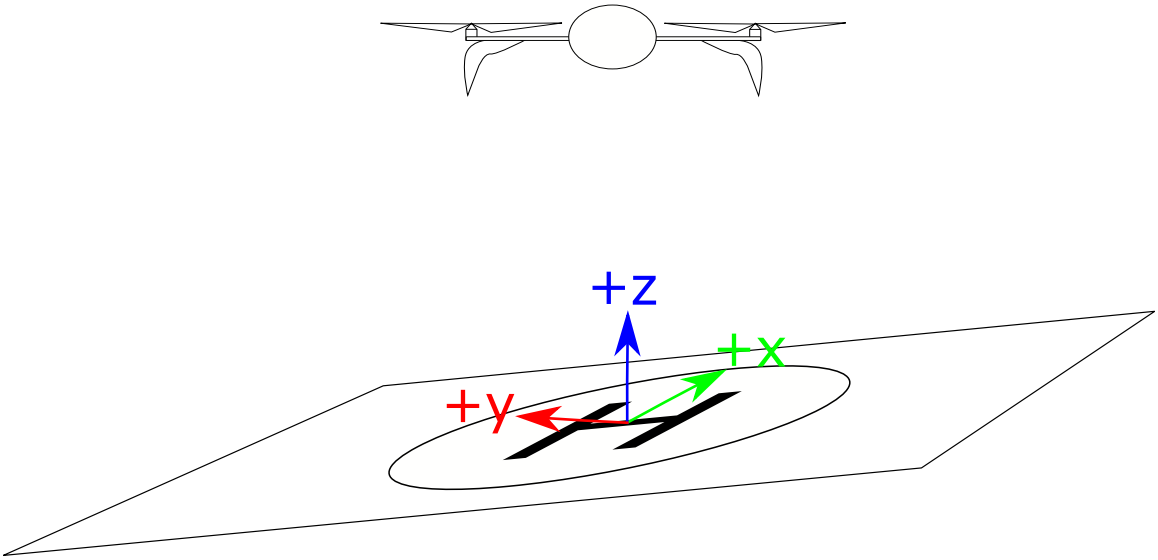

Figure 4.3: Reference frame while ship is rolling

The pose of an UAV is defined as both its position and orientation. These two elements can be broken up and usually are found somewhat independently from one another. There are however some techniques where the two elements of pose are more coupled. The following sections describe how the position and orientation of the UAV are estimated relative to the ship.

Position

Numerous position estimation techniques have been demonstrated and tested in relation to autonomous landing of UAVs; the literature review on the topic reveals that the vast majority of these algorithms use some form of computer vision. Vision-based position estimation, as discussed earlier, have a few drawbacks. First, they limit the environments and conditions that the UAV can be autonomously recovered in. In

all of the existing vision-based methods, it is assumed that the UAV has clear line-of-sight to the ship and can see it well enough to extract features in the images. In environments such as the Arctic, this requirement cannot always be met, be it due to fog, precipitation or the 6 months of darkness. Secondly, vision-based techniques usually require specific landing pads that the UAV needs to see at all times and must land on as it cannot estimate its position otherwise. This means that the UAV cannot adapt and adjust to land at other locations on the ship if needed. It can only land on the designated landing pad.

Instead of relying on vision, this work uses an array of peer-to-peer acoustic sensors fused with the UAV and ship kinematic models through an EKF to estimate the position of the UAV. This increases the environmental conditions the landing algorithm works in as acoustic sensors are not dependant on line-of-sight. There is a trade-off however as they also are not likely to be as accurate, especially in high winds. The sensors can be placed anywhere on the ship so long as the UAV landing site has sufficient acoustic coverage; the UAV can land anywhere within the volume covered by the acoustic sensors. For testing the proposed algorithm, four sensors were used and placed at the four corners of the landing platform as shown in Figure 4.4.

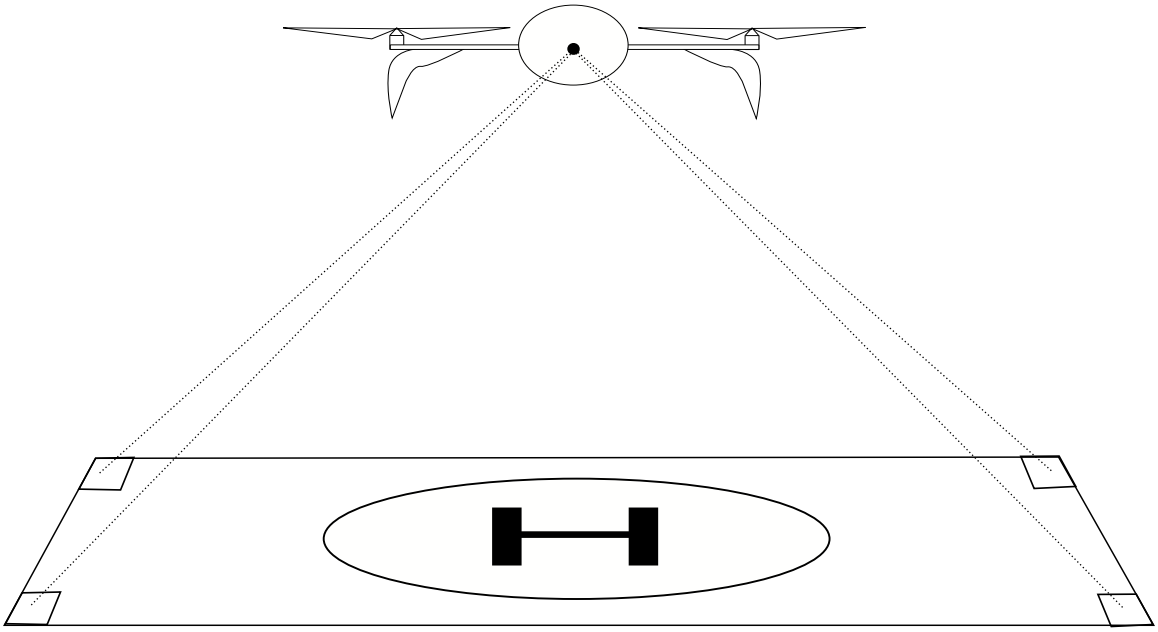

Figure 4.4: Layout for acoustic position estimator, with acoustic sensors at each corner

The UAV state used by the position estimator is defined by a vector of its linear positions and velocities with respect to the reference frame defined previously. The kinematic model of the UAV/ship will be used for the prediction step. This model is linear, and does not need to be approximated using a first-order Taylor series expansion:

$$x_k = Fx_{k-1} + B_k u_k. \tag{3.2}$$

A linear model is used to help simplify the problem, and also because the input to the system is the measured relative acceleration of the ship and UAV via an IMU sensor mounted on each. The sensors used currently have a lot of noise and since two noisy sensors are being differenced, there is even more uncertainty in their readings. Therefore, the EKF will be biased away from the model and this estimate will primarily be used to seed the non-linear measurement model. If a vehicle had a well defined motion model, it could be used instead of the constant velocity model. The process equation F and input matrix B are defined assuming a constant acceleration over the time step from $k-1$ to k. Note, in this equation each element of the matrix is a 3×3 diagonal matrix (i.e. F is a 6×6 matrix):

$$F = \begin{bmatrix} 1 & dt \\ 0 & 1 \end{bmatrix}, \tag{4.1}$$

$$B = \begin{bmatrix} \frac{dt^2}{2} \\ dt \end{bmatrix}. \tag{4.2}$$

At every time step, the EKF also predicts the covariance matrix P_{k-1}^k of the UAV pose as described earlier:

$$P_k = FP_{k-1}F^T + Q_k. \tag{3.3}$$

The motion model noise matrix Q_k is defined according to the noise present in the acceleration measurement (this is known and published with the IMU sensor information):

$$Q = BB^T\sigma_a^2 = \begin{bmatrix} \frac{dt^4}{4} & \frac{dt^3}{2} \\ \frac{dt^3}{2} & dt^2 \end{bmatrix} \sigma^2_{acceleration}. \tag{4.3}$$

The EKF updates the state estimate with the landing site acoustic measurements when they are available. The relation between the state and set of acoustic distances is non-linear.

$$y_k = h(x_k) = \sqrt{\sum (x_{x,y,z} - p_{x,y,z})^2}. \tag{4.4}$$

The measurement model can be linearised through a first order Taylor series expansion around the predicted state estimate:

$$H = \frac{\partial h}{\partial X_{x,y,z}} = \frac{X_{x,y,z} - p_{x,y,z}}{\sqrt{\sum (X_{x,y,z} - p_{x,y,z})^2}}. \tag{4.5}$$

Following the EKF algorithm described earlier, the Kalman gain is then found as follows:

$$K_k = P_k H_k^T (H_k P_k H_k^T + R)^{-1}. \tag{3.5}$$

Finally, the state and covariance are then updated:

$$x_k = x_k + K_k(y_k - h(x_k)), \tag{3.13}$$

$$P_k = P_k - K_k P_k H_k^T. \tag{3.7}$$

The measurement noise matrix R_k is defined as the acoustic sensor noise:

$$R = \begin{bmatrix} 1 & 0 & 0 & 0 \\ 0 & 1 & 0 & 0 \\ 0 & 0 & 1 & 0 \\ 0 & 0 & 0 & 1 \end{bmatrix} \sigma^2_{acoustic}. \tag{4.6}$$

The position estimate is relative to the position and orientation (attitude) of the ship transom. It needs to be transformed to be relative to real-world orientation as per the defined desired reference frame described previously. To do so, the filtered position can be pre-multiplied by the transpose of the rotation matrix describing the orientation of the ship relative to the world axis:

$$x_{world} = Rot^{ship}_{world} x_{ship}. \tag{4.7}$$

The EKF has a few advantages relative to trilateration often used with these types of peer-to-peer range measurements (like GPS):

- use redundant sensors allows for larger arrays to be used;
- does not require a ping from a specific sensor, just needs at least 3 of the 4;
- takes into account the known motion of the ship and UAV; and
- does not require multiple iterations for convergence.

Orientation

The UAV requires an estimate of its orientation to complete its pose. The orientation within the literature is often found using a few sensors. The pitch, roll and yaw were extracted by some researchers using vision, however this has the same pitfalls as before where it relies on line-of-sight and specific landing pads. Others simply use IMUs for pitch and roll, which for this project makes the most sense since these orientations are relative to the world frame and therefore the measurement can be used as they are. IMUs are sensors that work well in most environments on Earth as

they are based on gravitational fields and angular velocities. The UAV heading (yaw) on the other hand, defined relative to the ships heading, is not as trivial without vision. The method for heading proposed here depends on the vehicle used and the environment in which it is landing.

For most applications, a magnetic compass can be employed with great success. One on the ship and one on the UAV can be differenced to give the relative heading. However, magnetic compasses lose their effectiveness the farther north/south they are. This is usually attributed to a few factors. First, the magnetic meridians do not converge radially around the Magnetic North Pole. This means at high latitudes the compass will not always point to magnetic north or true north. For this application, this is not a problem since the measure of the UAV is relative to the ship, meaning any biases would be eliminated. As the ship moves further north, it no longer becomes a straight forward bias and the compass behaves more erratically. Within $20 - 30^{\circ}$ of magnetic north, the magnetic field points more down into the Earth and the horizontal component is often no longer strong enough to overcome the frictional forces within the compass bearings, rendering the compass inert. Metal ships in motion can also cause perturbations in compass measurements. While high quality INS sensors could track the heading changes, they also can be costly and can require long calibration times. In these cases, there are two other options that could be employed.

One is to use the angular velocity of the Earth by way of a gyrocompass. These systems are commonly used for naval applications where the hull and systems on the ship may cause interference for a magnetic compass. The downside to using a gyrocompass is that these sensors need to be precisely built and require high-accuracy gyroscopes. They also require accurate vehicle velocity estimates, as uncertainty in the vehicle velocity can contribute to uncertainties in the heading estimate. The gyrocompass is also known to lose some of their effectiveness as it moves closer to True North.

A more appropriate solution for the poles specifically is to find the heading based on a body-fixed vector. In this case, the position of 2 points on the UAV would need to be known. Using the vector between these 2 points, the heading can be extracted by knowing the geometry of the vehicle. For instance, if the two points are along the

y-axis of the UAV, its heading can the always be found as the line perpendicular to the vector connecting the sensors. This can easily be applied in this project by adding a second sensor to the UAV, assuming the vehicle is large enough to have adequate space between them (there would be space big enough on a work-class UAV). This also would increase the precision of the overall position estimate as the noise in the sensors will begin to cancel out. Assume sensor A is mounted at location $X_a = (x_a, y_a, z_a)$ in the UAV frame which measures its world location as $X_A = (x_A, y_A, z_A)$. Likewise, sensor B is mounted at $X_b = (x_b, y_b, z_b)$ in the UAV frame and measures its world location at $X_B = (x_B, y_B, z_B)$. The position can be expressed mathematically as follows:

$$X_{UAV} = \frac{X_A + X_B}{2} - X_{offset}. \tag{4.8}$$

X_{offset} is the offset from the center off mass of the UAV where the position estimate is required to the spot located directly between the two sensors. It would be most convenient if the two sensors were equally spaced out along either the x-axis or y-axis so that the offset is equal to 0s. For heading, it can also be expressed mathematically:

$$\theta_{UAV} = \tan\left(\frac{y_B - y_A}{x_B - x_A}\right) + \theta_{offet}. \tag{4.9}$$

Similar to before, θ_{offet} is the offset angle between the line made by connecting the two sensors and the x axis of the UAV.

4.2.2 Guidance

The guidance system has two primary functions that contribute towards achieving the high level algorithm design. First, it is responsible for determining where the UAV should go at each time step, and second it is responsible for generating the control inputs to have the UAV follow the prescribed trajectory while working in tandem with the control subsystem. In essence, it is responsible for compensating for internal forces and changes to the system, like the ship heave or observed obstacles, while also

directing the UAV to it's goal location.

Most applications use proportional or pursuit where the UAV simply maintains a constant angle or velocity vector towards the landing site. There is no compensation for obstacles nor is there the ability to move the UAV around in the space as needed. The goal position for the UAV will also be constantly changing, not only as the ship translates but also as it rotates in roll and pitch. This is because the UAV wants to station-keep+ over the landing site in the defined frame (not ship) coordinates. This is to ensure the UAV is always in the right position when the ship levels out. To execute the dynamically defined path while also avoiding obstacles, a potential fields approach is proposed. As previously mentioned, the potential fields approach defines a potential at every location within the space, then drives the robot to travel in the direction from high to low potential. The potential at a point is the sum of all attractive and repulsive potentials experienced at that location as previously defined:

$$U = U_a + U_r. \tag{3.14}$$

The attractive potential is a combination of a conical function and a quadratic function. The potential well is located at the three-dimensional goal position and moves as necessary.

$$\nabla U_a = \begin{cases} -\frac{(q-q_g)}{d_{q,q_g}} & \text{if } d_{q,q_g} > d^*, \\ -(q-q_g) & \text{if } d_{q,q_g} <= d^*. \end{cases} \tag{3.19}$$

Repulsive potentials are defined as obstacles. This could be any component on the ship that could damage the UAV, be damaged by the UAV or airspace the UAV should avoid. The one guaranteed obstacle to modelled in this way is the ship deck. This done to slow the UAV during landing and also to bias it away from the ship deck during heave motions as the deck is coming up towards the UAV. For the ship deck to be modelled this way, d_{q,q_o} is the one-dimensional distance above the deck (elevation), as it does not matter where above the deck the UAV is, it will always apply an upward repulsive force on the UAV:

$$\nabla U_r = \begin{cases} -\zeta_r \left(\frac{1}{d_{q,q_o}} - \frac{1}{d_o^*}\right) \frac{1}{d_o^{*2}} \frac{q-q_o}{d_o^*} & \text{if } d_{q,q_g} < d_o^*, \\ 0 & \text{if } d_{q,q_o} >= d_o^*. \end{cases} \tag{3.21}$$

The total potential gradient is then found as the sum of the forces:

$$F_{tot} = F_{att} + F_{rep} = -\nabla U_{att} - \nabla U_{rep}. \tag{3.22}$$

These forces are applied to the robot as generalized velocities. This helps to generalize the algorithm as the velocities are independent of the UAVs specific dynamics, which are easier to compensate for within the control loop instead.

4.2.3 Recovery

The recovery considers how/when the UAV makes contact with the ground/ship. The UAV needs to land without damaging itself, the ship, the environment or crew. With rotary wing UAVs, the complexities involved in recovery are not so much in the touch down like fixed-wing UAVs, but in the decision of when to land. The difficultly in selecting the best time to land is further exacerbated as the sea states worsen. Traditional techniques provide no compensation for the ship motions, or use very case specific ship models to predict future landing windows. This severely limits the conditions where the UAV can be safely recovered. Here, an active learning predictor is used to look-ahead into the future for potential landing windows the UAV can take advantage of. The UAV can then have a head start or be prepared to land when the window arrives.

Even though the transom of the ship can move in all 6 degrees-of-freedom (DOF), not all contribute equally to the dangers of landing. The motions that need to be most compensated for within the context of a safe recovery are roll, pitch and heave (relative heave velocity); surge, sway and yaw are rarely large enough even at sea state 5 (for the case study ship used) to make a difference. The potential fields guidance algorithm is designed to mitigate the heave velocity by modelling the ship

deck as an obstacle and allowing the potential forces to slow the UAV velocity relative the the ship's. Pitch and roll however need their own form of recovery mitigation. It is reccomended in full-scale manned helicopter piloting manuals that landings on surfaces that are tilted more than 10° [122] should not be attempted as the tilt is too much for the vehicle to safely land. Using this criteria with the inclusion of a safety factor, recoveries within the autonomous control will only happen at times when the ship rotation in the pitch and roll directions are less than 5°. In order to achieve this, recovery is proposed based on 3 situations:

1. low amplitude motion ($< 5°$): the UAV does not need to compensate for pitch and roll and can land when otherwise convenient;

2. high amplitude ($> 5°$) low frequency motion: the UAV can monitor the ship for landing windows and begin landing once it detects a new window;

3. high amplitude ($> 5°$) high frequency motion: the UAV will look ahead in time for potential landing windows and time it's landing to coincide with this window.

The first two cases do not require additional sensors or capabilities beyond what is already used. The UAV can simply monitor the ship and land whenever the pitch and roll do not go over 5° or it can search actively for a window using the IMU present from the position estimator and land when it predicts one, assuming the ship frequency is slow and the UAV can land at a higher speed. In the third case, where the UAV needs to look-ahead to estimate future roll and pitch values, the predictor will be used. From what is known about the pitch and roll, it can be expected that they will be somewhat periodic, although with some randomness inherent to it. The roll and pitch time history and predictions will be unique to the conditions and ship the UAV is trying to land in. Lastly, the predictions do not need to be exact roll pitch values, nor do they need to be highly accurate at the extremes, they just need to be close around the zeros where the optimal landing conditions can be found to determine landing windows. For all these reason, best predictor architecture found and tested was a MLP neural network. Since seas are dynamic environments, a situation dependant batch-trained classic neural network would not be practical, as it would be specific

to the environment in which the training was performed, meaning the solution would very quickly become obsolete. Instead, an on-line EKF learning algorithm is used, allowing the predictor to continually adapt to the evolving conditions while sacrificing some of the neural network accuracy.

The network design and training algorithm are shown in the following equations. In this case, the state used in the EKF are the network weights (W^1 is the array of weights contained in the first layer and W^2 is the array of weights contained in the second) and biases (b^1 is the array of biases contained in the first layer and b^2 is the array of biases contained in the second) all arranged in a column vector:

$$x_k = \begin{bmatrix} W^1 \\ b^1 \\ W^2 \\ b^2 \end{bmatrix}. \tag{4.10}$$

The prediction stage then occurs. Since the weights are not changing within the time step The state vector also stays the same. However the covariance matrix P is still augmented with the model noise Q. While normally Q in the EKF algorithm represents model noise, in the network training law it is a diagonal matrix indicating the confidence in the current weight values and how much weight past training data is given in the next update:

$$x_k = F_k x_{k-1}, \tag{3.2}$$

$$P_k = F_k P_{k-1} F_k^T + Q. \tag{3.3}$$

The matrix Q and P are (n_w, n_w) where n_w is the number of states (i.e. number of weights and biases in the neural network). The training law then uses the currently available training data to update the weights. The measurement equation is given by the neural network definition. It is non-linear so it has to be linearised by taking the partial derivative of the defining equation for each output with respect to each weight

and bias within the network itself. The process function F_k is an identity matrix. Next the Kalman gain is calculated:

$$K_k = P_k H_k^T (H_k P_k H_k^T + R)^{-1}. \tag{3.5}$$

The matrix H is $(n_w,\ n_y * n_s)$, where n_y is the number of network outputs and n_s is the number of samples being trained at a time. Each element in the matrix is given by the partial derivative of the measurement model (i.e. the equation for the neural network) for each individual output with respect to each weight and bias. For example, it a single training point (i.e. 1 training pitch and roll value), the matrix H_k would take the following form:

$$H_k = \frac{\partial h}{\partial X}\Big|_{X_k} = \begin{bmatrix} \frac{\partial h_1}{\partial W_1^1} & \frac{\partial h_1}{\partial W_2^1} & \cdots & \frac{\partial h_1}{\partial b_1^1} & \cdots & \frac{\partial h_1}{\partial W_1^2} & \cdots & \frac{\partial h_1}{\partial b_1^2} & \frac{\partial h_1}{\partial b_2^2} \\ \frac{\partial h_2}{\partial W_1^1} & \frac{\partial h_2}{\partial W_2^1} & \cdots & \frac{\partial h_2}{\partial b_1^1} & \cdots & \frac{\partial h_2}{\partial W_1^2} & \cdots & \frac{\partial h_2}{\partial b_1^2} & \frac{\partial h_2}{\partial b_2^2} \end{bmatrix}. \tag{4.11}$$

The partial derivative of h with respect to each weight and bias can be simplified depending on which layer the weight and bias is located. This gives 4 potential solutions, as shown in the following expression:

$$\frac{\partial h}{\partial X_i}\Big|_{X_k} = \begin{cases} W_i^2 x_i (1 - tanh^2(\sum_{j=1}^{nx} W_{j,i}^1 x + b_i^1)) & \text{if } X_i = W^1, \\ W_i (1 - tanh^2(\sum_{j=1}^{nx} W_{j,i}^1 x + b_i^1)) & \text{if } X_i = b^1, \\ tanh^2(\sum_{j=1}^{nx} W_{j,i}^1 x + b_i^1) & \text{if } X_i = W^2, \\ 1 & \text{if } X_i = b^2. \end{cases} \tag{4.12}$$

Finally the network weights are updated as:

$$x_k^k = x_{k-1}^k + K_k(y_k - h(x_k)), \tag{3.13}$$

$$P_k^k = P_{k-1}^k - K_k P_k H_k^T. \tag{3.7}$$

The matrix R is ($n_y * n_s$, $n_y * n_s$) and represents the weight applied to the new training data.

Since the algorithm is on-line and begins with random weights, it needs some time before it can be used. Training can be performed while the UAV is on mission or while the UAV is in landing phase 1. Once the network has been trained, the UAV can move to phase 2. During operation, the current ship state will need to be buffered. Once the look-ahead time has been reached, the saved states can be used to train the network.

4.2.4 Control

The control system is the part of the algorithm that actively compensates for external and unmodelled forces acting on the system. Many controllers have been tested for UAV landing, mostly focussed on fixed-wing applications. For rotary wing UAVs, most researchers use PID controllers since they work very effectively due to the simpler control required of rotary wing UAVs compared to fixed-wings. As previously mentioned, PID control works by adding an additional corrective term to the current input. This corrective term is proportional to the error measured within the system in the previous time step. This means that PID control is a form of feedback control; there must be a difference between the setpoint and feedback state before any corrections will be applied.

The path as defined by the guidance portion of the algorithm uses generalized velocity commands to move the UAV within the space. This is convenient since many flight control units have pre-built velocity controllers. This is true for the PX4 flight stack [123] used for the research here, as it uses a velocity controller for

its low-level controller. This simplifies the application of the vehicle landing autonomy and also makes applications to other vehicles more trivial as velocity controllers are well-defined systems made for easy integration. The PX4 controller used is a proportional-integral-differential (PID) controller that also includes anti-reset windup. The error for the velocity controller is defined as the difference between the feedback and setpoint velocities:

$$e(t) = v_{SP} - v_{MS}. \tag{4.13}$$

Here v_{SP} is the set point velocity and v_{MS} is the measured, or feedback, velocity. The feedback control loop then generates a control input that is sent to the UAV:

$$u(t) = K_p e(t) + K_i \int_0^t e(t) + K_d \dot{e}(t). \tag{4.14}$$

The variables K_p, K_i and K_d represent the proportional, integral and differential gains respectively. They can be tuned to achieve the desired system response.

The PID controller is hosted on-board the flight stack. In order to fly with these controllers and an external velocity setpoint, the PX4 must receive an internal position estimate from the acoustic position estimator. The velocity measurement is also a noisy measurement meaning the PX4 stack, even with motion capture systems, have some drift and non-ideal motions. The control block diagram for PID velocity control is shown in Figure **??**.

4.2.5 Mission Planner

While not included with the subsystems as found in the literature, there is a 5th subsystem used in this work. The final subsystem in this algorithm is the mission planner. The mission planner is the main hub where the low level components are integrated to fulfill the high level autonomy. The mission planner is responsible for collecting the acoustic pose estimate, constructing the sea state characterization,

determining when to move to the next landing phases and setting the goal position for the guidance. It is the middleware that acts as the go-between for each individual subsystem and the vehicle itself. It represents the high level design that all of the low level subsystems are contributing to achieve.

4.3 Contributions

This thesis contains new theoretical contributions to the field of ship based autonomous UAV landing. The contributions are highlighted below:

- a three-phase based approach for landing with modular subsystem components;
- development of an acoustic-based position estimator for use with a moving landing zone that is not reliant on vision or specific landing pads;
- development of a potential field map for ship-based landing including elements for obstacle avoidance and biasing to prevent collisions with the ship deck;
- an adaptive predictor to predict landing windows while also learning on-line and adapting to changing sea conditions.

Chapter 5

Experimental Environment

The autonomy as discussed in the previous chapter was tested and demonstrated experimentally, both in simulation and with hardware. This chapter introduces the experimental environments and equipment used to validate and assess the solution. The autonomy was demonstrated in incrementally more complex environments, beginning with a simulation environment and moving up into a dynamic lab setting. Each step has changes in complexity and in information payout. Simulations are performed in controlled environments without communication loss, inherent noise, or unmodelled vehicle dynamics. The next step, static lab testing, continues to control the environment and eliminate the wind and limits the control authority requirement, however it considers the actual vehicle and ship dynamics and real-world interaction. Dynamic lab testing adds another layer by requiring more motion of the UAV, taxing the tracking algorithm and demonstrating more components of the autonomy. External forces can also be modelled in a controlled manner. Future tests would include insitu testing and full-scale testing, each adding in further random and difficult to model environmental considerations like wind, eddies, turbulence, full ship speed, deck obstacles, etc.

This chapter details only the testing environment used in this porject: the individual experiments and the results from all the flight tests will be presented in the following chapter.

5.1 Middleware

The Robotic Operating System (ROS) was used to handle the flow of information in this project, both in simulation and hardware. ROS is the middleware used in many robotic applications; the main function of ROS is to help different modules of code (called nodes) communicate with each other (through channels called messages). The ROSCORE is the master that advertises and connects nodes based on the desired message requests. The ROSCORE is located on the flight computer, that also runs the other nodes and code snippets that make up the landing autonomy. This flight computer for these tests is a base station computer acting as if it was ship-mounted; however, in practice, it could be placed on the UAV so long as the ship-based IMU can be wirelessly communicated to the UAV itself. Having the landing algorithm located on the ship also means that the predictor can be trained while the UAV is completing its mission. The base computer communicates with the real UAV through mavROS [124] over a WIFI connection, to the ship IMU over USB and to the acoustic sensors over radio frequency. The Stewart platform is also connected to the base computer over USB; however, it is controlled in MATLAB and independent of the landing autonomy. In simulation, the ship IMU, acoustic sensors and UAV all communicated through ROS and are hosted on the same PC. Other smaller nodes were also built to handle smaller convenient tasks like the joystick switches, manual overrides for safety, etc. The overall code flow can be seen in Figure 5.1.

5.2 Simulations

The autonomy developed was first tested in simulation. The simulation test objectives were to:

1. validate the individual landing components prior to hardware implementation;

2. demonstrate and evaluate the landing procedure as a whole; and

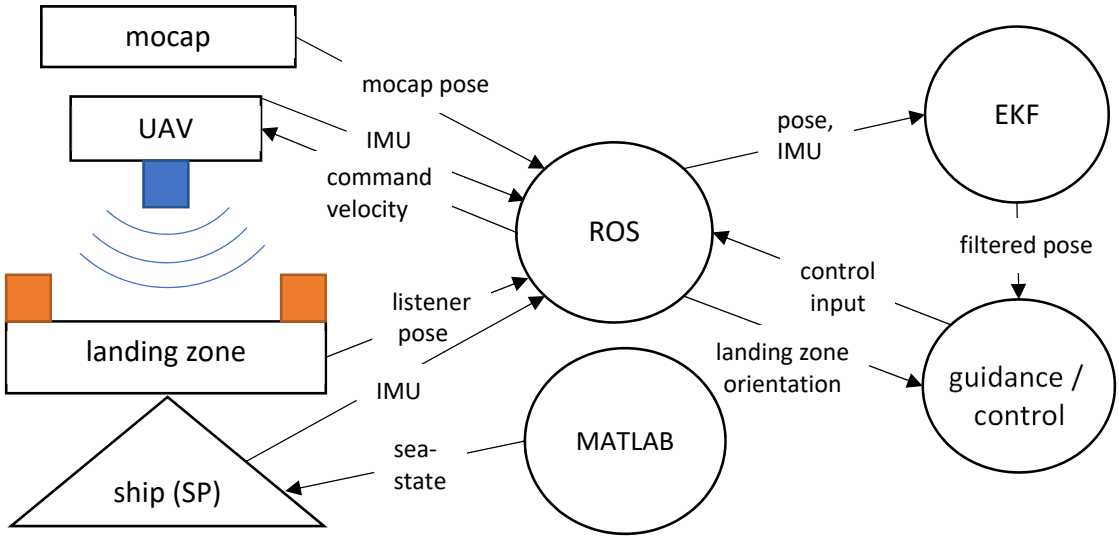

Figure 5.1: Code flow for the landing autonomy

3. analyze the effects of environmental conditions that cannot be achieved with the hardware tests.

These objectives were met using multiple simulation environments built using multiple modelling tools and physics engines. This was done to best suit each component, or each test to demonstrate the subsystems both individually and as a whole. The primary modelling tools and physics engines used were MATLAB and Gazebo.

5.2.1 MATLAB Modelling

The first simulations were preformed in MATLAB. The purpose of this environment was to evaluate the feasibility of initial ideas and individual "proof-of-concept" for each element in the overall project. The UAV and ship were modelled as point robots to simplify the control components and to simplify some of the mechanical factors like inertia, mass, etc.

MATLAB was also used for much of the tuning since it is an easy and quick environment for multiple tests in succession. This was the case for the position estimator and guidance algorithms. However, in these cases collected hardware data was used to ensure the validity of the tuning once moved back into real-world applications.

MATLAB was also used heavily with the demonstration of the ship state predictor. Again, real-world ship data was used for all sensor measurements. Finally, MATLAB was used to analyse the results of the high level and low level algorithm components.

5.2.2 Gazebo Modelling

Once the elements were validated in MATLAB, the algorithm was simulated using Gazebo and its Open Dynamic Engine (ODE) physics engine. This environment allowed the world parameters that were removed in the MATLAB simulations to be added back into the system. The world itself was modelled using the open source UUV unmanned underwater vehicle) simulator package. The UUV simulator package, while designed for underwater vehicles, can simulate surface water interactions as well. The UAV was simulated using the open source Hector Quadrotor ROS package [125]. The Hector Quadrotor accepts the same *geomety_msgs/Twist* ROS messages as the UAV used in hardware tests for its command velocity setpoints. These setpoints are in turn used in the PID velocity controller for loop closure. The simulated UAV was the barebones model with no sensors, and no changes were made to the UAV (i.e. the PID controllers were used as is). The ship was simulated using the Aurora ship model available within the UUV simulator package [126]. These allowed for larger scale tests and focused on the overall procedure. A second ship simulant was also developed for this environment. It consisted of a flat plate that could be easily moved and twisted. This was done because the UUV simulator package cannot model surface waves, so the plate could instead maneuver and rotate to simulate the ship deck motions in sea states easier than manipulating the whole ship. This plate is loaded and used in the Gazebo model the same way as the Aurora; by directly spawning the in the position defined by its forward motion and orientation as desired.

The second Gazebo environment was also built to emulate the hardware environment to allow one final calibration and verification of the subsystems prior to use in hardware. This also can be used to validate the simulation environment itself if the hardware results match the simulation results. This simulation environment kept the Hector Quadrotor ROS package as the main UAV simulator, however switched to a

Stewart platform package [127] to simulate the ship. It was modelled in a simple empty world available through the Gazebo package. Once a subsystem was working in simulation it was then tested in hardware. These two environments are shown in Figure 5.2.

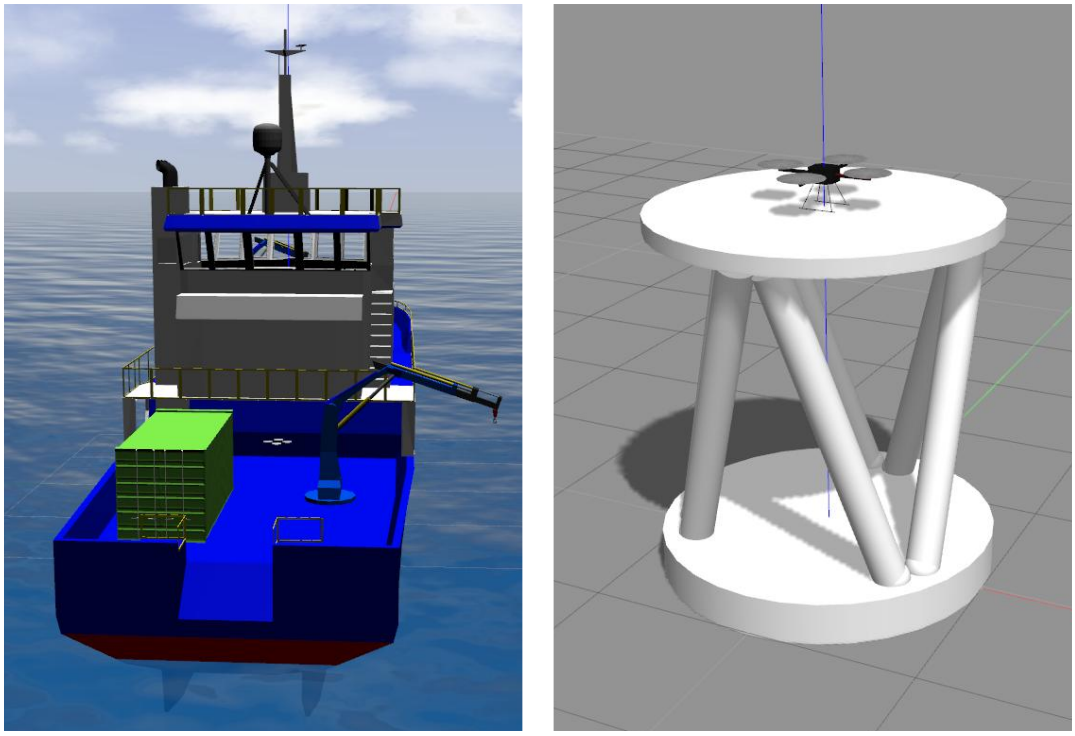

(a) Open water world environment (b) Hardware environment simulate

Figure 5.2: Gazebo simulation environments used for validation and testing of the UAV landing autonomy

The acoustic sensors and IMUs need to be simulated in the Gazebo environment as well. Gazebo automatically publishes the pose of every object within its environment through a *tf* (transform) broadcaster published over ROS by Gazebo. This feature is built into Gazebo and can be freely accessed. The sensor measurements were extracted directly from this message. Where needed, the measurements were converted to raw sensor measurements (i.e. breaking position into linear range measurements) or used as is with or without the addition of expected sensor noise, depending on the test being performed.

5.3 Hardware Testing

One of the primary goals of this thesis was to demonstrate as much of the landing autonomy in hardware as possible, while replicating real-world environments and conditions. To do this, a sophisticated and novel testing environment was developed for use within the flight spaces available at Dalhousie University.

5.3.1 Equipment

Unmanned Aerial Vehicle

One of the difficulties to generate generic UAV autonomy is the large differences between UAVs currently used in marine-based missions. The goal for the UAV selection is to design and tune the UAV to both perform and have capabilities similar to, or worse, than current industry standard vehicles. The theory being if this vehicle can perform as required, then a more able vehicle will definitely meet the requirement. There are many UAVs that can be used in almost any application that can be conceived, however there are two UAVs that are well documented for use in marine environments by the Canadian and American military and also deployed from ships. They are the Aeryon Skyranger R70 [128] and the Fire Scout MQ-8B [10] (this vehicle was discussed in the literature review as having a demonstrated autonomous landing capability).

The Aeryon Skyranger R70 and the Fire Scout MQ-8B are representative of the range of UAVs used, including size, type, use, performance etc. Their basic properties are listed in Table 5.1. These properties were used to define the requirements and design parameters for the vehicle used in testing, with the goal for the project to develop a landing autonomy that can be used in as many vehicles as possible. Therefore, the primary design vehicles are for quadrotors (similar to the Aeryon R70 in form factor) as opposed to the single-rotor Fire Scout. The technology will be transferable so long as the differences in control and maneuverability are accounted for.

Table 5.1: Properties of UAVs used in sea-based military applications [10, 128]

Parameter	**Aeryon R70**	**Fire Scout**
vehicle type	quadrotor	single-rotor
max ground speed	14 m/s	44 m/s
max accent/decent	3-4 m/s	4-8 m/s
mass	4.5 kg	1430 kg
dimensions	1.02 x 1.02 m	7.3 x 1.9 m

The UAV used in the project was an in-house built drone called the Prism M1 (seen in Figure 5.3). The UAV itself operates using the Pixracer flight control unit (FCU) which was running version 1.8.2 of the PX4 software.

Figure 5.3: The Prism M1 UAV build by the Intelligent Systems Lab used in testing.

The UAV was designed to fly and respond more conservatively in comparison to the Aeryon R70 and Fire Scout. (Again, having parameters and dynamics more similar to the Aeryon R70 than the Fire Scout). This was done by under-sizing the propellers. The UAV essentially was designed to react like a larger drone even though its form factor is much smaller. In terms of commands, the Pixracer allows for custom velocity or position commands to be sent to the internal controllers so long as the board itself is also receiving a position estimate from a source. The key design parameters for the Prism M1 are shown in Table 5.2.

Table 5.2: Properties of the Prism M1 UAV

Parameter	**Value**
vehicle type	quadrotor
max ground speed	5 m/s
max accent/decent	1 m/s
mass	0.691 kg
dimensions	20 cm x 25 cm
FCU	Pixracer
flight software	PX4 1.8.2
propellers	Gemfan Flash 4052
motors	Emax RS2205 2300kV
max thrust	3.12 kg

Ship

A Stewart platform was used to emulate the motion of the ship's transom during landing. Specifically, the platform was designed to simulate full scale pitch, heave, roll and surge of the HMCS Nipigon, shown in Figure 5.4. The HMCS Nipigon is an Annapolis-class destroyer that was decommissioned in 1998, however it is similar to the current Halifax-class Canadian Patrol Frigates which are currently equipped to deploy helicopters and UAVs. Performance data for HMCS Nipigon in a sea state is available to assist with the algorithm testing.

Pitch and roll data exists for this ship at 3 different sea states: 3, 4 and 5, at 3 different velocities: 10 knots, 15 knots and 20 knots, and 3 different wave aspects: head (ship travels 180° to wave direction), bow (ship travels 45° to wave direction) and beam seas (ship travels perpendicular to wave direction). A 60 second clip of this data for 10 knots for all three headings is plotted in Figure 5.5. While most ships will be in head seas for manned aircraft or UAV landing, that cannot be guaranteed. RAOs are also specific to an individual ship so the response across ships will be different for given sea states, velocities and wave aspects. With the Nipigon, the ship dynamics are such that the pitch and roll never become greater than 5° with head waves even in sea-state 5. However, with bow and beam waves roll can exceed 10°.

The Stewart platform uses a 60 second set of time histories, derived from validated

Figure 5.4: The HMCS Nipigon, photo courtesy National Archives under NAID 6409100

RAOs as inputs. This was due to data constraints on the micro-controller on the platform itself. Once the 60 seconds has passed, the motion is repeated. The Stewart platform itself was designed to replicate the ship response of HMCS Nipigon up to, and including, sea state 3, however it can model the response roll and pitch of Nipigon up to and including sea state 5.

Table 5.3: Limits of the Stewart platform designed to simulate ship motion

Direction	**Min (mm or deg)**	**Max (mm or deg)**	**Max Freq. (Hz)**
heave	0	550	0.5
surge	0	550	0.5
roll	-45	45	0.5
pitch	-45	45	0.5

The Stewart platform is equipped with a landing platform (61 cm $\times$ 61cm), the acoustic sensor beacons and an IMU. This platform is shown in Figure 5.6.

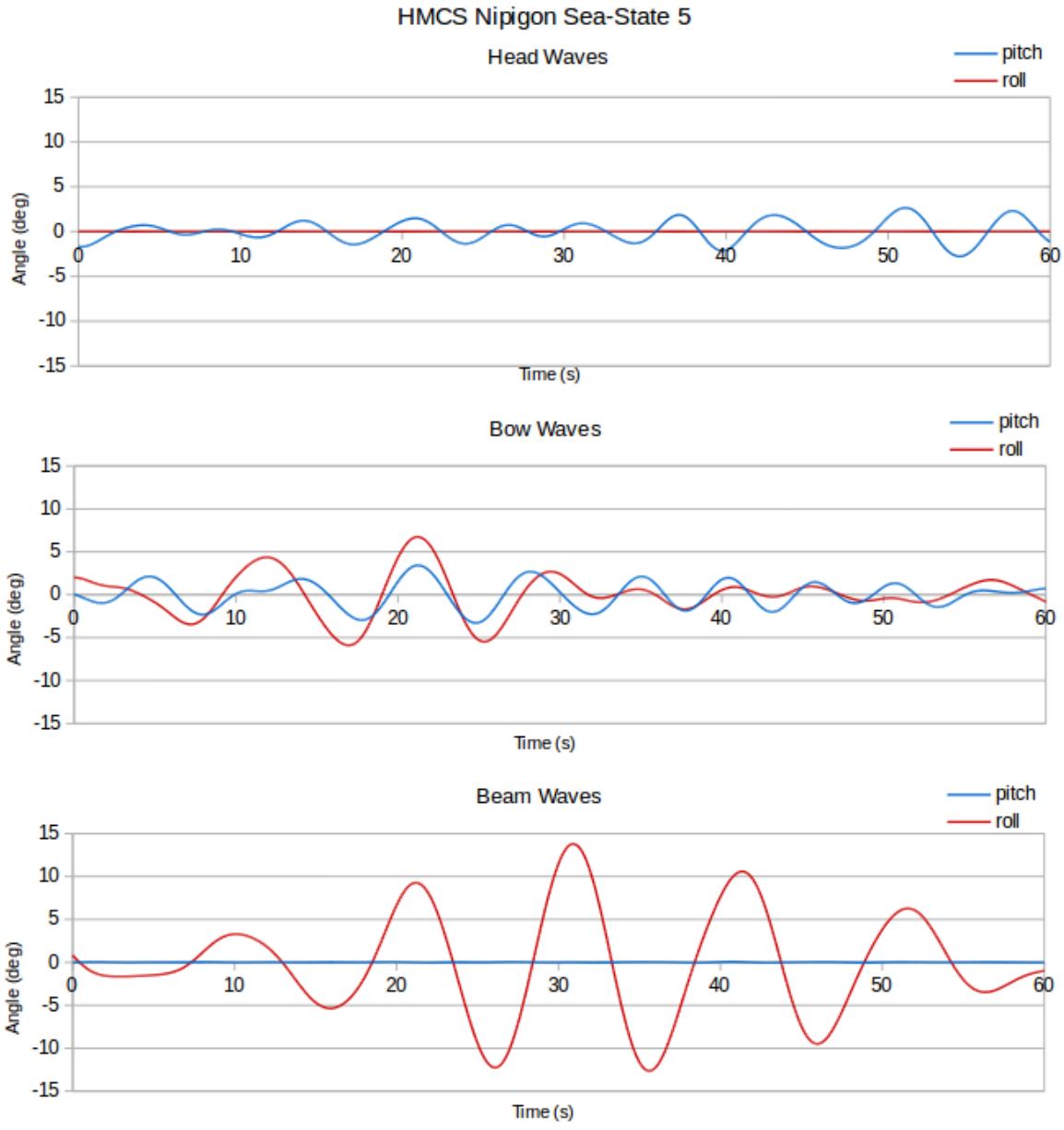

Figure 5.5: Pitch and Roll for the Nipigon travelling 10 knots in sea-state 5 with head, bow and beam waves

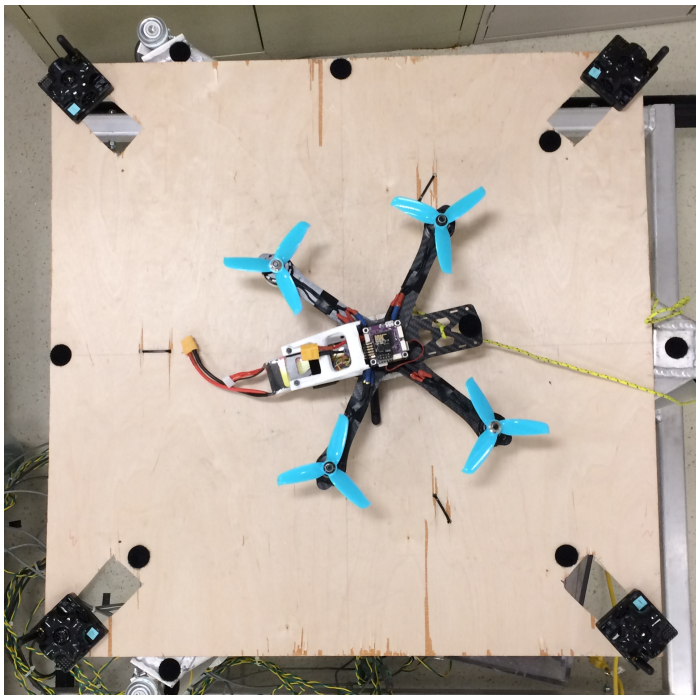

Figure 5.6: The landing platform with the 4 acoustics sensors on the corners. An IMU is mounted on the underside.

Validation

A ground truth for the UAV and Stewart platform is used within the flight spaces to validate the results. The Intelligent Systems Lab is equipped with a movable motion capture system (mocap) and this system was used to provide ground truth. The ISL mocap is an eight-camera system that can encompass a space as large as 10×15 meters with tracking errors on the scale of only a few millimeters (or less) depending on the size of the markers, camera set-up, covered region, etc. The actual tracking is done using Velcro-adhered reflective dots. These dots are placed strategically, and the software is taught the layout for the object. The mocap can track the object and determine its pose if four of the dots are visible in at least two of the eight cameras. The mocap was used to monitor and quantify the error in the subsystems of the landing algorithm as well as the overall landing efficiency.

As previously mentioned, the PX4 software requires a constant position estimate to use off-board control mode. Off-board control mode allows the UAV to use custom trajectories and waypoints, and is the mode used in all experiments. The acoustic

position estimator is not always available at the beginning of flights due to the initial set-up of each flight test. Therefore, to begin flight tests, the UAV gets its position directly from the motion capture system. Once it is manually flown in range of the acoustic sensors (i.e. above the landing zone on the platform itself), it switches to the acoustic position estimator and the landing algorithm is given the control authority.

5.3.2 Flight Space

The autonomous landing algorithm was tested with hardware in two controlled flight spaces. These flight spaces were located on campus at Dalhousie University: one in the Intelligent Systems Lab (ISL) dedicated flight space located in the Oceans Technology Hub at Sexton Campus and the other was a larger temporary location set-up in the Dalhousie University Sexton Gymnasium. The set-up and equipment used for each location were identical; the primary differences being the area captured and the tests performed in the space.

ISL Dedicated Flight Space

The first flight space was ISL's dedicated flight space. The capture space available for flight is a box approximately $3 \times 4 \times 3$ meters. This flight space has highly controllable parameters, with no fluctuations in light or ambient noise to affect the motion capture system or other sensors in the process. The space however is primarily suitable for mostly stationary or low speed tests due to the small capture volume available. The majority of the tests were performed in this environment, which can be seen in Figure 5.7.

Dalhousie University Gymnasium

The second flight space was a temporary space set-up in the Sexton Gymnasium. This space had a capture volume of approximately $10 \times 15 \times 4$ meters. There are more fluctuating parameters in this space, primarily due to the light penetrating through

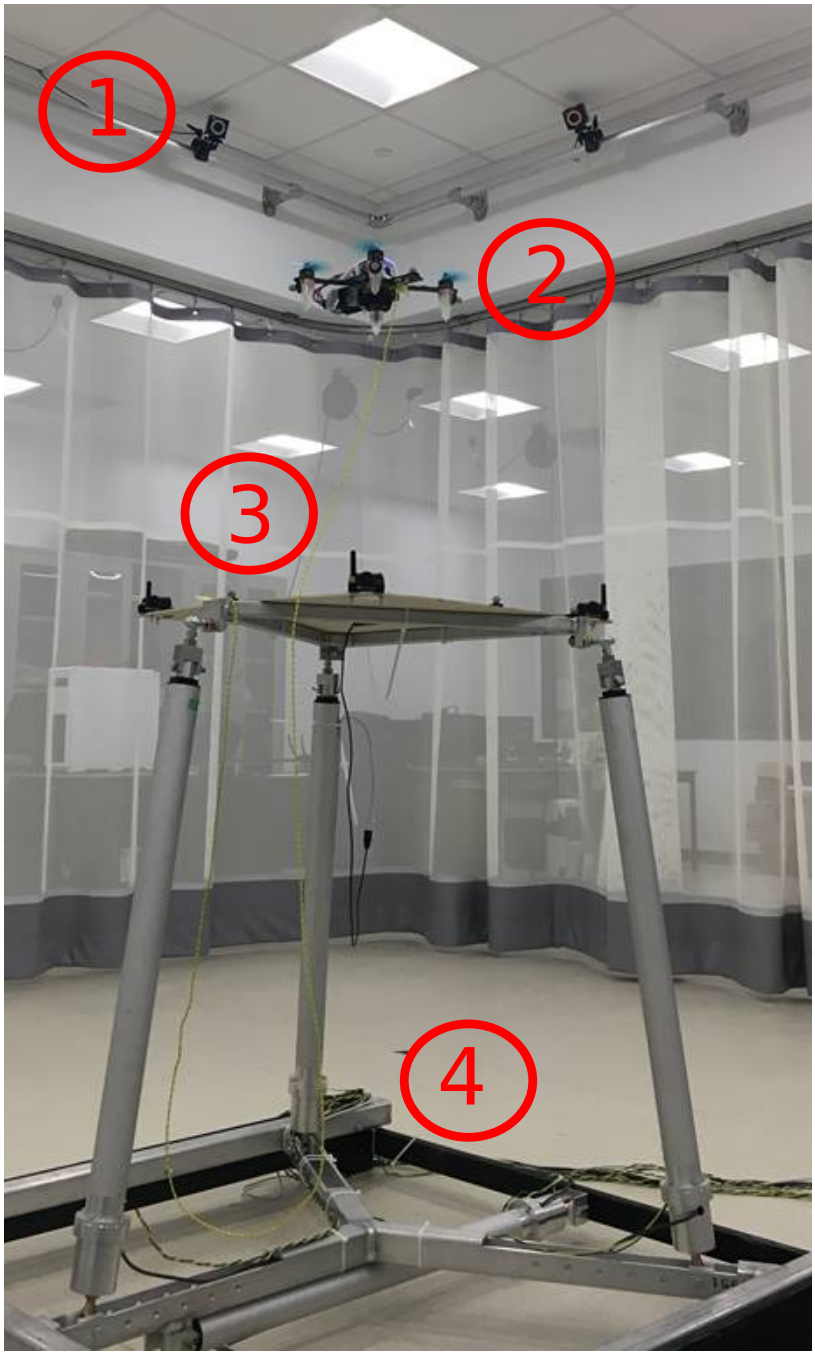

Figure 5.7: Hardware experimental environment within the ISL flight space: 1) Motion capture cameras (2 of 8). 2) Drone. 3) Acoustic sensors. 4) Stewart Platform

large windows that cause fluctuations in the accuracy and stability of the motion capture system. This meant that starting a test was more difficult as the UAV could have position dropouts until it entered the range of the acoustic position estimator. It also meant that more filtering was needed to process the results. However, this allowed for higher altitude flights and for tests to be done while the ship is moving at a constant velocity. The Sexton Gym testing environment is shown in Figure 5.8.

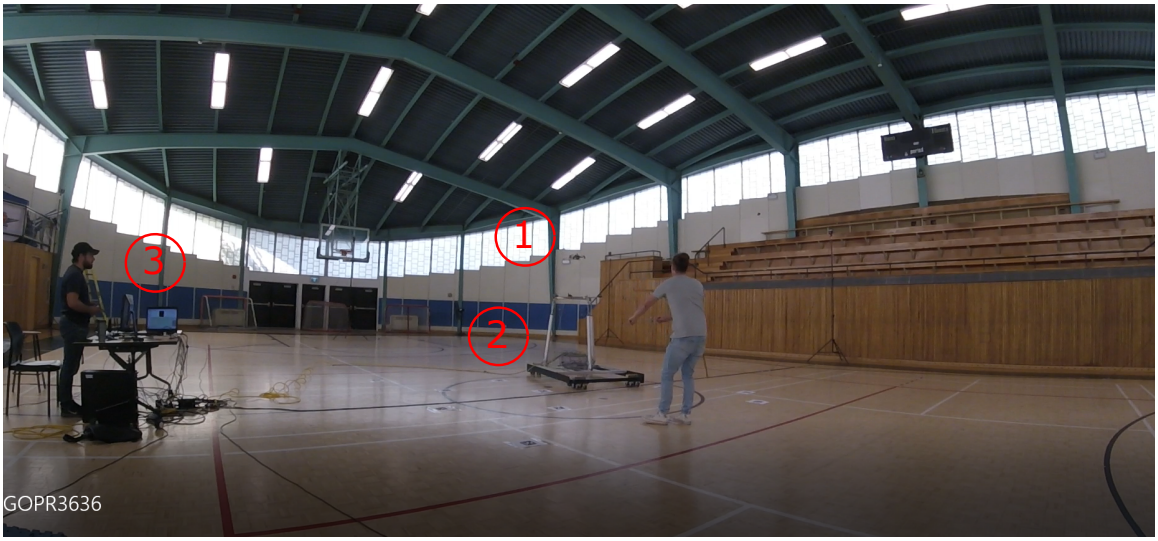

Figure 5.8: Hardware experimental environment within the Sexton gym flight space: 1) UAV. 2) Stewart Platform. 3) Base Station

5.4 Contributions

This thesis contains new experimental contributions to the field of ship-based autonomous UAV landing, namely the development of an experimental platform including a ship motion emulator that can use full-scale RAOs for motion inputs. This testing platform will be used to:

- validate and verify of the individual subsystems involved in landing; and
- demonstrate a full-scale end-to-end ship-based landing in sea state 3 and partially demonstrate for sea state 5.

Chapter 6

Landing Components Results

The individual sub components of the landing autonomy were put through a series of tests and experiments, both in simulation and in hardware. The goal of the tests was to validate each subsystem individually (as decoupled as possible from the whole landing autonomy). All of the subsystems were tested in simulation and in hardware, however the hardware experimental results are viewed as being more valuable, and are the primary focus for discussion. There are however a few exceptions. Due to constraints on space within the flight spaces and available resources, not all aspects of the landing autonomy can be fully tested in hardware. The conditions that cannot be tested fully in hardware are as follows:

- The surge and heave in sea state 5 for the HMCS Nipigon exceed the limits of the Stewart platform. It can achieve sea state 3.

- The sea state data for Nipigon is taken up to 20 knots (10 m/s). There is not enough space to have the translational velocity of the Stewart platform (ship) to get that high while also staying within the range of the mocap system and the flight spaces available. The fastest the platform can be safely towed is approximately 1.0 m/s.

- Wind is a known disturbance in landing. The full-scale sea state wind at sea state 5 cannot be demonstrated within the flight space. Using fans, a wind

speed of approximately 2-4 m/s can be achieved.

- The phase 1 hover height is meant to be set at 5-10 m. The ceiling for the ISL flight space and size of the Stewart platform means the UAV can only hover approximately 1.5 m above the landing site. In the Sexton gym, this can be expanded depending on camera coverage to approximately 2-3 m. This is still short of the desired 5-10 m.

Since these elements cannot be demonstrated or tested fully in hardware, they will alternatively be examined in simulation. The other element that will be tested primarily in simulation is the sea state predictor. This is because the Stewart platform can only play approximately 60 s of ship response data on a loop due to the design. This small sample size on repeat makes it far too easy for the predictor to learn the ship motion and it makes it look more effective than it actually is. However, it should be reinforced that all of the sensor data used to test and vet the system comes from real-world RAO measurements and therefore the simulated results should be close to what is expected in real-world applications. Simulations also makes it easier and much quicker to do individual experiments as each RAO data set consists of 30 minutes worth of measurements.

6.1 Acoustic Position Tests

The first set of tests were devised to test the position estimator using acoustic sensors. The first goal of the acoustic position tests were to determine the accuracy of the estimator and how the accuracy might change or respond in real-world applications. Specifically, an understanding of how the accuracy changes as the ship responds to transitioning in a sea state. The sensor layout is also scaled down for testing and can be any configuration on the ship. The second goal is to determine how the layout size might affect the position estimate and how the accuracy changes with the scale of the sensor layout.

Single Sensor Position with Ship Motion

The first test was designed to assess how the acoustic position estimator would respond to ship motion i.e. how the estimation accuracy would change as the motion DOF increased. To test this, the Stewart platform was fitted with 4 acoustic listeners (receivers) and the UAV fitted with 1 beacon (transmitter). The Stewart platform was given ship transom motion trajectories to follow consisting of 0, 1, 2, 3, and 4 DOFs. The amplitude and frequency of these motions were representative of sea state 3 for surge and heave, and sea state 5 for pitch and roll, based on the limitations of the Stewart platform. The UAV was flown manually around the flight space (both the ISL lab and Sexton Gym) and the position estimates from the acoustic system and motion capture system were both recorded. The mean square error at each time step was calculated and the results are summarized in Table 6.1. Since the mean square error is used, it automatically creates a lower boundary at $MSE = 0$, as the MSE cannot be negative. This results in the data being positively skewed (as opposed to a Normal distribution). Traditionally, in statistics, when a data set is positively or negatively skewed the median is used instead of the mean to better interpret the results. This is because the mean is highly susceptible to large outliers where as the median is robust to such errors. Both the mean and median are reported in the results summary. The tolerances for positively skewed data are usually given as the first and third quantile, which are also given with the figures.

Table 6.1: Acoustic position error with respect to various degrees-of-freedom in ship motion using a single beacon. First quantile: -1.5cm, third quantile: +2.1 cm

DOF in Ship Motion	**Mean error (cm)**	**Median error (cm)**
0	7.04	6.11
1 (pitch)	7.09	6.24
2 (pitch, heave)	8.06	6.04
3 (pitch, heave, surge)	8.02	6.38
4 (pitch, heave, surge, roll)	8.82	7.01

An example test flight with four DOF motion is shown in Figure 6.1. The top part of the figure shows the Euclidean distance from the center of the landing area. The bottom part of the figure shows the elevation above the area. The motion capture

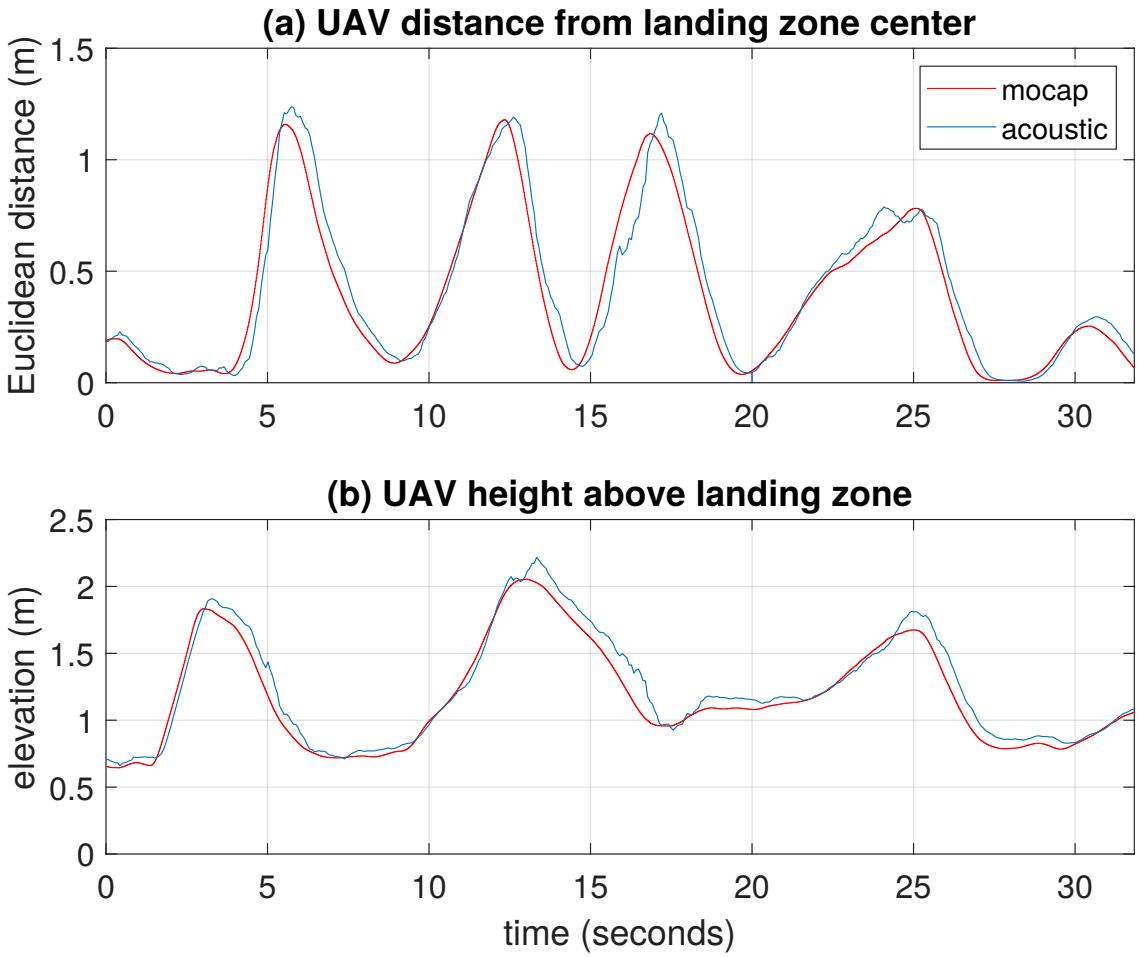

Figure 6.1: Position estimation error between acoustic estimator and motion capture system with 4 DOF ship motion. The top figure shows the error in the $x-y$ plane and the bottom figure shows the error in the elevation.

data taken from the flight is shown in red and the acoustic positioning data is shown in blue.

Single Sensor Position with Varying Scales

The second test was to quantify how the scale of the area used for the sensors will affect the system accuracy. This time, four acoustic listeners were placed on the floor at set distances from the center of the space, and one beacon was mounted to the UAV. The UAV was once again flown around the space and the UAV position estimate

and motion capture data were recorded. The lengths of the area edges tested were 0.5 m, 1.0 m, 2.0 m, 3.0 m, and 6.0 m × 10.0 m, which is the maximum distance capable within the Sexton Gym flight space. Once again the mean square error was calculated at every time step. The results for these tests are summarized in Table 6.2, showing both the mean and median.

Table 6.2: Acoustic position error with respect to different sensor layouts using a single beacon. First quantile: -1.5cm, third quantile: +2.1 cm.

Sensor layout (m)	**Mean error (cm)**	**Median error (cm)**
0.5	7.95	7.48
1.0	7.56	6.58
2.0	7.09	4.38
3.0	7.51	5.72
6.0 × 10.0	7.83	5.22

Multi-sensor Position/Yaw with Varying Scales

A two-sensor array on the UAV was also tested for cases where the UAV is not able to rely on a magnetic compass. This will have two effects on the overall system. First, it will increase the accuracy of the overall position estimate and second, it will allow for UAV attitudes to be extracted. Since this estimate is the average between the two sensors, the distance in between does not affect the overall results. The same scaling test used for the single sensor, where the UAV was flown in an environment with the beacons placed at increasing distances from one another, was repeated for the two sensor UAV case. The results for the new position error and median are shown in Figure 6.3.

Table 6.3: Acoustic position error with respect to different sensor layouts using multiple beacons. First quantile: -0.8cm, third quantile: +1.3 cm

Sensor layout (m)	**Mean error (cm)**	**Median error (cm)**
0.5	7.03	7.00
1.0	6.51	6.58
2.0	6.20	4.75
3.0	6.18	4.71
6.0 × 10.0	6.14	4.65

Attitude, on the other hand is related to the distance between the two sensors mounted on the UAV. To determine the accuracy of this estimate, the same scale tests were performed once again with two sets of UAV mounted sensor spacings: one with 0.5 m and one with 1.0 m. The sensors were both mounted on the y axis of the UAV. The mean and median heading was calculated for each distance at each scale. The results are summarized in Figure 6.4

Table 6.4: Acoustic orientation error with respect to different sensor layouts with multiple beacons. First quantile: -2.0 deg, third quantile: +3.3 deg

Sensor layout (m)	**UAV sensors 0.5 m apart**		**UAV sensors 1.0 m apart**	
	Mean error (deg)	**Median error (deg)**	**Mean error (deg)**	**Median error (deg)**
0.5	5.95	4.30	2.85	2.16
1.0	5.99	4.90	2.96	2.45
2.0	4.62	3.70	2.31	1.83
3.0	4.69	3.34	2.42	1.76
6.0 × 10.0	4.53	3.24	2.45	1.81

6.1.1 Discussion

Single Sensor

The acoustic position estimator is responsible for giving positional feedback to the UAV for guidance and control purposes. It, with a single beacon, was shown to have a mean error of approximately 7-9 cm with a median of 6-7 cm. These results are, as expected, slightly higher than what was shown within the literature using vision-based systems. These results are however much better than what is capable with GPS. The system showed accuracy and precision when increasing the DOF of the motion on the Stewart platform and by association, the listeners' performance as they were attached to the landing site. It also was not affected by increasing the separation over which the listeners' sensors were placed. In fact, there was a slight improvement when increasing the area for the sensors. This can be explained by looking at the UAV flight path relative to the listener layout. It could be observed from the data and test results that the largest errors and most outliers occurred when the UAV was

flying outside of the area covered by the sensor placement. With a larger area, the UAV spends more time within this "cone" created by the sensors and therefore the error decreased slightly.

One concern with the position estimator that could not be fully tested on hardware in the lab environment is the effect wind has on the estimate. The effect of wind on the accuracy of the position estimate needs to be considered because acoustic sound propagation can be changed by the moving air. As sound is the vibration of particles in a medium, if that medium is moving then the apparent speed of sound will change by the same amount. As such, the distance measurements from each acoustic sensor may be skewed. There are techniques to compensate for this digitally at a signal processing level [129–131], or an anemometer could be used to approximate the wind speed and limit its effect manually. However, assuming that there is no compensation for the wind speed, the effect this will have on the overall system can estimated mathematically and be verified with stored data.

According to the Beaufort scale, at sea state 5 (2.5 to 4-meter waves), the expected wind speeds are 8.0 - 17.2 m/s. Assuming the worst case scenario, where the landing zone is not protected, there are no boundary-layer effects at the ship deck and the highest rated wind speed of 17.2 m/s, the apparent speed of sound could be anywhere from 326-360 m/s, instead of the 343 m/s (or close to, as there is compensation for temperature and density done within the sensor). This would cause the distance measured by each individual sensor to be biased along the direction of the moving air. If the sensor to UAV vector is directly parallel to the wind, the distance error for each sensor could be as high a 50 cm over a 10 m range, 25 cm for distances of 5 m and 10 cm for distances of 2 m.

Testing the system with each sensor error being 50 cm in the same direction (which should give the absolute worst result) gave rise to a mean position estimation error of 52 cm, while a 10 cm sensor error produced a mean position error of 11 cm and 5 cm sensor error produced a mean position error of approximately 9 cm. This shows that estimating position in the highest expected winds for sea state 5 only increases the average position error by approximately 2 cm when in the final landing stages assuming a non-realistic worst-case scenario. It can be concluded that the wind speeds

at sea state 5 would not change the sensor measurements enough to affect the final stage of the landing algorithm.

When the UAV is higher in the air however, the position error is also quite high. At high elevations, the autonomy does not require a highly accurate position estimate for the UAV, as it only needs to hover or track during this phase. It is not until the UAV comes into its ready-to-land position that it requires a good position estimate and by that time it will be low enough that the error will have reduced significantly as shown.

Noise, attenuation and refraction also affect sound waves while travelling through winds. Noise can be filtered and reduced at the sensor level minimizing its impact, while increased attenuation and refraction are not concerning at the 10 m scale that is being considered in this application.

Multi-sensor Pose Estimation

When switching to a multi-sensor UAV layout, there were incremental improvements to the mean and median of the position estimate, approximately 1-2 cm in both cases. This improvement was expected since the position estimator is now able to average some of the error within the estimate. It was able to operate at the same minimal 15 Hz frequency that the single sensor system operated even with the inclusion of a second beacon sensor.

The wind is expected to affect the two sensor system identically to the single sensor, because the direction of the wind is the same for both sensors the errors induced by each sensor will be very similar and will not cancel.

In terms of heading, a UAV that is capable of separating the sensors by 0.5 m was able to determine its heading with a mean error of approximately 4.5-6 degrees and median of 3-5 degrees. Spacing the sensors out a bit more on a larger UAV to 1.0 m improved the heading estimate error range mean and median to 2-3 degrees and 1.5-2.5 degrees respectively. This heading accuracy is comparable to higher end magnetic compasses, whose errors can range from 1 degree to as high as 15 or more. In terms

of wind, the wind should have little to no affect at all on the heading estimate. As stated previously, the wind is affecting the range measurement in the same direction and therefore even though the position estimates might be slightly off, the vector connecting the two sensors should be the same, meaning the heading measurement will not change.

6.2 Goal Tracking Tests

The guidance and control components are highly coupled. The guidance generates the velocity commands required for motion and the control algorithm ensures that the desired commands are implemented. Since they are so coupled, they cannot be fully decoupled during testing. However, experiments can be designed to task one more than the other. Experiments were devised to test the capabilities of the guidance and control and how they function.

Tracking Ship Motion

The first test was to determine how well the UAV could track goal locations above the Stewart platform while it was undergoing sea state 3 surge and heave and sea state 5 pitch and roll. This test was designed to evaluate the guidance algorithm and how well it could have the UAV respond to internal measured disturbances. The UAV was set to hover 1 meter above the platform and set to stay at that height centered above the platform the landing site moves and rotates. The UAV's position was measured and the mean and median error relative to the desired goal positions were calculated. The results are summarized and shown in Table 6.5.

Tracking at Low Altitude

The next test was to determine how well the UAV could adapt to heave and surge at sea state 5 while avoiding colliding with the ship deck during the final stages of landing. This was once again designed to test primarily the guidance algorithm. The

Stewart platform was tuned to heave and surge at velocities that would be expected in sea state 5 with only half the amplitude due to platform constraints. The full scale heave and surge amplitudes were tested in simulation. The UAV's position was measured and the mean and median error relative to the desired goal positions were calculated. The results are summarized and shown in Table 6.5.

Tracking a Moving Target (Ship)

The next test was devised to test primarily the control subsystem and how well it can respond to constant external forces. The most common instances in landing would be the actual real-world velocity of the ship. The landing zone was placed on a cart and was towed approximately 0.5-1.0 m/s and the UAV was set to hover 1 m above the platform. This experiment was repeated in simulation using full-scale ship velocities (10 m/s). The UAV's position was measured and the mean and median error relative to the desired goal positions were calculated. The results are summarized and shown in Table 6.5.

Tracking with External Forces

The last test in this category was to determine how well the control subsystem could respond to external forces that are not constant, like wind and turbulence. Fans were used on an oscillate setting to apply a force and the UAV was set to once again hover above the platform. This experiment was repeated in simulation using wind speeds similar to what would be seen in sea state 3 and sea state 5 using the wind speed message available with the Hector quad-rotor ROS package. The UAV's position was measured and the mean and median error relative to the desired goal positions were calculated. The results are summarized and shown in Table 6.5.

Table 6.5: Tracking error throughout guidance/control tests. First quantile: -1.5cm, third quantile: +2.1 cm.

Test	Mean Error (cm)	Median Error (cm)
Ship Motion	11.4	10.2
Traversing (0.5-1.0 m/s)	11.6	10.5
(sim) Traversing (10 m/s)	11.9	10.6
Low Altitude	12.3	11.7
Wind (2-4 m/s)	11.4	10.3
(sim) Wind (10 m/s)	15.4	12.9

6.2.1 Discussion

The potential field guidance algorithm is responsible for setting velocity commands to have the UAV track the goal position. It considers internal measured forces and as such, the best tests to explain and demonstrate the abilities of the potential field approach are the ship tracking and low altitude tracking tests. This is because the motion of the ship is measured by the IMU attached to the ship and the guidance algorithm can push the UAV towards the constantly changing goal position.

For the ship tracking tests, the platform was moving at sea state 3 heave and surge and sea state 5 pitch and roll. This means the goal position could theoretically be anywhere within a 1.0 m $\times$ 1.0 m $\times$ 1.0 m box and continuously moving. The potential fields in conjunction with the controllers were able to keep the UAV within 11 cm of the goal position on average. It also adequately drove the UAV away from the landing platform as the UAV elevation decreased. While there was a slight increase in the tracking error, this increase in error was found to be primarily in the "z" direction. This is because the UAV was low enough that it felt in danger of hitting the landing platform as it was heaving at sea state 5 velocities. The potential fields algorithm put an extra force upwards so when the ship accelerated towards the UAV, it would avoid the collision. It is biased so that any error in tracking would occur away from the ship as opposed to closer to it. This was corroborated with what was seen in simulation as well.

The PID controller is responsible for ensuring the desired motion is actually carried out, while also compensating for external forces that are acting on the UAV. Its

performance in this context can be best seen in the tracking tests that are exposed to external forces. These experiments were unable to be demonstrated at full-scale in hardware so simulation results are used to supplement the analysis.

In hardware, the PID controller was able to quickly adapt to the slow moving target (the ship). The maximum velocity of the UAV was designed so even at the slow ship speed, the UAVs control authority was still somewhat taxed. In simulation, the UAV was able to move quicker and could still track the faster moving vehicle. This is because the UAV can still move much quicker than the ship and the frequency of the position estimator is fast enough that the control loop is able to compensate for the growing errors fast enough to track the vehicle. Once the forces were made to be more random using wind, there was an increase in the mean tracking error, however it was still able to land on the platform. This was also shown with higher wind speeds in simulation.

6.3 Sea State Predictor Tests

The next set of tests were designed to quantify the capabilities and define the extremes of the sea state look-ahead predictor. Different neural network sizes and structures were also tested. Each test began with random network weights and was allowed 5 minutes of training (≈ 25 wave cycles) before the outputs were used in any decision-making process. After the 5 minute training period, the network outputs were used to predict ship orientations and landing windows while also continually training to new data as it became available. This portion of the test used 25 minutes of training data. The predicted landing windows were compared to the actual ship orientation to determine whether the predictor correctly identified a landing window. This was repeated for 9 different ship aspects and velocity pairs, generated from the 3 different ship aspects (head, bow and beam waves) and 3 different ship speeds (10, 15 and 20 knots).

The majority of the training and validation for the sea state predictor was performed in simulation. However, the measurements were not simulated, and instead

the RAO data for Nipigon at sea state 5 was used directly. After pruning, little improvements in performance was seen in the MLP neural network after 12 hidden neurons in a single hidden layer. The network used the current and 2 previous time instances of the ships roll, pitch, roll rate and pitch rate to predict the pitch and roll of the ship a set time step into the future. The network structure is shown in Figure 6.2.

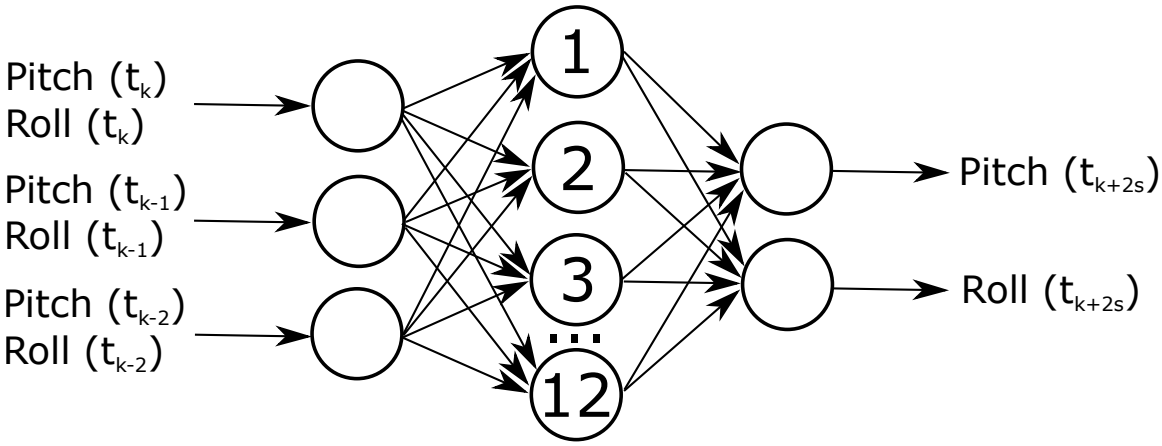

Figure 6.2: Look ahead ship state predictor looking ahead 2 seconds

Using the predicted pitch and roll, a decision was made as to whether or not the ship orientation at that time would be suitable for landing (As previously mentioned, a landing window was defined as any time the ship pitch and roll was under 5°). The time steps selected for testing were 1, 2, 3, 4 and 5 seconds. The results for the sea state predictor tests are summarized in Table 6.6.

For use in Table 6.6, 2 values are given for each time/heading/wave data point. The value highlighted in green is the percentage of time the predictor determines the UAV will get a landing window and a landing window actually materializes after the predictor time step has passed i.e. the predictor has correctly predicted a landing window. Highlighted in red is the percentage of time the predictor predicts a landing window however the actual orientation of the ship after the time step was such that the ship was critically tilted. As previously mentioned, a "critical tilt" was defined as a ship roll or pitch that is more than 10°, from the operator guidelines for full-scale manned helicopters [122].

Table 6.6: Landing window predictor results for HMCS Nipigon RAOs

Ship Landing Window Predictor									
Time (s)	Head Waves			Bow Waves			Beam Waves		
	10 kn	15 kn	20 kn	10 kn	15 kn	20 kn	10 kn	15 kn	20 kn
1	100	100	100	99.9	100	100	100	100	100
	0	0	0	0	0	0	0	0	0
2	100	100	100	99.9	99.9	100	97.7	97.4	96.0
	0	0	0	0	0	0	0	0	0
3	100	100	100	99.8	99.9	100	89.9	91.4	91.9
	0	0	0	0	0	0	0.11	0.01	0.01
4	100	100	100	99.7	100	100	88.0	90.2	90.7
	0	0	0	0	0	0	0.1	0.04	0.03
5	100	100	100	99.3	99.9	100	88.6	91.7	93.3
	0	0	0	0	0	0	0.11	0.07	0.06

The second test attempted to define the extremes where the sea state predictor begins to break down, since RAOs are specific to the ship for which they are taken and may not be what is seen with Nipigon. To do this, the pitch and roll at bow seas were artificially scaled. This will give insight into using the predictor at larger sea states and for smaller vessels that may be less stable. For each ship speed, the pitch, roll, pitch velocity and roll velocity were multiplied by a factor of 2, 3 and 5. At a factor of 5, the pitch and roll angles and velocities were all over $40°$ and $35°/s$ respectively which is unrealistically large for any ship attempting to land a UAV. The test was preformed in the same manner as before using the new dataset and the results are shown in Table 6.7

6.3.1 Discussion

The purpose of the sea state predictor is to give the UAV some advanced notice as to when the ship will be in a state suitable for landing. The predictor was allowed 5 minutes of training time before the results were used, however it was determined during the trials that there was not a significant improvement in the results after 2 minutes for the most extreme sea conditions and even less for more mild cases.

The predictor exists to ensure UAVs that either need more time to descend or

Table 6.7: Landing window predictor results for exaggerated RAOs

Ship Landing Window Predictor									
Time (s)	Bow Waves x2			Bow Waves x3			Bow Waves x5		
	10 kn	15 kn	20 kn	10 kn	15 kn	20 kn	10 kn	15 kn	20 kn
1	100	99.7	99.4	99.5	98.5	97.2	96.7	97.2	95.0
	0	0	0	0	0.02	0	0.51	0.46	0.59
2	94.5	93.3	93.7	74.8	77.8	77.9	50.6	47.23	49.3
	0.32	0.08	0	3.13	0.7	0.39	16.6	11.22	10.32
3	90.7	89.2	92.9	70.6	69.1	75.6	35.4	42.7	42.7
	0.06	0.06	0	4.02	1.31	0.57	25.8	14.3	11.4
4	87.0	89.4	92.6	57.4	63.3	71.1	25.2	32.9	36.1
	0.44	0.06	0	5.84	2.03	1.11	27.9	20.6	17.7
5	82.3	89.9	94.3	49.4	64.3	74.8	17.2	26.7	38.7
	0.82	0.07	0	9.15	1.40	1.11	38.7	24.5	18.8

that may respond slower have the chance to begin the process early enough to land safely. With HMCS Nipigon, this was only required in sea states greater than 3 as below this number the ship deck orientation was never more than 5° no matter the speed or heading. The results from Table 6.6 show how often the predictor works effectively and how often the predictor would cause a dangerous landing assuming no other safe guards are in place. The RAOs and ship response are very different for different sea/bow interactions and speeds, and this can be seen in the table as well. For head seas at 10 knots, the predictor is 100% correct no matter how far in advance it is looking. The same is true for ship speeds of 15 and 20 knots. This is because at no point in time does the pitch (roll is ≈ 0 for head waves) exceed the 5° threshold for landing. In theory, the UAV would have recognised this during the landing and would have found that the predictor was not necessary. The trade off here is that if the UAV would have incorrectly assumed the predictor was in fact needed, it would have indicated that there were going to be times when the ship was unsuitable for landing even though it actually was. This is because the predictor has the most difficulty estimating given extremes in pitch (and roll in subsequent tests). Normally this is not an issue as the predictor is meant to find zeros, not extremes, however it does mean that there will be times when the UAV hesitates when it does not have to. For 10 knots at head waves, this occurred less than 1% of the time.

When the ship heading changes the need for the predictor becomes more pronounced as the ship will pitch and roll more vigorously due to the difference in the latitudinal and longitudinal stability/inertia common with almost all ships. With HMCS Nipigon, there were instances while travelling in bow seas at all speeds the ships x-y orientation was greater than the desired 5° setpoint threshold. In these cases, the predictor correctly predicted landing windows up to 5 seconds in the future 99.3% of the time. Once again, some real landing windows were missed however the trade-off for being certain of the ship conditions outweighs the few missed landing opportunities.

While landing a UAV, the standard is to have the ship travel at head seas and generally landings would not be attempted at beam seas as beam seas are traditionally the most difficult to land in. Figure 5.5 demonstrates why as the ship routinely exceeds the desired 5° landing setpoint and often even exceeds the 10° potential critical failure tilt as well. While HMCS Nipigon only exhibited this extreme behaviour in the worst case scenario for landing, other ships may present this motion in head seas, bow seas or even at lower sea states. Also, the heading of the ship should not be a constraint for landing. In these cases a large disparity was seen in the accuracy for the predictor as the look-ahead times became greater and greater, being accurate at least 96% of the time with no critical failures with a 2 second look-ahead and dropping to 88.6% a critical failure 0.24% of the time with a 5 second look-ahead. The errors that are inherent within this kind of system are mitigated through other elements of the landing autonomy. The UAV uses this information as an estimate to help it decide when to begin its decent however it is still monitoring the current state as it comes down. If the pitch and roll do not level out as predicted, the UAV aborts the landing attempt and returns to phase 2 of the landing process.

It is also important to notice that the predictor performs better at faster ship velocities. At higher velocities, the effective wave-ship interaction frequency also increases for head waves and bow waves. As such, the higher frequency waves are easier for the ship to dampen and the motion of the transom is reduced. The result is the predictor has an easier time predicting the motion of the ship since the motion is more stable.

To determine the point when the sea state predictor would breakdown, the RAO training values were all scaled up. Predictably, the predictor had a harder time properly finding landing windows with the much larger orientation angles and faster rotation frequencies. There was a clear drop in performance when doubling the response of the ship however the worse case is still 82.3% which is still within the realm of useful with the addition of the "bailout" process mentioned before. At 3 times the scale the predictor began to breakdown. While using it with 2-3 look ahead times might be viable at 4-5 seconds it begins to become more paramount that there is more care in protecting the UAV from mis-information as it descends. At 5 times the input, any more than 2 second look ahead will find that there are scenarios where the UAV is critically wrong more often than not.

Chapter 7

Autonomous Landing Results

7.1 End-to-End Landing Tests

Once all the tests on the individual low-level subsystems were performed, the landing autonomy could be tested as a whole. These tests were designed to validate the algorithm in its entirety and demonstrate the novel landing capabilities from start to finish.

7.1.1 Landing in Sea State 3

The initial goal of this thesis autonomous UAV landings in sea state 3. As such, a few hundred landings were performed in rapid succession using the novel autonomous landing algorithm. For each landing, the Stewart platform simulated Nipigon experiencing sea state 3 conditions using the RAOs data mentioned previously. Landings were grouped based on the 9 different heading/velocity pairs. The Stewart platform can only repeat 60 seconds worth of data by design, so every 3-5 landings, a new 60 second snippet of data from the 3 hours available was randomly selected. All recoveries for sea state 3 fell into either category 1 or category 2, and therefore the sea state predictor was not needed. The UAV began each test in it's phase 1 "hover" position

(set at only 1.0 m) due to height constraints) and began each individual landing from this point. The motion capture system was used to determine exactly where on the platform the UAV landed.

ISL Flight Space

The first of the sea state 3 tests were done in the ISL flight space with a stationary platform and fans running to simulate wind. Ten landings from each heading/velocity pair were randomly taken for demonstration purposes and are shown in Figure 7.1. Each sub-figure shows the area of the available landing area that is on the Stewart platform. The red "x" represents the center of the landing area, which is also the goal location of the UAV. Red circles are drawn in 10 cm increments to aid with spatial visualization when viewing the figure. The blue "x"s are the final landed locations of the UAV after landing.

Sexton Gym Flight Space

The previous tests were repeated within the Sexton Gym flight space without the fans adding wind. Instead the Stewart platform was towed at approximately 1 m/s to model a constant ship speed. The UAV was also permitted to hover slightly higher (approximately 1 m) during the "Hover" phase and "Ready" phase. Once again, 10 random landings were selected and are shown in Figure 7.2. This time the landings are not grouped into velocity/heading pairs and instead are all combined.

7.1.2 Landing in Sea State 5

The previous tests were repeated for sea state 5 with the omission of the tests done in the Sexton Gym due to time constraints on the space. The focus of this test was less on where the UAV lands, as this should be very similar to what is seen in sea state 3, but more on when the UAV lands and the orientation of the ship at touchdown.

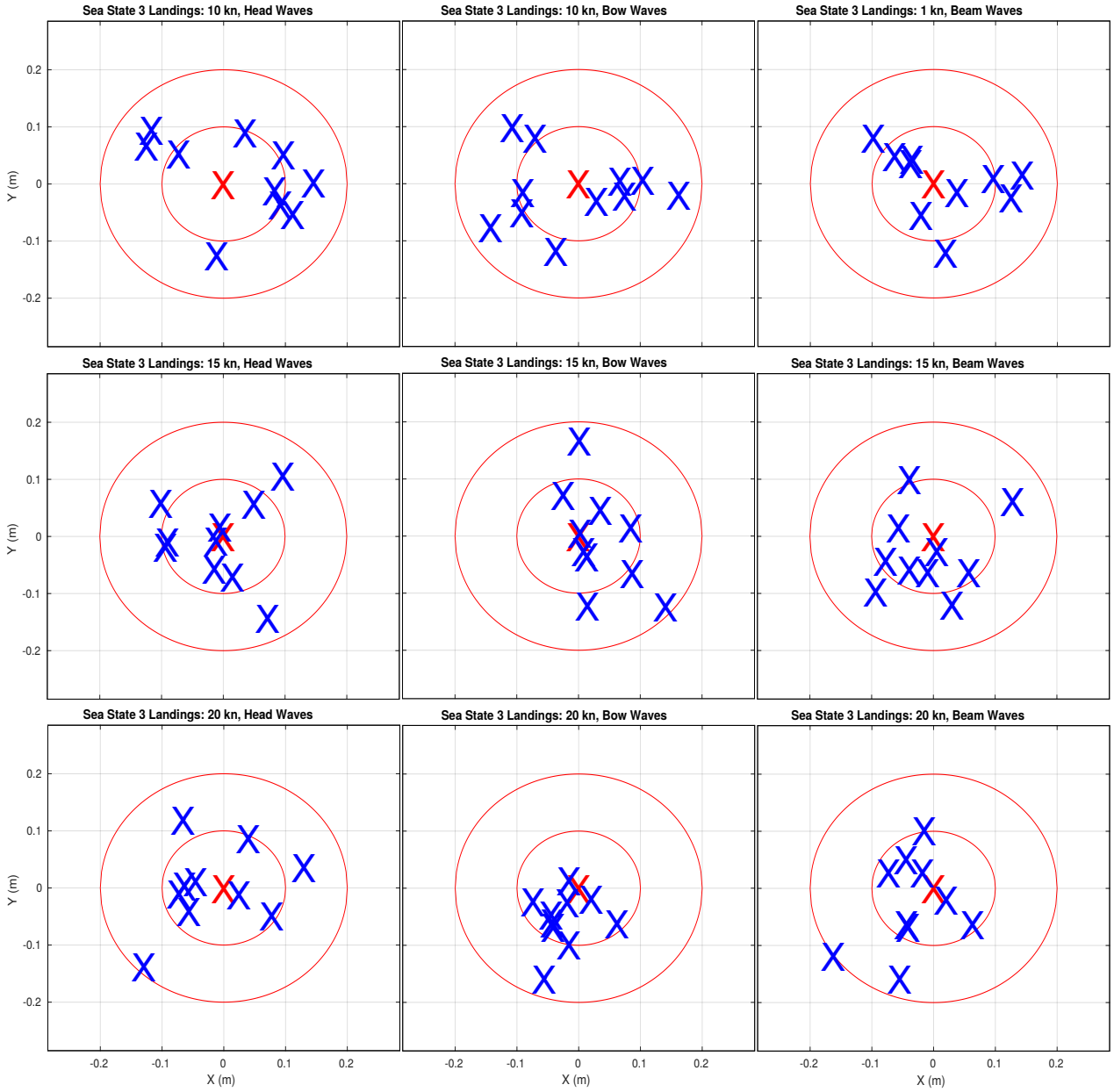

Figure 7.1: Sea State 3 landing locations for ISL flight space tests. The red "x" represents the desired UAV landing point. Blue "x" represents final landed locations. Tolerance: +/- 0.3 cm

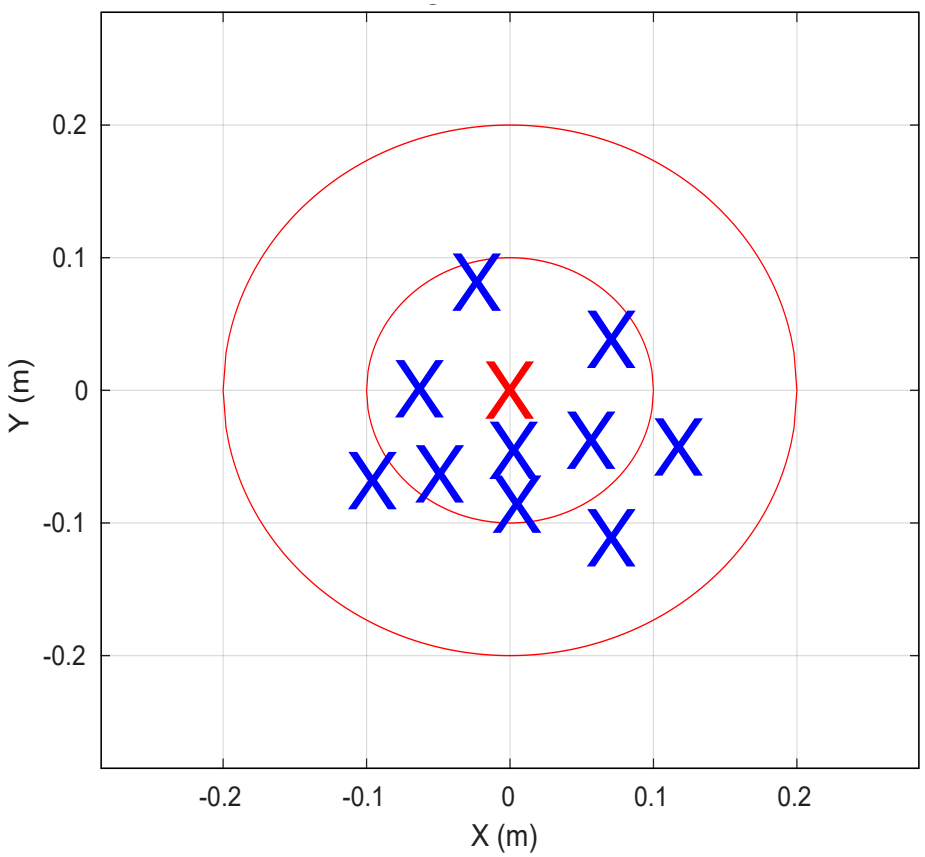

Figure 7.2: Sea State 3 landing locations for Sexton gym tests. The red "x" represents the desired UAV landing point. Blue "x" represents final landed locations. Tolerance: +/- 0.3 cm

For these tests, the predictor was integrated into the overall landing procedure and the Stewart platform was allowed run for a few minutes before each test to allow the predictor to learn enough of the motion without draining the UAV batteries. The UAV would then perform a set of landings before changing the conditions and restarting the test. Each landing assumed the UAV required 2 seconds to to touch down and therefore that is how long into the future the predictor looked. In reality, it took less than a second so the UAV would just stall before landing. Once again, the of landings were preformed for different ship speeds/headings. The differences now were that there was a little more time between landings as the UAV had to wait longer between available landing windows. Figure 7.3 shows three landing cross-sections. The landings include bow waves, beam waves and an exaggerated bow waves set to demonstrate the capabilities in much harsher conditions. The figure

shows the different stages the UAV goes through in landing beginning at the hover phase, then motion matching, then the decision to land, the beginning of the landing itself and touchdown. At each time instance, the correlating ship orientation is also approximated.

7.2 Discussion

All of the individual subsystems are integrated to create the landing autonomy. While each subsystem is important, it is meaningless if they cannot combine to generate consistent, trustworthy and safe landings.

7.2.1 Landing Phase 1: Hover

Sea State 3

The hover phase could only be demonstrated to an altitude of approximately 1-1.5 meters within the ISL flight space and up to 2 meters within the Sexton Gymnasium flight space. In simulation, the hover could be tested at any height, however 5-10 meters were used. At higher altitudes, there was a small difference in the drift of the vehicle relative to lower altitudes. At 2 meters, the drift was still observed and measured to be under 25 cm from the goal location during the phase. In simulation, the drift at high altitudes was similar to what was seen in hardware. The drift is due to errors in the acoustic position and errors in the orientation of the ship. Since the position estimate is rotated to a real-world orientation, errors incurred here are magnified as the distance from the center of the rotation increases. The goal location is also rotated with the ship meaning its position relative to the ship deck is constantly changing. At sea state 3, the UAV had no issues staying within the range of the acoustic sensors even while traversing 20 knots in simulation and approximately 0.5 m/s in hardware. The 2 m stand-off was more than enough to avoid the ship at the peak of its heave motion. Since the UAV determined no predictor was necessary in

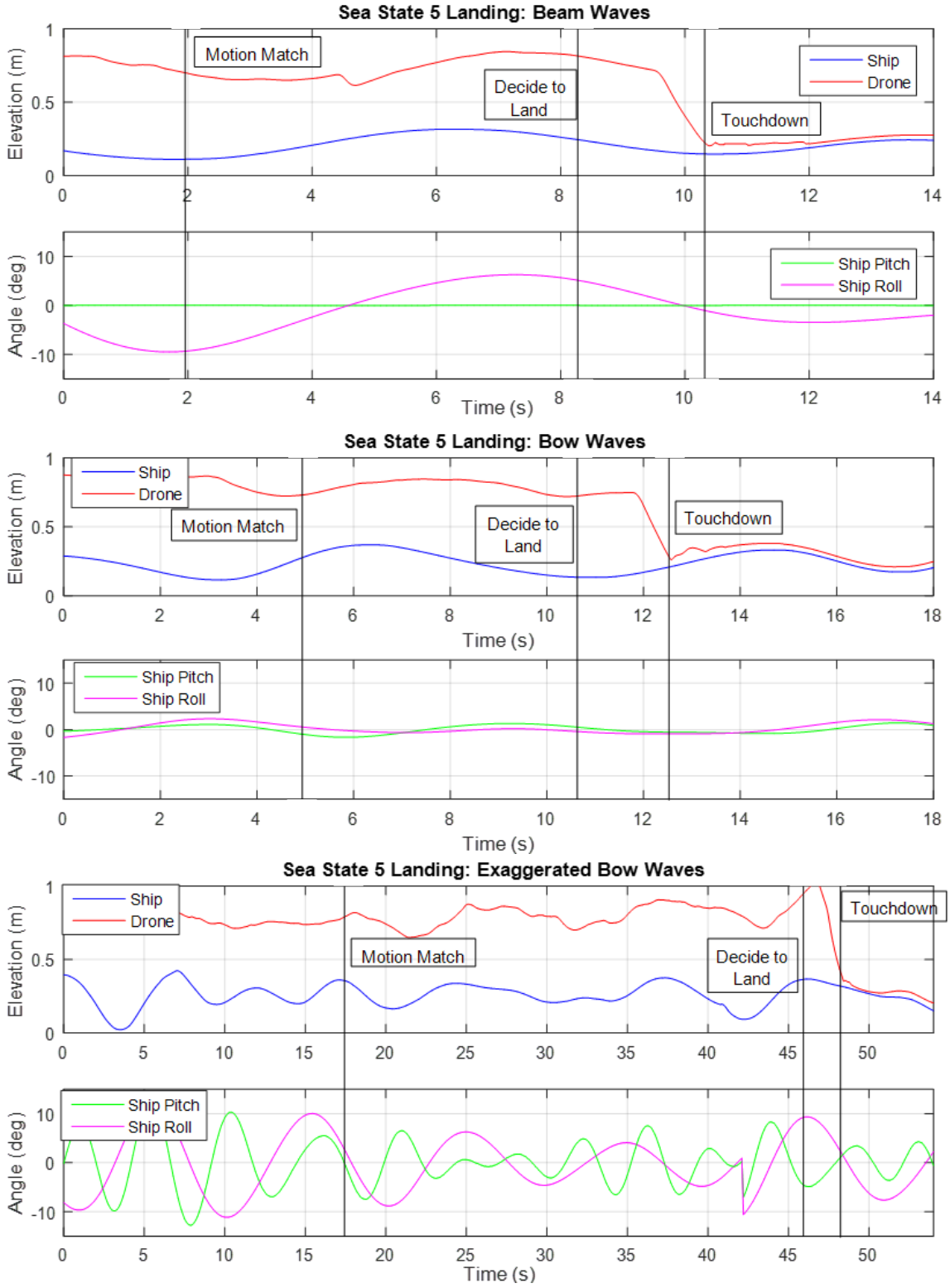

Figure 7.3: Pitch and Roll for HMCS Nipigon travelling 10 knots in sea-state 5 with head, bow and beam waves

any of the phase 3 tests, the phase lasted only the 15 second minimum hover time.

Sea State 5

Similar to sea state 3, the hover phase in sea state 5 could only be demonstrated to an altitude of approximately 1-1.5 meters within the ISL flight space, up to 2 meters within the Sexton Gymnasium flight space and 5-10 meters in simulation. The UAV's ability to follow the ship while traversing in hardware and simulation was unchanged. Due to the limits of the Stewart platform, sea state 5 heave could not be observed. However, simulation showed that a 5-10 m stand off was adequate to avoid hitting the ship deck during heave. It was observed in both simulation and in hardware that the drift during this phase increase slightly as the more aggressive angles now seen by the ship deck propagated to the goal location. It in essence is moving faster meaning the UAV has to move further to correct for the goal location translating. The UAV found that a predictor was necessary at all times for bow and beam seas, and sometimes for head seas depending on the sea conditions at the instant of landing. Therefore, this phase last approximately 5 minutes in simulation. In hardware, due to flight time constraints, the UAV was allowed to model the motions of the platform prior to take-off. The Stewart platform also only allows for 60 s of data to be used and repeated therefore the predictor did not require as much time to model the ship motion.

7.2.2 Landing Phase 2: Ready

The UAV then entered the ready phase. In hardware the the ready elevation was set at 0.5 m and in simulation the elevation was set at 1.0 m. The UAV drift reduced slightly. The UAV still had no problems remaining above the landing site while traversing in simulation and in hardware At sea state 3, since no predictor was needed the UAV simply entered the landing phase when it was centered over the landing site. Visually, there is not a large difference in this phase for sea state 3 and sea state 5. At sea state 5, the motion matching UAV travels much fast and further to compensate for the large motions of the ship. It also remains in this phase longer as the UAV is looking for potential landing windows.

7.2.3 Landing Phase 3: Land

The actual touchdown landing is the most important phase as it has the highest potential for damage or injury. At sea state 3 for HMCS Nipigon the risk was fairly low since the pitch and roll are low. In Figure 7.1 it can be seen that for hardware testing the UAV could consistently land within 20 cm of the desired landing site, with approximately 60% of those landings being within 10 cm of the desired landing location. This break down remains consistent when the Stewart platform was moving at the 0.5-1.0 m/s tow velocity. At the full-scale ship velocity in simulation, the UAV landed with more precision, which is expected due to the simplification of the environment.

Traditionally, head seas are ideal for landing. In sea state 3, there is not a large difference between landing in head, beam or bow seas as seen in Figure 7.1. This is because the motions of the HMCS Nipigon were not significantly different from each other at each wave aspect to drastically increase the difficulty for the algorithm.

Sea State 5

Landing locations for sea state 5 were very similar to what was seen with sea state 3. The landing locations diverged by only 1-2 cm from what had been seen with the lesser ship motion. However, with sea state 5, one of the more important is when the UAV lands and what the ship is doing at the time. Many landings were tested, and none of the landings landed when the ship was critically tilted. While for the longer look ahead winds there was a need for the "bailout" a few times, no crashes or damage to the UAV or ship were experienced.

At sea state 3, there was not a large difference between landing in different wave aspects. At sea state 5 however the differences increase to a point where the results are noticeable. While difficult to see in Figure **??**, the sea state predictor results, as previously indicated, are more accurate for head seas. This means that this algorithm, like the current standard, will function better with the ship traversing through head seas at higher sea states because, even though the UAV can track the ship just as

well in other wave aspects, the prediction of when to land is more accurate at head seas.

7.2.4 Other Considerations

There are a few other considerations that also need to be addressed in relation to landing before concluding on the overall effectiveness of the autonomous landing algorithm as described and demonstrated.

Control Authority

The first consideration is the concept of control authority. Control authority traditionally refers to human-robot interactions and determining what input has the most influence over the action the robot takes. In this context, the battle over control authority refers to the balance between what the UAV needs to do to track the ship and what the UAV needs to do to land i.e. the PID control and guidance subsystems. The ability of a UAV to land at sea is dependent on its capabilities. For it to land on a ship moving 10 m/s, the UAV itself must be able to fly at 10 m/s and have enough control authority left to perform the motion matching and other landing sequence items. The landing algorithm was designed to require as little control authority as possible for this reason. For the most part this is successful as simple side-to-side x-y plane corrections do not require much of the UAV. The most control authority intensive part of the landing algorithm is the motion matching occurring along the vertical plane, as it will often have to oscillate up and down faster than moving side-to-side (not including the ship velocity). In cases where the control authority of the UAV is taxed compensating for wind and ship velocity, the UAV may not be able to move fast enough to avoid the ship during heave motions. In these cases (control authority is related to air speed and therefore some understanding of how taxed the UAV will be given a ship and wind speed will be known), the solution is to have the UAV motion match at a higher elevation and use the predictor to help predict further into the future. This will give the UAV more time to avoid the ship deck as it heaves

towards it and the UAV can often motion match outside of the heave range of the ship itself.

Scalability and Wind

Control authority is also related to the scalability of the landing system and how wind may affect each vehicle. Naturally, UAVs of different specifications and sizes are affected differently by wind and drag. Thankfully, a commonly reported measure for UAVs is air speed, which includes these considerations. Since drag is a function of the air moving over the body of the vehicle, only the relative interaction matters, not the absolute UAV speed. This makes it much easier to predict how the UAV will function in wind at different sizes. For instance, if a UAV has an airspeed of 10 m/s and it is flying in 5 m/s head winds, the maximum ground speed the UAV can fly at is 5 m/s before drag overcomes its maximum thrust. This then relates back to control authority as this UAV would not be able to land on a ship moving faster than 5 m/s. With that measure, the constraining parameter on the UAVs control authority in this system is airspeed, assuming the position estimator is running at a high enough frequency. There is an omission here that is related to wind and that is turbulence. Turbulence is known to affect helicopters and UAVs during landing, as a bi-product of turbulence is buffeting which would also impact control authority and controllability for the UAV. Turbulence is highly specific to the actual case; further research into the effects of turbulence on this landing system is an element for future research.

Inertia

While airspeed is a good indication of a UAVs capabilities, in a reactive system there also needs to be a consideration for how fast the UAV can react to changing velocities as the ship moves, especially in heave. Larger UAVs have more inertia and take longer to change direction, accelerate and decelerate. The response and reaction frequency of even large UAVs is still much faster than the ship's motion and therefore this should not be an issue in most applications. As previously mentioned, the test UAV had

artificial delays designed into it to model a worse case slow reaction vehicle. With slow reacting vehicles, an adjustment to the hover height will give the vehicle the time it needs to react and prevent collisions with the ship deck upon touchdown.

Chapter 8

Conclusions

In order for UAVs to be used for a wider breadth of applications, operational elements like ship based landing need to be in place. A novel autonomous landing technique was described and tested that includes the following components:

- three-phase autonomous landing high level design;
- acoustic-based localization to increase the environmental conditions the UAV can be recovered under;
- potential field based path planner to allow for more adaptive tracking and obstacle avoidance;
- prediction-based recovery to allow the UAV to be landed in harsher sea states;
- PID velocity controllers to simplify the portability of the algorithm to different UAVs.

Each system was tested individually and as a whole. Individually, the acoustic localization was shown to have an error in the range of 7-9 cm which can be reduced to 6-8 cm with the use of an additional beacon, which also allows the heading to be estimated to within 3-5 degrees. The guidance and control algorithms allow the

UAV to track moving goal positions within 10-15 cm for different internal and external forces like ship motions and wind. The recovery predictor was shown able to accurately predict landing winds up to 5 seconds into the future 88% of the time.

As a whole, the UAV was able to land to within 20 cm of the center of the landing platform and within 10 cm 60% of those landings. These results were retained with the addition of some wind and ship velocity. When the predictor was integrated, these results remain constant while also ensuring the UAV only landed when the ship was level enough to do so.

The described solution has great impact on the current state of marine UAVs. The ability to reliably recover UAVs at sea in a variety of sea states allows UAVs to have a wider breadth of applications.

8.1 Summary of Contributions

This thesis has made numerous theoretical and experimental contributions to the field of autonomous ship-based landing of UAVs. These contributions are summarized below.

Theoretical

- A new three-phase based approach for landing with modular subsystem components
- Development of an acoustic based position estimator for use with a moving landing zone that is not reliant on vision of specific landing pads
- Development of a potential field map for ship based landing including elements for obstacle avoidance and biasing to prevent crashes on the ship deck
- An adaptive predictor to predict future landing windows while also learning on-line and adapting to evolving sea conditions

Experimental

- Development of an experimental platform including a ship motion emulator simulant that can use full scale RAOs for ship motion inputs

- Demonstration of a full scale end-to-end ship-based landing in sea state 3 and partial demonstration for sea state 5 in hardware

Academic Contributions

- **Conference papers and presentations**
  (1) J. Ross, J. Lindsay, E. Gregson, A. Moore, J. Patel, and M. Seto. Collaboration of multi-domain marine robots towards above and below-water characterization of floating targets. *Proceedings of the 13th IEEE International Symposium on Robotic and Sensors Environments*, 2019 (awarded best student paper at the conference)

  (2) J. Ross, M. Seto, and C. Johnston. Zero visibility autonomous landing of quadrotors on underway ships in a sea state. *Proceedings of the 13th IEEE International Symposium on Robotic and Sensors Environments*, 2019

  (3) J. Ross, M. Seto, and C. Johnston. Autonomous zero visibility landing of quadrotors on underway ships in a sea state. *Proceedings of the 2019 OCEANS Conference & Exposition*, 2019

- **Submitted journal papers**
  J. Ross, M. Seto and C. Johnston. End-to-end autonomous landing of rotary-wing UAVs on an underway ship in a sea state. submitted to *The Journal of Intelligent and Robotic Systems*

8.2 Future Work

While this work demonstrated and end-to-end capability, there are still areas that can be further expanded and understood. These are outside of the scope of the work or were not explored due to constraints on space, resources or time.

- **Full scale in-situ testing**. At this point in time, the landing autonomy is ready for the next stage of testing, which would have the system move outdoor and on a ship. The ship can be stationary at first, however this is the logical next progression for the research. Part of this testing will also look into the effects of the ship ambient noise on the acoustic sensors and whether more filtering or Doppler compensation may be needed.

- **Effects of turbulence on the UAV motion and control authority**. The turbulence experienced by the UAV in landing is a known problem for flight. The turbulence experienced by the UAV depends on the ship environment, and therefore this study will be specific to each application.

- **Improvements to the sea state predictor**. While the sea state predictor works well as demonstrated in this work, there is room for improvement. Further study into different neural network structures, feed forward predictors or on-line training techniques could improve the effectiveness of the predictor

- **Further validation with different vehicles**. The ISL lab has access to 2 different vehicles, the Prism M1 and the Parrot AR Drone 2.0. While the Prism M1 was the primary research vehicle, some landings early on were performed with the AR Drone. Future testing with a wider variety of vehicles could further validate the system as a whole.

Bibliography

[1] NOAA. How much of the ocean have we explored? *National Ocean Service website*, 2018.

[2] BBC. Uav-based data gathering using an artificial potential fields approach. *BBC Website*, 2019.

[3] B. Davies. Subglacial lakes. *Antartic Glaciers Website*, 2018.

[4] P. Schermerhorn and M. Scheutz. Dynamic robot autonomy: Investigating the effects of robot decision-making in a human-robot team task. *Proceedings of the 11th International Conference on Multimodal Interfaces*, 2008.

[5] R. Parasuraman, T. Sheridan, and C. Wickens. A model for types and levels of human interaction with automation. *IEEE Transactions on Systems, Man, and Cybernetics-Part A: Sytems and Humans*, 30:286–297, 2000.

[6] M. Dzindolet, S. Peterson, R. Pomranky, L. Pierce, and H. Beck. The role of trust in automation reliance. *International Journal of Human-Computer Studies*, 2003.

[7] K.S. Barber and C.E. Martin. Specification, measurement, and adjustment of agent autonomy: Theory and implementation. *Autonomous Agents and Multi-Agent Systems*, 1999.

[8] A. Gautam, P. Sujit, and S. Saripalli. A survey of autonomous landing techniques for uavs. *International Conference on Unmanned Aircraft Systems*, pages 1210–1218, 2014.

[9] W. Kong, D. Zhou, D. Zhang, and J. Zhang. Vision-based autonomous landing system for unmanned aerial vehicle: A survey. *International Conference on Multisensor Fusion and Information Integrationfor Intelligent Systems (MFI)*, pages 1–8, 2014.

[10] Northrop Grumman. Mq-8b fire scout, 2010.

[11] S. Moore. Superaccurate gps chips coming to smartphones in 2018. *IEEE Spectrum*, 2017.

[12] F. Amzajerdian, L. Petway, G. Hines, B. Barnes, D. Pierrottet, and G. Lockard. Doppler lidar sensor for precision landing on the moon and mars. *IEEE Aerospace Conference*, pages 1–7, 2012.

[13] O. Shakernia, Y. Ma, T. koo, and S. Sastry. Landing an unmanned air vehicle: Vision based motion estimation and nonlinear control. *Asian Journal of Control*, 1:128–145, 1999.

[14] S. Saripalli, J. Montgomery, and G. Sukhatme. Vision-based autonomous landing of an unmanned aerial vehicle. *IEEE International Conference on Robotics and Automation*, 3:2799–2804, 2002.

[15] S. Saripalli, J. Montgomery, and G. Sukhatme. Visually guided landing of an unmanned aerial vehicle. *IEEE Transactions on Robotics and Automation*, 19:371–380, 2003.

[16] S. Saripalli and G. Sukhatme. Landing on a moving target using an autonomous helicopter. *International Conference on Field and Service Robotics*, 2003.

[17] T. Merz, Simone Duranti, and G. Conte. Autonomous landing of an unmanned helicopter based on vision and inertial sensing. In *Experimental Robotics IX*, pages 343–352. Springer, 2006.

[18] C. Sharp, O. Shakernia, and S. Sastry. A vision system for landing an unmanned aerial vehicle. *IEEE International Conference on Robotics and Automation*, 2:1720–1727, 2001.

[19] O. Shakernia, R. Vidal, C. Sharp, Y. Ma, and S. Sastry. Multiple view motion estimation and control for landing an unmanned aerial vehicle. *IEEE International Conference on Robotics and Automation*, 3:2793–2798, 2002.

[20] Y. Fan, S. Haiqing, and W. Hong. A vision-based algorithm for landing unmanned aerial vehicles. *International Conference on Computer Science and Software Engineering*, 1:993–996, 2008.

[21] C. Martinez, I. Mondragon, M. Olivares-Mendez, and P. Campoy. On-board and ground visual pose estimation techniques for uav control. *Journal of Intellegent Robotic Systems*, 61:301–320, 2011.

[22] S. Arora, S. Jain, S. Scherer, S. Nuske, and L. Chamberlain. Infrastructure-free shipdeck tracking for autonomous landing. *IEEE International Conference on Robotics and Automation*, pages 323–330, 2013.

[23] S. Yang, S. Scherer, and A. Zell. An onboard monocular vision system for autonomous takeoff, hovering and landing of a micro aerial vehicle. *Journal of Intelligent and Robotic Systems*, 1-4:499–515, 2013.

[24] J. Sanchez-Lopez, J. Pestana, S. Saripalli, and P. Campoy. An approach toward visual autonomous ship board landing of a vtol uav. *Journal of Intellegent Robotic Systems*, 74:113–127, 2014.

[25] R. Mebarki, V. Lippiello, and B. Siciliano. Autonomous landing of rotary-wing aerial vehicles by image-based visual servoing in gps-denied environments. *IEEE International Symposium on Safety, Security, and Rescue Robotics*, 2015.

[26] Y. Shuo, Y. Jiahang, Y. Lu, and L. Zexiang. Precise quadrotor autonomous landing with srukf vision perception. *IEEE International Conference on Robotics and Automation*, pages 2196–2201, 2015.

[27] B. Edwards, J. Archibald, W. Fife, and D. Lee. A vision system for precision mav targeted landing. *International Symposium on Computational Intelligence in Robotics and Automation*, pages 125–130, 2007.

[28] A. Masselli and A. Zell. A novel marker based tracking method for position and attitude control of mavs. *International Micro Air Vehicle Conference and Flight Competition*, pages 1–6, 2012.

[29] Y. Bi and H. Duan. Implementation of autonomous visual tracking and landing for a low-cost quadrotor. *Optik - International Journal for Light and Electron Optics*, 124:3296–3300, 2013.

[30] I. Borshchova and S. O'Young. Visual servoing for autonomous landing of a multi-rotor uas on a moving platform. *Journal of Unmanned Vehicle Systems*, 5:13–26, 2017.

[31] I. Borshchova and S. O'Young. Marker-guided auto-landing on a moving platform. *Journal of Intelligent Unmanned Systems*, 5:28–42, 2017.

[32] A. Beyeler, C. Mattiussi, J-C. Zufferey, and D. Floreano. Vision based altitude and pitch estimation for ultra-light indoor microflyers. *IEEE International Conference on Robotics and Automation*, 2006.

[33] B. Barber, S. Griffiths, T. McLain, and R. Beard. Autonomous landing of miniature aerial vehicles. *Journal of Aerospace Computing, Information , and Communication*, 4:770–784, 2007.

[34] S. Lange, N. Sunderhauf, and P. Protzel. Autonomous landing for a multirotor uav using vision. *International Conference on Simulation, Modeling and Programming for Autonomous Robots*, pages 482–491, 2008.

[35] S. Lange, N. Sunderhauf, and P. Protzel. A vision based onboard approach for landing and position control of an autonomous multirotor uav in gps-denied environments. *International Conference on Advanced Robotics*, pages 1–6, 2009.

[36] O. Arrar, N. Aouf, and I. Vitanov. Vision based autonomous landing of multirotor uav on moving platform. *Journal of Intellegent and Robotic Systems*, 85:369–384, 2017.

[37] S. Dotenco, F. Gallwitz, and E. Angelopoulou. Autonomous approach and landing for a low-cost quadrotor using monocular cameras. *Computer Vision - ECCV 2014 Workshops*, pages 209–222, 2014.

[38] J. Kim, Y. Jung, D. Lee, and D.H. Shim. Outdoor autonomous landing on a moving platform for quadrotors using an omnidirectional camera. *International Conference on Unmanned Aircraft Systems*, pages 1243–1252, 2014.

[39] L. Qui, Z. Song, and W. Shen. Computer vision scheme used for the automate landing of unmanned helicopter on ship deck. *Acta Aeronautica Et Astronautica Sinica*, 24:351–354, 2003.

[40] C. Xu, L. Qiu, M. Liu, B. Kong, and Y. Ge. Stereo vision based relative pose and motion estimation for unmanned helicopter landing. *IEEE Internation conferenc eon Information Aquisition*, pages 31–36, 2006.

[41] K. Hsia, S. Lien, and J. Su. Height estimation via stereo vision system for unmanned helicopter autonomous landing. *International Symposium on Computer Communication Control and Automation*, 2:257–260, 2010.

[42] Z. Yu, K. Nonami, J. Shin, and D. Celestino. 3d vision based landing control of a small scale autonomous helicopter. *Journal of Control Theory and Applications*, 8:61–68, 2010.

[43] M. Fischle and R. Bollesr. Random sample consensus: a paradigm for model fitting with applications to image analysis and automated cartography. *Communications of the ACM*, 24:381–395, 1981.

[44] X. Pan, D. Ma, L. Jin, and Z. Jiang. Vision-based approach angle and height estimation for uav landing. *Congress on Image and Signal Processing*, 3:801–805, 2008.

[45] M. Sereewatana, M. Ruchanurucks, and S. Siddhichai. Depth estimation of markers for uav automatic landing control using stereo vision with a single camera. *ICICTES*, 2014.

[46] C. Patruno1, M. Nitti1, A. Petitti1, E. Stella1, and T. D'Orazio. A vision-based approach for unmanned aerial vehicle landing. *Journal of Intelligent and Robotic Systems*, pages 645–664, 2019.

[47] D. Pebrianti, F. Kendoul, S. Azrad, W. Wang, and K. Nonami. Autonomous hovering and landing of a quad-rotor micro aerial vehicle by means of on ground stereo vision system. *Journal of System Design and Dynamics*, 4:269–284, 2010.

[48] W. Kong, D. Zhou, Y. Zhang, D. Zhang, X. Wang, B. Zhao, C. Yan, L. Shen, and J. Zhang. A ground-based optical system for autonomous landing. *IEEE/RSJ International Conference on Intelligent Robots and Systems*, pages 4797–4804, 2014.

[49] O. Yakimenko, I. Kaminer, W. Lentz, and P. Ghyzel. Unmanned aircraft navigation for shipboard landing using infrared vision. *IEEE Transactions on Aerospace and Electronic Systems*, 38:1181–1200, 2002.

[50] K. Wenzel, P. Rosset, and A. Zell. Automatic take off, hovering and landing control for miniature helicopters with low-cost onboard hardware. *Proceedings of the AMS09, Autonome Mobile Systeme 2009*, pages 73–80, 2009.

[51] K. Wenzel, P. Rosset, and A. Zell. Low-cost visual tracking of a landing place and hovering flight control with a microcontroller. *Journal of Intellegent Robotic Systems*, 57:297–311, 2010.

[52] Y. Gui, P. Guo, H. Zhang, Z. Lei, X. Zhou, J. Ding, and Q. Yu. Airborne vision-based navigation method for uav accuracy landing using infrared lamps. *Journal of Intelligent Robotic Systems*, 72:197–218, 2013.

[53] M. Faessler, E. Mueggler, K. Schwabe, and D. Scaramuzza. A monocular pose estimation system based on infrared leds. *International Conference on Robotics and Automation*, 2014.

[54] G. Xu, Y. Zhang, S. Ji, Y. Cheng, and Y. Tian. Research on computer vision-based for uav autonomous landing on a ship. *Pattern Recognition Letters*, 2009.

[55] K. Wenzel, A. Masselli, and A. Zell. Automatic take off, tracking and landing of a miniature uav on a moving carrier vehicle. *Journal of Intelligent Robotic Systems*, 61:221–238, 2011.

[56] G. Xu, X. Chen, B. Wang, K. Li, J. Wang, and X. Wei. A search strategy of uavs automatic landing on ship in all weathe. *International Conference on Electrical and Control Engineering*, pages 2857–2860, 2011.

[57] W. Xiaa-Hong, X. Gui-Li, T. Yu-Peng, W. Biao, and W. Jing-Dong. Uavs automatic landing in all weather based on the cooperative object and computer vision. *Second International Conference on Instrumentation and Measurement, Computer, Communication and Control*, pages 1346–1351, 2012.

[58] W. Kong, D. Zhang, X. Wang, Z. Xian, and J. Zhang. Autonomous landing of an uav with a ground-based actuated infrared stereo vision system. *IEEE/ASJ*

International Conference on Intelligent Robots and Systems, pages 2963–2970, 2013.

[59] A. Smith, H. Balakrishnan, M. Goraczko, and N. Priyantha. *Tracking Moving Devices with the Cricket Location System*. 2004.

[60] M. Kim and Y. Kim. Multiple uavs nonlinear guidance laws for stationary target observation with waypoint incidence angle constraint. *International Journal of Aeronautical and Space Sciences*, 14:67–74, 2013.

[61] B. Min, M-J Tahk, D. Shim, and H. Bang. Guidance law for visionbased automatic landing of uav. *KSAS International Journal*, 8:46–53, 2007.

[62] S. Saripalli and . G. Sukhatme. Landing on a moving target using an autonomous helicopter. *IEEE International Conference on Robotics and Automation*, 2007.

[63] S. Saripalli. Vision-based autonomous landing of an helicopter on a moving target. *AIAA Guidance, Navigation and Control Conference*, 2009.

[64] C. Wu, J. Qi, D. Song, J. Ha, S. Key, and C. Academ. Lp based path planning for autonomous landing of an unmanned helicopter on a moving platform. *The Journal of Unmanned System Technology*, 1, 2013.

[65] J. Chahl, M. Srinivasan, and S. Zhang. Landing strategies in honeybees and applications to uninhabited airborne vehicles. *The International Journal of Robotics Research*, 23:101–110, 2004.

[66] F. Ruffier and N. Franceschini. Visually guided micro-aerial vehicle: Automatic take off, terrain following, landing and wind reaction. *IEEE International Conference on Robotics and Automation*, 3:2339–2346, 2004.

[67] C. McCarthy, N. Barnes, and R. Mahony. A robust docking strategy for a mobile robot using flow field divergence. *IEEE Transactions on Robotics*, 24:832–842, 2008.

[68] B. Herisse, F. Russotto, T. Hamel, and R. Mahony. Hovering flight and vertical landing control of a vtol unmanned aerial vehicle using optical flow. *IEEE/RSJ International Conference on Intelligent Robots and Systems*, pages 801–806, 2008.

[69] B. Herisse, T. Hamel, R. Mahony, and F-X Russotto. The landing problem of a vtol unmanned aerial vehicle on a moving platform using optical flow. *IEEE/RSJ International Conference on Intellegent Robots and Systems*, pages 1600–1605, 2010.

[70] B. Herisse, T. Hamel, R. Mahony, and F-X Russotto. Landing a vtol unmanned aerial vehicle on a moving platform using optical flow. *IEEE Transactions on Robotics*, 28:77–89, 2012.

[71] S. Thurrowgood, R. Moore, D. Soccol, M. Knight, and M. Srinivasan. A biologically inspired, vision-based guidance system for automatic landing of a fixed-wing aircraft. *Journal of Field Robotics*, 31:699–727, 2014.

[72] F. Kendoul and B. Ahmed. Bio-inspired taupilot for automated aerial 4d docking and landing of unmanned aircraft systems. *IEEE/RSJ International Conference on Intelligent Robots and Systems*, pages 480–487, 2012.

[73] F. Kendoul. Four-dimensional guidance and control of movement using time-to-contact: Application to automated docking and landing of unmanned rotorcraft systems. *International Journal of Robotics Research*, 33:237–267, 2014.

[74] T. Khuswendi, H. Hindersah, and W. Adiprawita. Vision-based hardware-in-the loop simulation test of vision-based net-recovery for fixed-wing unmanned aerial vehicles. *Proceedings of the 2011 International Conference on Electrical Engineering and Informatics*, 2011.

[75] A. Budiyanto, A. Cahyadi, T. Adji, and O. Wahyunggoro. Uav obstacle avoidance using potential field under dynamic environment. *2015 International Conference on Control, Electronics, Renewable Energy and Communications (ICCEREC)*, 2015.

[76] C. Tazibt, N. Achir, P. Muhlethaler, and T. Djamah. Uav-based data gathering using an artificial potential fields approach. *IEEE 88th Vehicular Technology Conference*, 2018.

[77] E. Falomir, S. Chaumette, and G. Guerrini. Mobility strategies based on artificial potential fields for swarms of unmanned aerial vehicles. *Journe de lEcole Doctorale de Mathmatiques et Informatique Bordeaux 2018*, 2018.

[78] S. Oh, K. Pathak, S. Agrawal, H. Pota, and M. Garratt. Approaches for a tether-guided landing of an autonomous helicopter. *IEEE Transactions on Robotics*, 22:536–544, 2006.

[79] A. Mulligan, A. Osbrink, and M. Patterson. Precision recovery capability for small uas. *23rd Bristol UAV Systems Conference*, 2008.

[80] S. Yoon and Y. Kim. Pursuit guidance law and adaptive backstepping controller design for vision-based net-recovery uav. *AIAA Guidance, Navigation and Control Conference and Exhibit*, 2008.

[81] S. Yoon, H. Kim, and Y. Kim. Spiral landing trajectory and pursuit guidance law design for vision-based net-recovery uav. *AIAA Guidance, Navigation, and Control Conference*, 30:600–605, 2009.

[82] S. Yoon, H. Kim, and Y. Kim. Spiral landing guidance law design for unmanned aerial vehicle net-recovery. *Journal of Aerospace Engineering*, 224:1081–1096, 2010.

[83] M. Kim, D. Lee, J. Park, C. Park, H. Kim, and Y. Kim. Vision-based hardware-in-the loop simulation test of vision-based net-recovery for fixed-wing unmanned aerial vehicles. *3rd Asia-Pasific International Symposium on Aerospace*, pages 2857–2860, 2011.

[84] H. Kim, M. Kim, H. Lim, C. Park, S. Yoon, D. Lee, H. Choi, G. Oh, J. Park, and Y. Kim. Fully autonomous vision-based net-recovery landing system for a fixed-wing uav. *IEEE/ASME Transactions on Mechatronics*, 18:1320–1333, 2013.

[85] W. Kai, S. Chunzhen, and J. Yi. Research on adaptive guidance technology of uav ship landing system based on net recovery. *Procedia Engineering*, 99:10271034, 2015.

[86] S. Huh and D. Shim. A vision-based landing system for small unmanned aerial vehicles using an airbag. *Control Engineering Practice 18*, 18:812–823, 2010.

[87] S. Huh and D. Shim. A vision-based automatic landing method for fixed-wing uavs. *Journal of Intellegent Robotic Systems*, 57:217–231, 2010.

[88] B. Ferrier and R. Ernst. Fire scout launch and recovery considerations in unexpected ship roll motion conditions. *Naval Engineers Journal*, 129:87–98, 2017.

[89] P. Moriarty, R. Sheehy, and P. Doody. Neural networks to aid the autonomous landing of a uav on a ship. *Drones*, 2, 2018.

[90] S. Abujoub, J. McPhee, C. Westin, and R. Irani. Unmanned aerial vehicle landing on maritime vessels using signal prediction of the ship motion. *OCEANS 2018 MTS/IEEE Charleston*, 2018.

[91] B. Erginer and E. Altug. Modeling and pd control of a quadrotor vtol vehicle. *IEEE Intellegent Vehicles Symposium*, pages 894–899, 2007.

[92] J. Hervas, M. Reyhanoglu, and H. Tang. Automatic landing control of unmanned aerial vehicles on moving platforms. *2014 IEEE 23rd International Symposium on Industrial Electronics (ISIE)*, 2014.

[93] M. Bodson and M. Athans. Multivariable control of vtol aircraft for shipboard landing. *AIAA Guidance and Control Conference*, 1985.

[94] Y. Feng, C. Zhang, S. Baek, S. Rawashdeh, and A. Mohammadi. Autonomous landing of a uav on a moving platform using model predictive control. *2017 28th Irish Signals and Systems Conference (ISSC)*, 2017.

[95] B. Prasad and S. Pradeep. Automatic landing system design using feedback linearization method. *AIAA Infotech Aerospace 2007 Conference and Exhibit*, 2007.

[96] H. Voos and B. Nourghassemi. Nonlinear control of stabilized flight and landing for quadrotor uavs. *7th Workshop on Advanced Control and Diagnosis*, 2009.

[97] L. Marconi and A. Isidori. Robust output regulation for autonomous vertical landing. *39th IEEE Conference on Decision and Control*, 4:3590–3595, 2000.

[98] L. Marconi, A. Isidori, and A. Serrani. Autonomous vertical landing on an oscillating platform: an internal-model based approach. *Automatica*, 38:21–32, 2002.

[99] T. Lee and Y. Kim. Nonlinear adaptive flight control using backstepping and neural networks controller. *Journal of Guidance, Control and Dynamics*, 24:675–682, 2001.

[100] S. Bouabdallah and R. Siegwart. Backstepping and sliding-mode techniques applied to an indoor micro quadrotor. *Proceedings on the International Conference on Robotics and Automation*, pages 2247–2252, 2005.

[101] B. Ahmed and H. Pota. Backstepping-based landing control of a ruav using tether incorporating flapping correction dynamics. *Proceedings of the American Control Conference*, pages 2728–2733, 2008.

[102] B. Ahmed and H. Pota. Flight control of a rotary wing uav using backstepping. *IEEE International Conference on Control and Automation*, 57:1780–1785, 2009.

[103] S. Yoon, Y. Kim, and S. Park. Constrained adaptive backstepping controller design for aircraft landing in wind disturbance and actuator stuck. *International Journal of Aeronautical and Space Sciences*, 13:74–89, 2012.

[104] D. Lee, T. Ryan, and H. Kim. Autonomous landing of a vtol uav on a moving platform using image-based visual servoing. *IEEE International Conference on Robotics and Automation*, pages 971–976, 2012.

[105] H. Shin, D. You, and D. Shim. Autonomous shipboard landing algorithm for unmanned helicopters in crosswind. *International Conference on Unmanned Aircraft Systems*, pages 769–778, 2013.

[106] M. Livchitz, A. Abershitz, U. Soudak, and A. Kandel. Development of an automated fuzzy-logic-based expert system for unmanned landing. *Fuzzy Sets and Systems*, 93:145–159, 1998.

[107] K. Nho and R. Agarwal. Automatic landing system design using fuzzy logic. *Journal of Guidance, Navigation and Control*, 23:298–304, 2000.

[108] M. Olivares-Mendez, I. mondragon, and P. Campoy. Fuzzy controller for uav-landing task using 3d-position visual estimation. *IEEE International Conference on Fuzzy Systems*, pages 1–8, 2010.

[109] T. Koo and S. Sastry. Hybrid control of unmanned aerial vehicles for autonomous landing. *2nd AIAA Unmanned Unlimited Systems, Technologies, and Operations Conference*, 2003.

[110] S. Malaek, N. Sadati, H. Izadi, and M. Pakmehr. Intelligent autolanding controller design using neural networks and fuzzy logic. *5th Asian Control Conference*, 1:365–373, 2004.

[111] S. Khantsis and A. Bourmistrova. Uav controller design using evolutionary algorithms. In *AI 2005: Advances in Artificial Intelligence*, pages 1025–1030. Springer, 2005.

[112] F. Liao, J. Wang, E. Poh, and D. Li. Fault-tolerant robust automatic landing control design. *Journal of Guidance, Control, and Dynamics*, 28:854–871, 2005.

[113] S. Shue and R. Agarwal. Design of automatic landing systems using mixed h_2/h_∞ control. *Journal of Guidence, Control, and Dynamics*, 22:103–114, 1999.

[114] W. Wang, G. Song, K. Nonami, M. Hirata, and O. Miyazawa. Autonomous control for micro-flying robot and small wireless helicopter x.r.b. *IEEE/RSJ International Conference on Intelligent Robots and Systems*, pages 2906–2911, 2006.

[115] R. Wang, Z. Zhou, and Y. Shen. Flying-wing uav landing control and simulation based on mixed h_2/h_∞. *International Conference on Mechatronics and Automation*, pages 1523–1528, 2007.

[116] P.J. Braspenning, F. Thuijsman, and A.J.M.M. Weijters. *Artificial Neural Networks*. Springer, 1991.

[117] G. Cybenko. Approximation by superposition of a sigmoidal function. *Mathematics of Control, Signals, and Systems*, pages 303–314, 1989.

[118] S. Haykin. *Neural Networks: A Comprehensive Foundation*. Pearson, 2 edition, 1999.

[119] G. Santharam and P.S. Sastry. A reinforcement learning neural network for adaptive control of markov chains. *IEEE Transactions on Systems, Man, and Cybernetics - Part A: Systems and Humans*, 27:588 – 600, 1997.

[120] I.R. Young. *Wind Generated Ocean Waves*, volume 2. Elsevier Ltd., 1 edition, 1999.

[121] E.C. Tupper. Introduction to naval architecture. 2004.

[122] T. McAdams. Slope limits. *Aircraft Owners and Pilots Association*, 2012.

[123] Dronecode. Controller diagrams. *PX4 Development Guide (v1.9.0)*, 2019.

[124] Vladimir Ermakov. Mavlink to ros gateway with proxy for ground control station. `https://github.com/mavlink/mavros`, 2019.

[125] Johannes Meyer, Alexander Sendobry, Stefan Kohlbrecher, Uwe Klingauf, and Oskar von Stryk. Comprehensive simulation of quadrotor uavs using ros and gazebo. In *3rd Int. Conf. on Simulation, Modeling and Programming for Autonomous Robots (SIMPAR)*, page to appear, 2012.

[126] Musa Morena Marcusso Manhães, Sebastian A. Scherer, Martin Voss, Luiz Ricardo Douat, and Thomas Rauschenbach. UUV simulator: A gazebo-based package for underwater intervention and multi-robot simulation. In *OCEANS 2016 MTS/IEEE Monterey*. IEEE, sep 2016.

[127] Daniel Ingram. Simulating a stewart platform in gazebo using a plugin to allow control of a closed loop manipulator with ros. `https://github.com/daniel-s-ingram/stewart`, 2019.

[128] Aeryon SkyRanger. The benchmark in vtol suas flight performance, reliability and ease-of-use, 2016.

[129] W.-J Wang and T.-Z Shen. New doppler compensation algorithm for stepped-frequency signal processing. 26:353–364, 2006.

[130] S. Hirata, M. Kurosawa, and T. Katagiri. Ultrasonic distance and velocity measurement by low-calculation-cost doppler-shift compensation and high-resolution doppler velocity estimation with wide measurement range. *Acoustical Science and Technology*, 30:220–223, 2009.

[131] H. Roudsari and J.-F. Bousquet. Autonomous zero visibility landing of quadrotors on underway ships in a sea state. *Sensors*, 1, 2019.

[132] J. Ross, J. Lindsay, E. Gregson, A. Moore, J. Patel, and M. Seto. Collaboration of multi-domain marine robots towards above and below-water characterization of floating targets. *Proceedings of the 13th IEEE International Symposium on Robotic and Sensors Environments*, 2019.

[133] J. Ross, M. Seto, and C. Johnston. Zero visibility autonomous landing of quadrotors on underway ships in a sea state. *Proceedings of the 13th IEEE International Symposium on Robotic and Sensors Environments*, 2019.

[134] J. Ross, M. Seto, and C. Johnston. Autonomous zero visibility landing of quadrotors on underway ships in a sea state. *Proceedings of the 2019 OCEANS Conference & Exposition*, 2019.

SPRINGER NATURE LICENSE TERMS AND CONDITIONS

Mar 25, 2020

This Agreement between Dalhousie University Faculty of Engineering -- Jordan Ross ("You") and Springer Nature ("Springer Nature") consists of your license details and the terms and conditions provided by Springer Nature and Copyright Clearance Center.

License Number	4767920717188
License date	Feb 14, 2020
Licensed Content Publisher	Springer Nature
Licensed Content Publication	Journal of Intelligent and Robotic Systems
Licensed Content Title	An Approach Toward Visual Autonomous Ship Board Landing of a VTOL UAV
Licensed Content Author	Jose Luis Sanchez-Lopez, Jesus Pestana, Srikanth Saripalli et al
Licensed Content Date	Jan 1, 2013
Licensed Content Volume	74
Licensed Content Issue	1
Type of Use	Thesis/Dissertation
Requestor type	academic/university or research institute
Format	print and electronic
Portion	figures/tables/illustrations
Number of figures/tables/illustrations	1
Will you be translating?	no
Circulation/distribution	1 - 29
Author of this Springer Nature content	no
Title	PhD Student
Institution name	Dalhousie University
Expected presentation date	Apr 2020
Portions	fig 3 on page 3 of paper, 115 of journal
Requestor Location	Dalhousie University Faculty of Engineering 5269 Morris Street Halifax, NS B3H 4R2 Canada Attn: Jordan Ross
Total	**0.00 USD**
Terms and Conditions	

Springer Nature Customer Service Centre GmbH
Terms and Conditions

This agreement sets out the terms and conditions of the licence (the **Licence**) between you and **Springer Nature Customer Service Centre GmbH** (the **Licensor**). By clicking 'accept' and completing the transaction for the material (**Licensed Material**), you also confirm your acceptance of these terms and conditions.

1. Grant of License

1. 1. The Licensor grants you a personal, non-exclusive, non-transferable, world-wide licence to reproduce the Licensed Material for the purpose specified in your order only. Licences are granted for the specific use requested in the order and for

no other use, subject to the conditions below.

1. 2. The Licensor warrants that it has, to the best of its knowledge, the rights to license reuse of the Licensed Material. However, you should ensure that the material you are requesting is original to the Licensor and does not carry the copyright of another entity (as credited in the published version).

1. 3. If the credit line on any part of the material you have requested indicates that it was reprinted or adapted with permission from another source, then you should also seek permission from that source to reuse the material.

2. Scope of Licence

2. 1. You may only use the Licensed Content in the manner and to the extent permitted by these Ts&Cs and any applicable laws.

2. 2. A separate licence may be required for any additional use of the Licensed Material, e.g. where a licence has been purchased for print only use, separate permission must be obtained for electronic re-use. Similarly, a licence is only valid in the language selected and does not apply for editions in other languages unless additional translation rights have been granted separately in the licence. Any content owned by third parties are expressly excluded from the licence.

2. 3. Similarly, rights for additional components such as custom editions and derivatives require additional permission and may be subject to an additional fee. Please apply to Journalpermissions@springernature.com/bookpermissions@springernature.com for these rights.

2. 4. Where permission has been granted **free of charge** for material in print, permission may also be granted for any electronic version of that work, provided that the material is incidental to your work as a whole and that the electronic version is essentially equivalent to, or substitutes for, the print version.

2. 5. An alternative scope of licence may apply to signatories of the STM Permissions Guidelines, as amended from time to time.

3. Duration of Licence

3. 1. A licence for is valid from the date of purchase ('Licence Date') at the end of the relevant period in the below table:

Scope of Licence	Duration of Licence
Post on a website	12 months
Presentations	12 months
Books and journals	Lifetime of the edition in the language purchased

4. Acknowledgement

4. 1. The Licensor's permission must be acknowledged next to the Licenced Material in print. In electronic form, this acknowledgement must be visible at the same time as the figures/tables/illustrations or abstract, and must be hyperlinked to the journal/book's homepage. Our required acknowledgement format is in the Appendix below.

5. Restrictions on use

5. 1. Use of the Licensed Material may be permitted for incidental promotional use and minor editing privileges e.g. minor adaptations of single figures, changes of format, colour and/or style where the adaptation is credited as set out in Appendix 1 below. Any other changes including but not limited to, cropping, adapting, omitting material that affect the meaning, intention or moral rights of the author are strictly prohibited.

5. 2. You must not use any Licensed Material as part of any design or trademark.

5. 3. Licensed Material may be used in Open Access Publications (OAP) before publication by Springer Nature, but any Licensed Material must be removed from OAP sites prior to final publication.

6. Ownership of Rights

6. 1. Licensed Material remains the property of either Licensor or the relevant third party and any rights not explicitly granted herein are expressly reserved.

7. Warranty

IN NO EVENT SHALL LICENSOR BE LIABLE TO YOU OR ANY OTHER PARTY OR ANY OTHER PERSON OR FOR ANY SPECIAL, CONSEQUENTIAL, INCIDENTAL OR INDIRECT DAMAGES, HOWEVER CAUSED, ARISING OUT OF OR IN CONNECTION WITH THE DOWNLOADING, VIEWING OR USE OF THE MATERIALS REGARDLESS OF THE FORM OF ACTION, WHETHER FOR BREACH OF CONTRACT, BREACH OF WARRANTY, TORT, NEGLIGENCE, INFRINGEMENT OR OTHERWISE (INCLUDING, WITHOUT LIMITATION, DAMAGES BASED ON LOSS OF PROFITS, DATA, FILES, USE, BUSINESS OPPORTUNITY OR CLAIMS OF THIRD PARTIES), AND
WHETHER OR NOT THE PARTY HAS BEEN ADVISED OF THE POSSIBILITY OF SUCH DAMAGES. THIS LIMITATION SHALL APPLY NOTWITHSTANDING ANY FAILURE OF ESSENTIAL PURPOSE OF ANY LIMITED REMEDY PROVIDED HEREIN.

8. Limitations

8. 1. ***BOOKS ONLY:***Where **'reuse in a dissertation/thesis'** has been selected the following terms apply: Print rights of the final author's accepted manuscript (for clarity, NOT the published version) for up to 100 copies, electronic rights for use only on a personal website or institutional repository as defined by the Sherpa guideline (www.sherpa.ac.uk/romeo/).

9. Termination and Cancellation

9. 1. Licences will expire after the period shown in Clause 3 (above).

9. 2. Licensee reserves the right to terminate the Licence in the event that payment is not received in full or if there has been a breach of this agreement by you.

Appendix 1 — Acknowledgements:

For Journal Content:
Reprinted by permission from [**the Licensor**]: [**Journal Publisher** (e.g. Nature/Springer/Palgrave)] [**JOURNAL NAME**] [**REFERENCE CITATION** (Article name, Author(s) Name), [**COPYRIGHT**] (year of publication)

For **Advance Online Publication papers:**
Reprinted by permission from [**the Licensor**]: [**Journal Publisher** (e.g. Nature/Springer/Palgrave)] [**JOURNAL NAME**] [**REFERENCE CITATION** (Article name, Author(s) Name), [**COPYRIGHT**] (year of publication), advance online publication, day month year (doi: 10.1038/sj.[JOURNAL ACRONYM].)

For Adaptations/Translations:
Adapted/Translated by permission from [**the Licensor**]: [**Journal Publisher** (e.g. Nature/Springer/Palgrave)] [**JOURNAL NAME**] [**REFERENCE CITATION** (Article name, Author(s) Name), [**COPYRIGHT**] (year of publication)

Note: For any republication from the British Journal of Cancer, the following credit line style applies:

Reprinted/adapted/translated by permission from [**the Licensor**]: on behalf of Cancer Research UK: : [**Journal Publisher** (e.g. Nature/Springer/Palgrave)] [**JOURNAL NAME**] [**REFERENCE CITATION** (Article name, Author(s) Name), [**COPYRIGHT]** (year of publication)

For **Advance Online Publication** papers:
Reprinted by permission from The [**the Licensor**]: on behalf of Cancer Research UK: [**Journal Publisher** (e.g.

Nature/Springer/Palgrave)] [**JOURNAL NAME**] [**REFERENCE CITATION** (Article name, Author(s) Name), [**COPYRIGHT**] (year of publication), advance online publication, day month year (doi: 10.1038/sj.[JOURNAL ACRONYM])

For Book content:
Reprinted/adapted by permission from [**the Licensor**]: [**Book Publisher** (e.g. Palgrave Macmillan, Springer etc) [**Book Title**] by [**Book author**(s)] [**COPYRIGHT**] (year of publication)

Other Conditions:

Version 1.2

Questions? customercare@copyright.com or +1-855-239-3415 (toll free in the US) or +1-978-646-2777.

ELSEVIER LICENSE TERMS AND CONDITIONS

Mar 25, 2020

This Agreement between Dalhousie University Faculty of Engineering -- Jordan Ross ("You") and Elsevier ("Elsevier") consists of your license details and the terms and conditions provided by Elsevier and Copyright Clearance Center.

License Number	4767930188245
License date	Feb 14, 2020
Licensed Content Publisher	Elsevier
Licensed Content Publication	Optik - International Journal for Light and Electron Optics
Licensed Content Title	Implementation of autonomous visual tracking and landing for a low-cost quadrotor
Licensed Content Author	Yingcai Bi,Haibin Duan
Licensed Content Date	Sep 1, 2013
Licensed Content Volume	124
Licensed Content Issue	18
Licensed Content Pages	5
Start Page	3296
End Page	3300
Type of Use	reuse in a thesis/dissertation
Portion	figures/tables/illustrations
Number of figures/tables/illustrations	1
Format	both print and electronic
Are you the author of this Elsevier article?	No
Will you be translating?	No
Title	PhD Student
Institution name	Dalhousie University
Expected presentation date	Apr 2020
Portions	figure 3 on third page of paper
Requestor Location	Dalhousie University Faculty of Engineering 5269 Morris Street Halifax, NS B3H 4R2 Canada Attn: Jordan Ross
Publisher Tax ID	GB 494 6272 12
Total	**0.00 USD**
Terms and Conditions	

INTRODUCTION

1. The publisher for this copyrighted material is Elsevier. By clicking "accept" in connection with completing this licensing transaction, you agree that the following terms and conditions apply to this transaction (along with the Billing and Payment terms and conditions established by Copyright Clearance Center, Inc. ("CCC"), at the time that you opened your Rightslink account and that are available at any time at http://myaccount.copyright.com).

GENERAL TERMS

2. Elsevier hereby grants you permission to reproduce the aforementioned material subject to the terms and conditions indicated.

3. Acknowledgement: If any part of the material to be used (for example, figures) has appeared in our publication with credit or acknowledgement to another source, permission must also be sought from that source. If such permission is not obtained then that material may not be included in your publication/copies. Suitable acknowledgement to the source must be made, either as a footnote or in a reference list at the end of your publication, as follows:
"Reprinted from Publication title, Vol /edition number, Author(s), Title of article / title of chapter, Pages No., Copyright (Year), with permission from Elsevier [OR APPLICABLE SOCIETY COPYRIGHT OWNER]." Also Lancet special credit - "Reprinted from The Lancet, Vol. number, Author(s), Title of article, Pages No., Copyright (Year), with permission from Elsevier."
4. Reproduction of this material is confined to the purpose and/or media for which permission is hereby given.
5. Altering/Modifying Material: Not Permitted. However figures and illustrations may be altered/adapted minimally to serve your work. Any other abbreviations, additions, deletions and/or any other alterations shall be made only with prior written authorization of Elsevier Ltd. (Please contact Elsevier at permissions@elsevier.com). No modifications can be made to any Lancet figures/tables and they must be reproduced in full.
6. If the permission fee for the requested use of our material is waived in this instance, please be advised that your future requests for Elsevier materials may attract a fee.
7. Reservation of Rights: Publisher reserves all rights not specifically granted in the combination of (i) the license details provided by you and accepted in the course of this licensing transaction, (ii) these terms and conditions and (iii) CCC's Billing and Payment terms and conditions.
8. License Contingent Upon Payment: While you may exercise the rights licensed immediately upon issuance of the license at the end of the licensing process for the transaction, provided that you have disclosed complete and accurate details of your proposed use, no license is finally effective unless and until full payment is received from you (either by publisher or by CCC) as provided in CCC's Billing and Payment terms and conditions. If full payment is not received on a timely basis, then any license preliminarily granted shall be deemed automatically revoked and shall be void as if never granted. Further, in the event that you breach any of these terms and conditions or any of CCC's Billing and Payment terms and conditions, the license is automatically revoked and shall be void as if never granted. Use of materials as described in a revoked license, as well as any use of the materials beyond the scope of an unrevoked license, may constitute copyright infringement and publisher reserves the right to take any and all action to protect its copyright in the materials.
9. Warranties: Publisher makes no representations or warranties with respect to the licensed material.
10. Indemnity: You hereby indemnify and agree to hold harmless publisher and CCC, and their respective officers, directors, employees and agents, from and against any and all claims arising out of your use of the licensed material other than as specifically authorized pursuant to this license.
11. No Transfer of License: This license is personal to you and may not be sublicensed, assigned, or transferred by you to any other person without publisher's written permission.
12. No Amendment Except in Writing: This license may not be amended except in a writing signed by both parties (or, in the case of publisher, by CCC on publisher's behalf).
13. Objection to Contrary Terms: Publisher hereby objects to any terms contained in any purchase order, acknowledgment, check endorsement or other writing prepared by you, which terms are inconsistent with these terms and conditions or CCC's Billing and Payment terms and conditions. These terms and conditions, together with CCC's Billing and Payment terms and conditions (which are incorporated herein), comprise the entire agreement between you and publisher (and CCC) concerning this licensing transaction. In the event of any conflict between your obligations established by these terms and conditions and those established by CCC's Billing and Payment terms and conditions, these terms and conditions shall control.
14. Revocation: Elsevier or Copyright Clearance Center may deny the permissions described in this License at their sole discretion, for any reason or no reason, with a full refund payable to you. Notice of such denial will be made using the contact information provided by you. Failure to receive such notice will not alter or invalidate the denial. In no event will Elsevier or Copyright Clearance Center be responsible or liable for any costs, expenses or damage incurred by you as a result of a denial of your permission request, other than a refund of the amount(s) paid by you to Elsevier and/or Copyright Clearance Center for denied permissions.

LIMITED LICENSE

The following terms and conditions apply only to specific license types:
15. **Translation**: This permission is granted for non-exclusive world **English** rights only unless your license was granted for translation rights. If you licensed translation rights you may only translate this content into the languages you requested. A professional translator must perform all translations and reproduce the content word for word preserving the integrity of the article.
16. **Posting licensed content on any Website**: The following terms and conditions apply as follows: Licensing material from an Elsevier journal: All content posted to the web site must maintain the copyright information line on the bottom of each image; A hyper-text must be included to the Homepage of the journal from which you are licensing at http://www.sciencedirect.com/science/journal/xxxxx or the Elsevier homepage for books at http://www.elsevier.com; Central Storage: This license does not include permission for a scanned version of the material to be stored in a central repository such as that provided by Heron/XanEdu.
Licensing material from an Elsevier book: A hyper-text link must be included to the Elsevier homepage at http://www.elsevier.com . All content posted to the web site must maintain the copyright information line on the bottom of each image.

Posting licensed content on Electronic reserve: In addition to the above the following clauses are applicable: The web site must

be password-protected and made available only to bona fide students registered on a relevant course. This permission is granted for 1 year only. You may obtain a new license for future website posting.

17. **For journal authors:** the following clauses are applicable in addition to the above:

Preprints:

A preprint is an author's own write-up of research results and analysis, it has not been peer-reviewed, nor has it had any other value added to it by a publisher (such as formatting, copyright, technical enhancement etc.).

Authors can share their preprints anywhere at any time. Preprints should not be added to or enhanced in any way in order to appear more like, or to substitute for, the final versions of articles however authors can update their preprints on arXiv or RePEc with their Accepted Author Manuscript (see below).

If accepted for publication, we encourage authors to link from the preprint to their formal publication via its DOI. Millions of researchers have access to the formal publications on ScienceDirect, and so links will help users to find, access, cite and use the best available version. Please note that Cell Press, The Lancet and some society-owned have different preprint policies. Information on these policies is available on the journal homepage.

Accepted Author Manuscripts: An accepted author manuscript is the manuscript of an article that has been accepted for publication and which typically includes author-incorporated changes suggested during submission, peer review and editor-author communications.

Authors can share their accepted author manuscript:

- immediately
  - via their non-commercial person homepage or blog
  - by updating a preprint in arXiv or RePEc with the accepted manuscript
  - via their research institute or institutional repository for internal institutional uses or as part of an invitation-only research collaboration work-group
  - directly by providing copies to their students or to research collaborators for their personal use
  - for private scholarly sharing as part of an invitation-only work group on commercial sites with which Elsevier has an agreement
- After the embargo period
  - via non-commercial hosting platforms such as their institutional repository
  - via commercial sites with which Elsevier has an agreement

In all cases accepted manuscripts should:

- link to the formal publication via its DOI
- bear a CC-BY-NC-ND license - this is easy to do
- if aggregated with other manuscripts, for example in a repository or other site, be shared in alignment with our hosting policy not be added to or enhanced in any way to appear more like, or to substitute for, the published journal article.

Published journal article (JPA): A published journal article (PJA) is the definitive final record of published research that appears or will appear in the journal and embodies all value-adding publishing activities including peer review co-ordination, copy-editing, formatting, (if relevant) pagination and online enrichment.

Policies for sharing publishing journal articles differ for subscription and gold open access articles:

Subscription Articles: If you are an author, please share a link to your article rather than the full-text. Millions of researchers have access to the formal publications on ScienceDirect, and so links will help your users to find, access, cite, and use the best available version.

Theses and dissertations which contain embedded PJAs as part of the formal submission can be posted publicly by the awarding institution with DOI links back to the formal publications on ScienceDirect.

If you are affiliated with a library that subscribes to ScienceDirect you have additional private sharing rights for others' research accessed under that agreement. This includes use for classroom teaching and internal training at the institution (including use in course packs and courseware programs), and inclusion of the article for grant funding purposes.

Gold Open Access Articles: May be shared according to the author-selected end-user license and should contain a CrossMark logo, the end user license, and a DOI link to the formal publication on ScienceDirect.

Please refer to Elsevier's posting policy for further information.

18. **For book authors** the following clauses are applicable in addition to the above: Authors are permitted to place a brief summary of their work online only. You are not allowed to download and post the published electronic version of your chapter, nor may you scan the printed edition to create an electronic version. **Posting to a repository:** Authors are permitted to post a summary of their chapter only in their institution's repository.

19. **Thesis/Dissertation**: If your license is for use in a thesis/dissertation your thesis may be submitted to your institution in either print or electronic form. Should your thesis be published commercially, please reapply for permission. These requirements include permission for the Library and Archives of Canada to supply single copies, on demand, of the complete thesis and include permission for Proquest/UMI to supply single copies, on demand, of the complete thesis. Should your thesis be published commercially, please reapply for permission. Theses and dissertations which contain embedded PJAs as part of the formal submission can be posted publicly by the awarding institution with DOI links back to the formal publications on ScienceDirect.

Elsevier Open Access Terms and Conditions

You can publish open access with Elsevier in hundreds of open access journals or in nearly 2000 established subscription journals that support open access publishing. Permitted third party re-use of these open access articles is defined by the author's choice of Creative Commons user license. See our open access license policy for more information.

Terms & Conditions applicable to all Open Access articles published with Elsevier:

Any reuse of the article must not represent the author as endorsing the adaptation of the article nor should the article be modified in such a way as to damage the author's honour or reputation. If any changes have been made, such changes must be clearly indicated.

The author(s) must be appropriately credited and we ask that you include the end user license and a DOI link to the formal publication on ScienceDirect.

If any part of the material to be used (for example, figures) has appeared in our publication with credit or acknowledgement to another source it is the responsibility of the user to ensure their reuse complies with the terms and conditions determined by the rights holder.

Additional Terms & Conditions applicable to each Creative Commons user license:

CC BY: The CC-BY license allows users to copy, to create extracts, abstracts and new works from the Article, to alter and revise the Article and to make commercial use of the Article (including reuse and/or resale of the Article by commercial entities), provided the user gives appropriate credit (with a link to the formal publication through the relevant DOI), provides a link to the license, indicates if changes were made and the licensor is not represented as endorsing the use made of the work. The full details of the license are available at http://creativecommons.org/licenses/by/4.0.

CC BY NC SA: The CC BY-NC-SA license allows users to copy, to create extracts, abstracts and new works from the Article, to alter and revise the Article, provided this is not done for commercial purposes, and that the user gives appropriate credit (with a link to the formal publication through the relevant DOI), provides a link to the license, indicates if changes were made and the licensor is not represented as endorsing the use made of the work. Further, any new works must be made available on the same conditions. The full details of the license are available at http://creativecommons.org/licenses/by-nc-sa/4.0.

CC BY NC ND: The CC BY-NC-ND license allows users to copy and distribute the Article, provided this is not done for commercial purposes and further does not permit distribution of the Article if it is changed or edited in any way, and provided the user gives appropriate credit (with a link to the formal publication through the relevant DOI), provides a link to the license, and that the licensor is not represented as endorsing the use made of the work. The full details of the license are available at http://creativecommons.org/licenses/by-nc-nd/4.0. Any commercial reuse of Open Access articles published with a CC BY NC SA or CC BY NC ND license requires permission from Elsevier and will be subject to a fee.

Commercial reuse includes:

- Associating advertising with the full text of the Article
- Charging fees for document delivery or access
- Article aggregation
- Systematic distribution via e-mail lists or share buttons

Posting or linking by commercial companies for use by customers of those companies.

20. **Other Conditions**:

v1.9

Questions? customercare@copyright.com or +1-855-239-3415 (toll free in the US) or +1-978-646-2777.

SPRINGER NATURE LICENSE TERMS AND CONDITIONS

Mar 25, 2020

This Agreement between Dalhousie University Faculty of Engineering -- Jordan Ross ("You") and Springer Nature ("Springer Nature") consists of your license details and the terms and conditions provided by Springer Nature and Copyright Clearance Center.

License Number	4767930928701
License date	Feb 14, 2020
Licensed Content Publisher	Springer Nature
Licensed Content Publication	Journal of Intelligent and Robotic Systems
Licensed Content Title	On-board and Ground Visual Pose Estimation Techniques for UAV Control
Licensed Content Author	Carol Martínez, Iván F. Mondragón, Miguel A. Olivares-Méndez et al
Licensed Content Date	Jan 1, 2010
Licensed Content Volume	61
Licensed Content Issue	1
Type of Use	Thesis/Dissertation
Requestor type	academic/university or research institute
Format	print and electronic
Portion	figures/tables/illustrations
Number of figures/tables/illustrations	1
Will you be translating?	no
Circulation/distribution	1 - 29
Author of this Springer Nature content	no
Title	PhD Student
Institution name	Dalhousie University
Expected presentation date	Apr 2020
Portions	figure 10 on page 12 of paper
Requestor Location	Dalhousie University Faculty of Engineering 5269 Morris Street Halifax, NS B3H 4R2 Canada Attn: Jordan Ross
Total	**0.00 USD**
Terms and Conditions	

Springer Nature Customer Service Centre GmbH
Terms and Conditions

This agreement sets out the terms and conditions of the licence (the **Licence**) between you and **Springer Nature Customer Service Centre GmbH** (the **Licensor**). By clicking 'accept' and completing the transaction for the material (**Licensed Material**), you also confirm your acceptance of these terms and conditions.

1. Grant of License

1. 1. The Licensor grants you a personal, non-exclusive, non-transferable, world-wide licence to reproduce the Licensed Material for the purpose specified in your order only. Licences are granted for the specific use requested in the order and for

no other use, subject to the conditions below.

1. 2. The Licensor warrants that it has, to the best of its knowledge, the rights to license reuse of the Licensed Material. However, you should ensure that the material you are requesting is original to the Licensor and does not carry the copyright of another entity (as credited in the published version).

1. 3. If the credit line on any part of the material you have requested indicates that it was reprinted or adapted with permission from another source, then you should also seek permission from that source to reuse the material.

2. Scope of Licence

2. 1. You may only use the Licensed Content in the manner and to the extent permitted by these Ts&Cs and any applicable laws.

2. 2. A separate licence may be required for any additional use of the Licensed Material, e.g. where a licence has been purchased for print only use, separate permission must be obtained for electronic re-use. Similarly, a licence is only valid in the language selected and does not apply for editions in other languages unless additional translation rights have been granted separately in the licence. Any content owned by third parties are expressly excluded from the licence.

2. 3. Similarly, rights for additional components such as custom editions and derivatives require additional permission and may be subject to an additional fee. Please apply to Journalpermissions@springernature.com/bookpermissions@springernature.com for these rights.

2. 4. Where permission has been granted **free of charge** for material in print, permission may also be granted for any electronic version of that work, provided that the material is incidental to your work as a whole and that the electronic version is essentially equivalent to, or substitutes for, the print version.

2. 5. An alternative scope of licence may apply to signatories of the STM Permissions Guidelines, as amended from time to time.

3. Duration of Licence

3. 1. A licence for is valid from the date of purchase ('Licence Date') at the end of the relevant period in the below table:

Scope of Licence	Duration of Licence
Post on a website	12 months
Presentations	12 months
Books and journals	Lifetime of the edition in the language purchased

4. Acknowledgement

4. 1. The Licensor's permission must be acknowledged next to the Licenced Material in print. In electronic form, this acknowledgement must be visible at the same time as the figures/tables/illustrations or abstract, and must be hyperlinked to the journal/book's homepage. Our required acknowledgement format is in the Appendix below.

5. Restrictions on use

5. 1. Use of the Licensed Material may be permitted for incidental promotional use and minor editing privileges e.g. minor adaptations of single figures, changes of format, colour and/or style where the adaptation is credited as set out in Appendix 1 below. Any other changes including but not limited to, cropping, adapting, omitting material that affect the meaning, intention or moral rights of the author are strictly prohibited.

5. 2. You must not use any Licensed Material as part of any design or trademark.

5. 3. Licensed Material may be used in Open Access Publications (OAP) before publication by Springer Nature, but any Licensed Material must be removed from OAP sites prior to final publication.

6. Ownership of Rights

6. 1. Licensed Material remains the property of either Licensor or the relevant third party and any rights not explicitly granted herein are expressly reserved.

7. Warranty

IN NO EVENT SHALL LICENSOR BE LIABLE TO YOU OR ANY OTHER PARTY OR ANY OTHER PERSON OR FOR ANY SPECIAL, CONSEQUENTIAL, INCIDENTAL OR INDIRECT DAMAGES, HOWEVER CAUSED, ARISING OUT OF OR IN CONNECTION WITH THE DOWNLOADING, VIEWING OR USE OF THE MATERIALS REGARDLESS OF THE FORM OF ACTION, WHETHER FOR BREACH OF CONTRACT, BREACH OF WARRANTY, TORT, NEGLIGENCE, INFRINGEMENT OR OTHERWISE (INCLUDING, WITHOUT LIMITATION, DAMAGES BASED ON LOSS OF PROFITS, DATA, FILES, USE, BUSINESS OPPORTUNITY OR CLAIMS OF THIRD PARTIES), AND
WHETHER OR NOT THE PARTY HAS BEEN ADVISED OF THE POSSIBILITY OF SUCH DAMAGES. THIS LIMITATION SHALL APPLY NOTWITHSTANDING ANY FAILURE OF ESSENTIAL PURPOSE OF ANY LIMITED REMEDY PROVIDED HEREIN.

8. Limitations

8. 1. ***BOOKS ONLY:***Where **'reuse in a dissertation/thesis'** has been selected the following terms apply: Print rights of the final author's accepted manuscript (for clarity, NOT the published version) for up to 100 copies, electronic rights for use only on a personal website or institutional repository as defined by the Sherpa guideline (www.sherpa.ac.uk/romeo/).

9. Termination and Cancellation

9. 1. Licences will expire after the period shown in Clause 3 (above).

9. 2. Licensee reserves the right to terminate the Licence in the event that payment is not received in full or if there has been a breach of this agreement by you.

Appendix 1 — Acknowledgements:

For Journal Content:
Reprinted by permission from [**the Licensor**]: [**Journal Publisher** (e.g. Nature/Springer/Palgrave)] [**JOURNAL NAME**] [**REFERENCE CITATION** (Article name, Author(s) Name), [**COPYRIGHT**] (year of publication)

For **Advance Online Publication papers:**
Reprinted by permission from [**the Licensor**]: [**Journal Publisher** (e.g. Nature/Springer/Palgrave)] [**JOURNAL NAME**] [**REFERENCE CITATION** (Article name, Author(s) Name), [**COPYRIGHT**] (year of publication), advance online publication, day month year (doi: 10.1038/sj.[JOURNAL ACRONYM].)

For Adaptations/Translations:
Adapted/Translated by permission from [**the Licensor**]: [**Journal Publisher** (e.g. Nature/Springer/Palgrave)] [**JOURNAL NAME**] [**REFERENCE CITATION** (Article name, Author(s) Name), [**COPYRIGHT**] (year of publication)

Note: For any republication from the British Journal of Cancer, the following credit line style applies:

Reprinted/adapted/translated by permission from [**the Licensor**]: on behalf of Cancer Research UK: : [**Journal Publisher** (e.g. Nature/Springer/Palgrave)] [**JOURNAL NAME**] [**REFERENCE CITATION** (Article name, Author(s) Name), [**COPYRIGHT]** (year of publication)

For **Advance Online Publication** papers:
Reprinted by permission from The [**the Licensor**]: on behalf of Cancer Research UK: [**Journal Publisher** (e.g.

Nature/Springer/Palgrave)] [**JOURNAL NAME**] [**REFERENCE CITATION** (Article name, Author(s) Name), [**COPYRIGHT**] (year of publication), advance online publication, day month year (doi: 10.1038/sj.[JOURNAL ACRONYM])

For Book content:
Reprinted/adapted by permission from [**the Licensor**]: [**Book Publisher** (e.g. Palgrave Macmillan, Springer etc) [**Book Title**] by [**Book author**(s)] [**COPYRIGHT**] (year of publication)

Other Conditions:

Version 1.2

Questions? customercare@copyright.com or +1-855-239-3415 (toll free in the US) or +1-978-646-2777.

ELSEVIER LICENSE TERMS AND CONDITIONS

Mar 25, 2020

This Agreement between Dalhousie University Faculty of Engineering -- Jordan Ross ("You") and Elsevier ("Elsevier") consists of your license details and the terms and conditions provided by Elsevier and Copyright Clearance Center.

License Number	4767931468143
License date	Feb 14, 2020
Licensed Content Publisher	Elsevier
Licensed Content Publication	Pattern Recognition Letters
Licensed Content Title	Research on computer vision-based for UAV autonomous landing on a ship
Licensed Content Author	Guili Xu,Yong Zhang,Shengyu Ji,Yuehua Cheng,Yupeng Tian
Licensed Content Date	Apr 15, 2009
Licensed Content Volume	30
Licensed Content Issue	6
Licensed Content Pages	6
Start Page	600
End Page	605
Type of Use	reuse in a thesis/dissertation
Portion	figures/tables/illustrations
Number of figures/tables/illustrations	1
Format	both print and electronic
Are you the author of this Elsevier article?	No
Will you be translating?	No
Title	PhD Student
Institution name	Dalhousie University
Expected presentation date	Apr 2020
Portions	figure 12 on page 5. only using 1 of the 6 images
Requestor Location	Dalhousie University Faculty of Engineering 5269 Morris Street Halifax, NS B3H 4R2 Canada Attn: Jordan Ross
Publisher Tax ID	GB 494 6272 12
Total	**0.00 USD**
Terms and Conditions	

INTRODUCTION

1. The publisher for this copyrighted material is Elsevier. By clicking "accept" in connection with completing this licensing transaction, you agree that the following terms and conditions apply to this transaction (along with the Billing and Payment terms and conditions established by Copyright Clearance Center, Inc. ("CCC"), at the time that you opened your Rightslink account and that are available at any time at http://myaccount.copyright.com).

GENERAL TERMS

2. Elsevier hereby grants you permission to reproduce the aforementioned material subject to the terms and conditions indicated.

3. Acknowledgement: If any part of the material to be used (for example, figures) has appeared in our publication with credit or acknowledgement to another source, permission must also be sought from that source. If such permission is not obtained then that material may not be included in your publication/copies. Suitable acknowledgement to the source must be made, either as a footnote or in a reference list at the end of your publication, as follows:
"Reprinted from Publication title, Vol /edition number, Author(s), Title of article / title of chapter, Pages No., Copyright (Year), with permission from Elsevier [OR APPLICABLE SOCIETY COPYRIGHT OWNER]." Also Lancet special credit - "Reprinted from The Lancet, Vol. number, Author(s), Title of article, Pages No., Copyright (Year), with permission from Elsevier."
4. Reproduction of this material is confined to the purpose and/or media for which permission is hereby given.
5. Altering/Modifying Material: Not Permitted. However figures and illustrations may be altered/adapted minimally to serve your work. Any other abbreviations, additions, deletions and/or any other alterations shall be made only with prior written authorization of Elsevier Ltd. (Please contact Elsevier at permissions@elsevier.com). No modifications can be made to any Lancet figures/tables and they must be reproduced in full.
6. If the permission fee for the requested use of our material is waived in this instance, please be advised that your future requests for Elsevier materials may attract a fee.
7. Reservation of Rights: Publisher reserves all rights not specifically granted in the combination of (i) the license details provided by you and accepted in the course of this licensing transaction, (ii) these terms and conditions and (iii) CCC's Billing and Payment terms and conditions.
8. License Contingent Upon Payment: While you may exercise the rights licensed immediately upon issuance of the license at the end of the licensing process for the transaction, provided that you have disclosed complete and accurate details of your proposed use, no license is finally effective unless and until full payment is received from you (either by publisher or by CCC) as provided in CCC's Billing and Payment terms and conditions. If full payment is not received on a timely basis, then any license preliminarily granted shall be deemed automatically revoked and shall be void as if never granted. Further, in the event that you breach any of these terms and conditions or any of CCC's Billing and Payment terms and conditions, the license is automatically revoked and shall be void as if never granted. Use of materials as described in a revoked license, as well as any use of the materials beyond the scope of an unrevoked license, may constitute copyright infringement and publisher reserves the right to take any and all action to protect its copyright in the materials.
9. Warranties: Publisher makes no representations or warranties with respect to the licensed material.
10. Indemnity: You hereby indemnify and agree to hold harmless publisher and CCC, and their respective officers, directors, employees and agents, from and against any and all claims arising out of your use of the licensed material other than as specifically authorized pursuant to this license.
11. No Transfer of License: This license is personal to you and may not be sublicensed, assigned, or transferred by you to any other person without publisher's written permission.
12. No Amendment Except in Writing: This license may not be amended except in a writing signed by both parties (or, in the case of publisher, by CCC on publisher's behalf).
13. Objection to Contrary Terms: Publisher hereby objects to any terms contained in any purchase order, acknowledgment, check endorsement or other writing prepared by you, which terms are inconsistent with these terms and conditions or CCC's Billing and Payment terms and conditions. These terms and conditions, together with CCC's Billing and Payment terms and conditions (which are incorporated herein), comprise the entire agreement between you and publisher (and CCC) concerning this licensing transaction. In the event of any conflict between your obligations established by these terms and conditions and those established by CCC's Billing and Payment terms and conditions, these terms and conditions shall control.
14. Revocation: Elsevier or Copyright Clearance Center may deny the permissions described in this License at their sole discretion, for any reason or no reason, with a full refund payable to you. Notice of such denial will be made using the contact information provided by you. Failure to receive such notice will not alter or invalidate the denial. In no event will Elsevier or Copyright Clearance Center be responsible or liable for any costs, expenses or damage incurred by you as a result of a denial of your permission request, other than a refund of the amount(s) paid by you to Elsevier and/or Copyright Clearance Center for denied permissions.

LIMITED LICENSE

The following terms and conditions apply only to specific license types:
15. **Translation**: This permission is granted for non-exclusive world **English** rights only unless your license was granted for translation rights. If you licensed translation rights you may only translate this content into the languages you requested. A professional translator must perform all translations and reproduce the content word for word preserving the integrity of the article.
16. **Posting licensed content on any Website**: The following terms and conditions apply as follows: Licensing material from an Elsevier journal: All content posted to the web site must maintain the copyright information line on the bottom of each image; A hyper-text must be included to the Homepage of the journal from which you are licensing at http://www.sciencedirect.com/science/journal/xxxxx or the Elsevier homepage for books at http://www.elsevier.com; Central Storage: This license does not include permission for a scanned version of the material to be stored in a central repository such as that provided by Heron/XanEdu.
Licensing material from an Elsevier book: A hyper-text link must be included to the Elsevier homepage at http://www.elsevier.com . All content posted to the web site must maintain the copyright information line on the bottom of each image.

Posting licensed content on Electronic reserve: In addition to the above the following clauses are applicable: The web site must

be password-protected and made available only to bona fide students registered on a relevant course. This permission is granted for 1 year only. You may obtain a new license for future website posting.

17. **For journal authors:** the following clauses are applicable in addition to the above:

Preprints:

A preprint is an author's own write-up of research results and analysis, it has not been peer-reviewed, nor has it had any other value added to it by a publisher (such as formatting, copyright, technical enhancement etc.).

Authors can share their preprints anywhere at any time. Preprints should not be added to or enhanced in any way in order to appear more like, or to substitute for, the final versions of articles however authors can update their preprints on arXiv or RePEc with their Accepted Author Manuscript (see below).

If accepted for publication, we encourage authors to link from the preprint to their formal publication via its DOI. Millions of researchers have access to the formal publications on ScienceDirect, and so links will help users to find, access, cite and use the best available version. Please note that Cell Press, The Lancet and some society-owned have different preprint policies. Information on these policies is available on the journal homepage.

Accepted Author Manuscripts: An accepted author manuscript is the manuscript of an article that has been accepted for publication and which typically includes author-incorporated changes suggested during submission, peer review and editor-author communications.

Authors can share their accepted author manuscript:

- immediately
    - via their non-commercial person homepage or blog
    - by updating a preprint in arXiv or RePEc with the accepted manuscript
    - via their research institute or institutional repository for internal institutional uses or as part of an invitation-only research collaboration work-group
    - directly by providing copies to their students or to research collaborators for their personal use
    - for private scholarly sharing as part of an invitation-only work group on commercial sites with which Elsevier has an agreement
- After the embargo period
    - via non-commercial hosting platforms such as their institutional repository
    - via commercial sites with which Elsevier has an agreement

In all cases accepted manuscripts should:

- link to the formal publication via its DOI
- bear a CC-BY-NC-ND license - this is easy to do
- if aggregated with other manuscripts, for example in a repository or other site, be shared in alignment with our hosting policy not be added to or enhanced in any way to appear more like, or to substitute for, the published journal article.

Published journal article (JPA): A published journal article (PJA) is the definitive final record of published research that appears or will appear in the journal and embodies all value-adding publishing activities including peer review co-ordination, copy-editing, formatting, (if relevant) pagination and online enrichment.

Policies for sharing publishing journal articles differ for subscription and gold open access articles:

Subscription Articles: If you are an author, please share a link to your article rather than the full-text. Millions of researchers have access to the formal publications on ScienceDirect, and so links will help your users to find, access, cite, and use the best available version.

Theses and dissertations which contain embedded PJAs as part of the formal submission can be posted publicly by the awarding institution with DOI links back to the formal publications on ScienceDirect.

If you are affiliated with a library that subscribes to ScienceDirect you have additional private sharing rights for others' research accessed under that agreement. This includes use for classroom teaching and internal training at the institution (including use in course packs and courseware programs), and inclusion of the article for grant funding purposes.

Gold Open Access Articles: May be shared according to the author-selected end-user license and should contain a CrossMark logo, the end user license, and a DOI link to the formal publication on ScienceDirect.

Please refer to Elsevier's posting policy for further information.

18. **For book authors** the following clauses are applicable in addition to the above: Authors are permitted to place a brief summary of their work online only. You are not allowed to download and post the published electronic version of your chapter, nor may you scan the printed edition to create an electronic version. **Posting to a repository:** Authors are permitted to post a summary of their chapter only in their institution's repository.

19. **Thesis/Dissertation**: If your license is for use in a thesis/dissertation your thesis may be submitted to your institution in either print or electronic form. Should your thesis be published commercially, please reapply for permission. These requirements include permission for the Library and Archives of Canada to supply single copies, on demand, of the complete thesis and include permission for Proquest/UMI to supply single copies, on demand, of the complete thesis. Should your thesis be published commercially, please reapply for permission. Theses and dissertations which contain embedded PJAs as part of the formal submission can be posted publicly by the awarding institution with DOI links back to the formal publications on ScienceDirect.

Elsevier Open Access Terms and Conditions

You can publish open access with Elsevier in hundreds of open access journals or in nearly 2000 established subscription journals that support open access publishing. Permitted third party re-use of these open access articles is defined by the author's choice of Creative Commons user license. See our open access license policy for more information.

Terms & Conditions applicable to all Open Access articles published with Elsevier:

Any reuse of the article must not represent the author as endorsing the adaptation of the article nor should the article be modified in such a way as to damage the author's honour or reputation. If any changes have been made, such changes must be clearly indicated.

The author(s) must be appropriately credited and we ask that you include the end user license and a DOI link to the formal publication on ScienceDirect.

If any part of the material to be used (for example, figures) has appeared in our publication with credit or acknowledgement to another source it is the responsibility of the user to ensure their reuse complies with the terms and conditions determined by the rights holder.

Additional Terms & Conditions applicable to each Creative Commons user license:

CC BY: The CC-BY license allows users to copy, to create extracts, abstracts and new works from the Article, to alter and revise the Article and to make commercial use of the Article (including reuse and/or resale of the Article by commercial entities), provided the user gives appropriate credit (with a link to the formal publication through the relevant DOI), provides a link to the license, indicates if changes were made and the licensor is not represented as endorsing the use made of the work. The full details of the license are available at http://creativecommons.org/licenses/by/4.0.

CC BY NC SA: The CC BY-NC-SA license allows users to copy, to create extracts, abstracts and new works from the Article, to alter and revise the Article, provided this is not done for commercial purposes, and that the user gives appropriate credit (with a link to the formal publication through the relevant DOI), provides a link to the license, indicates if changes were made and the licensor is not represented as endorsing the use made of the work. Further, any new works must be made available on the same conditions. The full details of the license are available at http://creativecommons.org/licenses/by-nc-sa/4.0.

CC BY NC ND: The CC BY-NC-ND license allows users to copy and distribute the Article, provided this is not done for commercial purposes and further does not permit distribution of the Article if it is changed or edited in any way, and provided the user gives appropriate credit (with a link to the formal publication through the relevant DOI), provides a link to the license, and that the licensor is not represented as endorsing the use made of the work. The full details of the license are available at http://creativecommons.org/licenses/by-nc-nd/4.0. Any commercial reuse of Open Access articles published with a CC BY NC SA or CC BY NC ND license requires permission from Elsevier and will be subject to a fee.

Commercial reuse includes:

- Associating advertising with the full text of the Article
- Charging fees for document delivery or access
- Article aggregation
- Systematic distribution via e-mail lists or share buttons

Posting or linking by commercial companies for use by customers of those companies.

20. **Other Conditions**:

v1.9

Questions? customercare@copyright.com or +1-855-239-3415 (toll free in the US) or +1-978-646-2777.

JOHN WILEY AND SONS LICENSE TERMS AND CONDITIONS

Mar 25, 2020

This Agreement between Dalhousie University Faculty of Engineering -- Jordan Ross ("You") and John Wiley and Sons ("John Wiley and Sons") consists of your license details and the terms and conditions provided by John Wiley and Sons and Copyright Clearance Center.

License Number	4767950443853
License date	Feb 14, 2020
Licensed Content Publisher	John Wiley and Sons
Licensed Content Publication	Journal of Field Robotics
Licensed Content Title	A Biologically Inspired, Vision-based Guidance System for Automatic Landing of a Fixed-wing Aircraft
Licensed Content Author	Saul Thurrowgood, Richard J. D. Moore, Dean Soccol, et al
Licensed Content Date	Jun 5, 2014
Licensed Content Volume	31
Licensed Content Issue	4
Licensed Content Pages	29
Type of Use	Dissertation/Thesis
Requestor type	University/Academic
Format	Print and electronic
Portion	Figure/table
Number of figures/tables	1
Original Wiley figure/table number(s)	figure 1 (a part of it)
Will you be translating?	No
Title of your thesis / dissertation	PhD Student
Expected completion date	Apr 2020
Expected size (number of pages)	1
Requestor Location	Dalhousie University Faculty of Engineering 5269 Morris Street Halifax, NS B3H 4R2 Canada Attn: Jordan Ross
Publisher Tax ID	EU826007151
Total	**0.00 USD**
Terms and Conditions	

TERMS AND CONDITIONS

This copyrighted material is owned by or exclusively licensed to John Wiley & Sons, Inc. or one of its group companies (each a"Wiley Company") or handled on behalf of a society with which a Wiley Company has exclusive publishing rights in relation to a particular work (collectively "WILEY"). By clicking "accept" in connection with completing this licensing transaction, you agree that the following terms and conditions apply to this transaction (along with the billing and payment terms and conditions established by the Copyright Clearance Center Inc., ("CCC's Billing and Payment terms and conditions"), at the time that you opened your RightsLink account (these are available at any time at http://myaccount.copyright.com).

Terms and Conditions

- The materials you have requested permission to reproduce or reuse (the "Wiley Materials") are protected by copyright.

- You are hereby granted a personal, non-exclusive, non-sub licensable (on a stand-alone basis), non-transferable, worldwide, limited license to reproduce the Wiley Materials for the purpose specified in the licensing process. This license, **and any CONTENT (PDF or image file) purchased as part of your order,** is for a one-time use only and limited to any maximum distribution number specified in the license. The first instance of republication or reuse granted by this license must be completed within two years of the date of the grant of this license (although copies prepared before the end date may be distributed thereafter). The Wiley Materials shall not be used in any other manner or for any other purpose, beyond what is granted in the license. Permission is granted subject to an appropriate acknowledgement given to the author, title of the material/book/journal and the publisher. You shall also duplicate the copyright notice that appears in the Wiley publication in your use of the Wiley Material. Permission is also granted on the understanding that nowhere in the text is a previously published source acknowledged for all or part of this Wiley Material. Any third party content is expressly excluded from this permission.

- With respect to the Wiley Materials, all rights are reserved. Except as expressly granted by the terms of the license, no part of the Wiley Materials may be copied, modified, adapted (except for minor reformatting required by the new Publication), translated, reproduced, transferred or distributed, in any form or by any means, and no derivative works may be made based on the Wiley Materials without the prior permission of the respective copyright owner.**For STM Signatory Publishers clearing permission under the terms of the STM Permissions Guidelines only, the terms of the license are extended to include subsequent editions and for editions in other languages, provided such editions are for the work as a whole in situ and does not involve the separate exploitation of the permitted figures or extracts,** You may not alter, remove or suppress in any manner any copyright, trademark or other notices displayed by the Wiley Materials. You may not license, rent, sell, loan, lease, pledge, offer as security, transfer or assign the Wiley Materials on a stand-alone basis, or any of the rights granted to you hereunder to any other person.

- The Wiley Materials and all of the intellectual property rights therein shall at all times remain the exclusive property of John Wiley & Sons Inc, the Wiley Companies, or their respective licensors, and your interest therein is only that of having possession of and the right to reproduce the Wiley Materials pursuant to Section 2 herein during the continuance of this Agreement. You agree that you own no right, title or interest in or to the Wiley Materials or any of the intellectual property rights therein. You shall have no rights hereunder other than the license as provided for above in Section 2. No right, license or interest to any trademark, trade name, service mark or other branding ("Marks") of WILEY or its licensors is granted hereunder, and you agree that you shall not assert any such right, license or interest with respect thereto

- NEITHER WILEY NOR ITS LICENSORS MAKES ANY WARRANTY OR REPRESENTATION OF ANY KIND TO YOU OR ANY THIRD PARTY, EXPRESS, IMPLIED OR STATUTORY, WITH RESPECT TO THE MATERIALS OR THE ACCURACY OF ANY INFORMATION CONTAINED IN THE MATERIALS, INCLUDING, WITHOUT LIMITATION, ANY IMPLIED WARRANTY OF MERCHANTABILITY, ACCURACY, SATISFACTORY QUALITY, FITNESS FOR A PARTICULAR PURPOSE, USABILITY, INTEGRATION OR NON-INFRINGEMENT AND ALL SUCH WARRANTIES ARE HEREBY EXCLUDED BY WILEY AND ITS LICENSORS AND WAIVED BY YOU.

- WILEY shall have the right to terminate this Agreement immediately upon breach of this Agreement by you.

- You shall indemnify, defend and hold harmless WILEY, its Licensors and their respective directors, officers, agents and employees, from and against any actual or threatened claims, demands, causes of action or proceedings arising from any breach of this Agreement by you.

- IN NO EVENT SHALL WILEY OR ITS LICENSORS BE LIABLE TO YOU OR ANY OTHER PARTY OR ANY OTHER PERSON OR ENTITY FOR ANY SPECIAL, CONSEQUENTIAL, INCIDENTAL, INDIRECT, EXEMPLARY OR PUNITIVE DAMAGES, HOWEVER CAUSED, ARISING OUT OF OR IN CONNECTION WITH THE DOWNLOADING, PROVISIONING, VIEWING OR USE OF THE MATERIALS REGARDLESS OF THE FORM OF ACTION, WHETHER FOR BREACH OF CONTRACT, BREACH OF WARRANTY, TORT, NEGLIGENCE, INFRINGEMENT OR OTHERWISE (INCLUDING, WITHOUT LIMITATION, DAMAGES BASED ON LOSS OF PROFITS, DATA, FILES, USE, BUSINESS OPPORTUNITY OR CLAIMS OF THIRD PARTIES), AND WHETHER OR NOT THE PARTY HAS BEEN ADVISED OF THE POSSIBILITY OF SUCH DAMAGES. THIS LIMITATION SHALL APPLY NOTWITHSTANDING ANY FAILURE OF ESSENTIAL PURPOSE OF ANY LIMITED REMEDY PROVIDED HEREIN.

- Should any provision of this Agreement be held by a court of competent jurisdiction to be illegal, invalid, or unenforceable, that provision shall be deemed amended to achieve as nearly as possible the same economic effect as the original provision,

and the legality, validity and enforceability of the remaining provisions of this Agreement shall not be affected or impaired thereby.

- The failure of either party to enforce any term or condition of this Agreement shall not constitute a waiver of either party's right to enforce each and every term and condition of this Agreement. No breach under this agreement shall be deemed waived or excused by either party unless such waiver or consent is in writing signed by the party granting such waiver or consent. The waiver by or consent of a party to a breach of any provision of this Agreement shall not operate or be construed as a waiver of or consent to any other or subsequent breach by such other party.

- This Agreement may not be assigned (including by operation of law or otherwise) by you without WILEY's prior written consent.

- Any fee required for this permission shall be non-refundable after thirty (30) days from receipt by the CCC.

- These terms and conditions together with CCC's Billing and Payment terms and conditions (which are incorporated herein) form the entire agreement between you and WILEY concerning this licensing transaction and (in the absence of fraud) supersedes all prior agreements and representations of the parties, oral or written. This Agreement may not be amended except in writing signed by both parties. This Agreement shall be binding upon and inure to the benefit of the parties' successors, legal representatives, and authorized assigns.

- In the event of any conflict between your obligations established by these terms and conditions and those established by CCC's Billing and Payment terms and conditions, these terms and conditions shall prevail.

- WILEY expressly reserves all rights not specifically granted in the combination of (i) the license details provided by you and accepted in the course of this licensing transaction, (ii) these terms and conditions and (iii) CCC's Billing and Payment terms and conditions.

- This Agreement will be void if the Type of Use, Format, Circulation, or Requestor Type was misrepresented during the licensing process.

- This Agreement shall be governed by and construed in accordance with the laws of the State of New York, USA, without regards to such state's conflict of law rules. Any legal action, suit or proceeding arising out of or relating to these Terms and Conditions or the breach thereof shall be instituted in a court of competent jurisdiction in New York County in the State of New York in the United States of America and each party hereby consents and submits to the personal jurisdiction of such court, waives any objection to venue in such court and consents to service of process by registered or certified mail, return receipt requested, at the last known address of such party.

WILEY OPEN ACCESS TERMS AND CONDITIONS

Wiley Publishes Open Access Articles in fully Open Access Journals and in Subscription journals offering Online Open. Although most of the fully Open Access journals publish open access articles under the terms of the Creative Commons Attribution (CC BY) License only, the subscription journals and a few of the Open Access Journals offer a choice of Creative Commons Licenses. The license type is clearly identified on the article.

The Creative Commons Attribution License

The Creative Commons Attribution License (CC-BY) allows users to copy, distribute and transmit an article, adapt the article and make commercial use of the article. The CC-BY license permits commercial and non-

Creative Commons Attribution Non-Commercial License

The Creative Commons Attribution Non-Commercial (CC-BY-NC)License permits use, distribution and reproduction in any medium, provided the original work is properly cited and is not used for commercial purposes.(see below)

Creative Commons Attribution-Non-Commercial-NoDerivs License

The Creative Commons Attribution Non-Commercial-NoDerivs License (CC-BY-NC-ND) permits use, distribution and reproduction in any medium, provided the original work is properly cited, is not used for commercial purposes and no modifications or adaptations are made. (see below)

Use by commercial "for-profit" organizations

Use of Wiley Open Access articles for commercial, promotional, or marketing purposes requires further explicit permission from Wiley and will be subject to a fee.

Further details can be found on Wiley Online Library http://olabout.wiley.com/WileyCDA/Section/id-410895.html

Other Terms and Conditions:

v1.10 Last updated September 2015

Questions? customercare@copyright.com or +1-855-239-3415 (toll free in the US) or +1-978-646-2777.

ELSEVIER LICENSE TERMS AND CONDITIONS

Mar 25, 2020

This Agreement between Dalhousie University Faculty of Engineering -- Jordan Ross ("You") and Elsevier ("Elsevier") consists of your license details and the terms and conditions provided by Elsevier and Copyright Clearance Center.

License Number	4770270914561
License date	Feb 15, 2020
Licensed Content Publisher	Elsevier
Licensed Content Publication	Control Engineering Practice
Licensed Content Title	A vision-based landing system for small unmanned aerial vehicles using an airbag
Licensed Content Author	Sungsik Huh,David Hyunchul Shim
Licensed Content Date	Jul 1, 2010
Licensed Content Volume	18
Licensed Content Issue	7
Licensed Content Pages	12
Start Page	812
End Page	823
Type of Use	reuse in a thesis/dissertation
Portion	figures/tables/illustrations
Number of figures/tables/illustrations	1
Format	both print and electronic
Are you the author of this Elsevier article?	No
Will you be translating?	No
Title	PhD Student
Institution name	Dalhousie University
Expected presentation date	Apr 2020
Portions	id like to use fig.15 in my literature review
Requestor Location	Dalhousie University Faculty of Engineering 5269 Morris Street Halifax, NS B3H 4R2 Canada Attn: Jordan Ross
Publisher Tax ID	GB 494 6272 12
Total	**0.00 USD**
Terms and Conditions	

INTRODUCTION

1. The publisher for this copyrighted material is Elsevier. By clicking "accept" in connection with completing this licensing transaction, you agree that the following terms and conditions apply to this transaction (along with the Billing and Payment terms and conditions established by Copyright Clearance Center, Inc. ("CCC"), at the time that you opened your Rightslink account and that are available at any time at http://myaccount.copyright.com).

GENERAL TERMS

2. Elsevier hereby grants you permission to reproduce the aforementioned material subject to the terms and conditions indicated.

3. Acknowledgement: If any part of the material to be used (for example, figures) has appeared in our publication with credit or acknowledgement to another source, permission must also be sought from that source. If such permission is not obtained then that material may not be included in your publication/copies. Suitable acknowledgement to the source must be made, either as a footnote or in a reference list at the end of your publication, as follows:
"Reprinted from Publication title, Vol /edition number, Author(s), Title of article / title of chapter, Pages No., Copyright (Year), with permission from Elsevier [OR APPLICABLE SOCIETY COPYRIGHT OWNER]." Also Lancet special credit - "Reprinted from The Lancet, Vol. number, Author(s), Title of article, Pages No., Copyright (Year), with permission from Elsevier."
4. Reproduction of this material is confined to the purpose and/or media for which permission is hereby given.
5. Altering/Modifying Material: Not Permitted. However figures and illustrations may be altered/adapted minimally to serve your work. Any other abbreviations, additions, deletions and/or any other alterations shall be made only with prior written authorization of Elsevier Ltd. (Please contact Elsevier at permissions@elsevier.com). No modifications can be made to any Lancet figures/tables and they must be reproduced in full.
6. If the permission fee for the requested use of our material is waived in this instance, please be advised that your future requests for Elsevier materials may attract a fee.
7. Reservation of Rights: Publisher reserves all rights not specifically granted in the combination of (i) the license details provided by you and accepted in the course of this licensing transaction, (ii) these terms and conditions and (iii) CCC's Billing and Payment terms and conditions.
8. License Contingent Upon Payment: While you may exercise the rights licensed immediately upon issuance of the license at the end of the licensing process for the transaction, provided that you have disclosed complete and accurate details of your proposed use, no license is finally effective unless and until full payment is received from you (either by publisher or by CCC) as provided in CCC's Billing and Payment terms and conditions. If full payment is not received on a timely basis, then any license preliminarily granted shall be deemed automatically revoked and shall be void as if never granted. Further, in the event that you breach any of these terms and conditions or any of CCC's Billing and Payment terms and conditions, the license is automatically revoked and shall be void as if never granted. Use of materials as described in a revoked license, as well as any use of the materials beyond the scope of an unrevoked license, may constitute copyright infringement and publisher reserves the right to take any and all action to protect its copyright in the materials.
9. Warranties: Publisher makes no representations or warranties with respect to the licensed material.
10. Indemnity: You hereby indemnify and agree to hold harmless publisher and CCC, and their respective officers, directors, employees and agents, from and against any and all claims arising out of your use of the licensed material other than as specifically authorized pursuant to this license.
11. No Transfer of License: This license is personal to you and may not be sublicensed, assigned, or transferred by you to any other person without publisher's written permission.
12. No Amendment Except in Writing: This license may not be amended except in a writing signed by both parties (or, in the case of publisher, by CCC on publisher's behalf).
13. Objection to Contrary Terms: Publisher hereby objects to any terms contained in any purchase order, acknowledgment, check endorsement or other writing prepared by you, which terms are inconsistent with these terms and conditions or CCC's Billing and Payment terms and conditions. These terms and conditions, together with CCC's Billing and Payment terms and conditions (which are incorporated herein), comprise the entire agreement between you and publisher (and CCC) concerning this licensing transaction. In the event of any conflict between your obligations established by these terms and conditions and those established by CCC's Billing and Payment terms and conditions, these terms and conditions shall control.
14. Revocation: Elsevier or Copyright Clearance Center may deny the permissions described in this License at their sole discretion, for any reason or no reason, with a full refund payable to you. Notice of such denial will be made using the contact information provided by you. Failure to receive such notice will not alter or invalidate the denial. In no event will Elsevier or Copyright Clearance Center be responsible or liable for any costs, expenses or damage incurred by you as a result of a denial of your permission request, other than a refund of the amount(s) paid by you to Elsevier and/or Copyright Clearance Center for denied permissions.

LIMITED LICENSE

The following terms and conditions apply only to specific license types:
15. **Translation**: This permission is granted for non-exclusive world **English** rights only unless your license was granted for translation rights. If you licensed translation rights you may only translate this content into the languages you requested. A professional translator must perform all translations and reproduce the content word for word preserving the integrity of the article.
16. **Posting licensed content on any Website**: The following terms and conditions apply as follows: Licensing material from an Elsevier journal: All content posted to the web site must maintain the copyright information line on the bottom of each image; A hyper-text must be included to the Homepage of the journal from which you are licensing at http://www.sciencedirect.com/science/journal/xxxxx or the Elsevier homepage for books at http://www.elsevier.com; Central Storage: This license does not include permission for a scanned version of the material to be stored in a central repository such as that provided by Heron/XanEdu.
Licensing material from an Elsevier book: A hyper-text link must be included to the Elsevier homepage at http://www.elsevier.com . All content posted to the web site must maintain the copyright information line on the bottom of each image.

Posting licensed content on Electronic reserve: In addition to the above the following clauses are applicable: The web site must

be password-protected and made available only to bona fide students registered on a relevant course. This permission is granted for 1 year only. You may obtain a new license for future website posting.

17. **For journal authors:** the following clauses are applicable in addition to the above:

Preprints:

A preprint is an author's own write-up of research results and analysis, it has not been peer-reviewed, nor has it had any other value added to it by a publisher (such as formatting, copyright, technical enhancement etc.).

Authors can share their preprints anywhere at any time. Preprints should not be added to or enhanced in any way in order to appear more like, or to substitute for, the final versions of articles however authors can update their preprints on arXiv or RePEc with their Accepted Author Manuscript (see below).

If accepted for publication, we encourage authors to link from the preprint to their formal publication via its DOI. Millions of researchers have access to the formal publications on ScienceDirect, and so links will help users to find, access, cite and use the best available version. Please note that Cell Press, The Lancet and some society-owned have different preprint policies. Information on these policies is available on the journal homepage.

Accepted Author Manuscripts: An accepted author manuscript is the manuscript of an article that has been accepted for publication and which typically includes author-incorporated changes suggested during submission, peer review and editor-author communications.

Authors can share their accepted author manuscript:

- immediately
  - via their non-commercial person homepage or blog
  - by updating a preprint in arXiv or RePEc with the accepted manuscript
  - via their research institute or institutional repository for internal institutional uses or as part of an invitation-only research collaboration work-group
  - directly by providing copies to their students or to research collaborators for their personal use
  - for private scholarly sharing as part of an invitation-only work group on commercial sites with which Elsevier has an agreement
- After the embargo period
  - via non-commercial hosting platforms such as their institutional repository
  - via commercial sites with which Elsevier has an agreement

In all cases accepted manuscripts should:

- link to the formal publication via its DOI
- bear a CC-BY-NC-ND license - this is easy to do
- if aggregated with other manuscripts, for example in a repository or other site, be shared in alignment with our hosting policy not be added to or enhanced in any way to appear more like, or to substitute for, the published journal article.

Published journal article (JPA): A published journal article (PJA) is the definitive final record of published research that appears or will appear in the journal and embodies all value-adding publishing activities including peer review co-ordination, copy-editing, formatting, (if relevant) pagination and online enrichment.

Policies for sharing publishing journal articles differ for subscription and gold open access articles:

Subscription Articles: If you are an author, please share a link to your article rather than the full-text. Millions of researchers have access to the formal publications on ScienceDirect, and so links will help your users to find, access, cite, and use the best available version.

Theses and dissertations which contain embedded PJAs as part of the formal submission can be posted publicly by the awarding institution with DOI links back to the formal publications on ScienceDirect.

If you are affiliated with a library that subscribes to ScienceDirect you have additional private sharing rights for others' research accessed under that agreement. This includes use for classroom teaching and internal training at the institution (including use in course packs and courseware programs), and inclusion of the article for grant funding purposes.

Gold Open Access Articles: May be shared according to the author-selected end-user license and should contain a CrossMark logo, the end user license, and a DOI link to the formal publication on ScienceDirect.

Please refer to Elsevier's posting policy for further information.

18. **For book authors** the following clauses are applicable in addition to the above: Authors are permitted to place a brief summary of their work online only. You are not allowed to download and post the published electronic version of your chapter, nor may you scan the printed edition to create an electronic version. **Posting to a repository:** Authors are permitted to post a summary of their chapter only in their institution's repository.

19. **Thesis/Dissertation**: If your license is for use in a thesis/dissertation your thesis may be submitted to your institution in either print or electronic form. Should your thesis be published commercially, please reapply for permission. These requirements include permission for the Library and Archives of Canada to supply single copies, on demand, of the complete thesis and include permission for Proquest/UMI to supply single copies, on demand, of the complete thesis. Should your thesis be published commercially, please reapply for permission. Theses and dissertations which contain embedded PJAs as part of the formal submission can be posted publicly by the awarding institution with DOI links back to the formal publications on ScienceDirect.

Elsevier Open Access Terms and Conditions

You can publish open access with Elsevier in hundreds of open access journals or in nearly 2000 established subscription journals that support open access publishing. Permitted third party re-use of these open access articles is defined by the author's choice of Creative Commons user license. See our open access license policy for more information.

Terms & Conditions applicable to all Open Access articles published with Elsevier:

Any reuse of the article must not represent the author as endorsing the adaptation of the article nor should the article be modified in such a way as to damage the author's honour or reputation. If any changes have been made, such changes must be clearly indicated.

The author(s) must be appropriately credited and we ask that you include the end user license and a DOI link to the formal publication on ScienceDirect.

If any part of the material to be used (for example, figures) has appeared in our publication with credit or acknowledgement to another source it is the responsibility of the user to ensure their reuse complies with the terms and conditions determined by the rights holder.

Additional Terms & Conditions applicable to each Creative Commons user license:

CC BY: The CC-BY license allows users to copy, to create extracts, abstracts and new works from the Article, to alter and revise the Article and to make commercial use of the Article (including reuse and/or resale of the Article by commercial entities), provided the user gives appropriate credit (with a link to the formal publication through the relevant DOI), provides a link to the license, indicates if changes were made and the licensor is not represented as endorsing the use made of the work. The full details of the license are available at http://creativecommons.org/licenses/by/4.0.

CC BY NC SA: The CC BY-NC-SA license allows users to copy, to create extracts, abstracts and new works from the Article, to alter and revise the Article, provided this is not done for commercial purposes, and that the user gives appropriate credit (with a link to the formal publication through the relevant DOI), provides a link to the license, indicates if changes were made and the licensor is not represented as endorsing the use made of the work. Further, any new works must be made available on the same conditions. The full details of the license are available at http://creativecommons.org/licenses/by-nc-sa/4.0.

CC BY NC ND: The CC BY-NC-ND license allows users to copy and distribute the Article, provided this is not done for commercial purposes and further does not permit distribution of the Article if it is changed or edited in any way, and provided the user gives appropriate credit (with a link to the formal publication through the relevant DOI), provides a link to the license, and that the licensor is not represented as endorsing the use made of the work. The full details of the license are available at http://creativecommons.org/licenses/by-nc-nd/4.0. Any commercial reuse of Open Access articles published with a CC BY NC SA or CC BY NC ND license requires permission from Elsevier and will be subject to a fee.

Commercial reuse includes:

- Associating advertising with the full text of the Article
- Charging fees for document delivery or access
- Article aggregation
- Systematic distribution via e-mail lists or share buttons

Posting or linking by commercial companies for use by customers of those companies.

20. **Other Conditions**:

v1.9

Questions? customercare@copyright.com or +1-855-239-3415 (toll free in the US) or +1-978-646-2777.